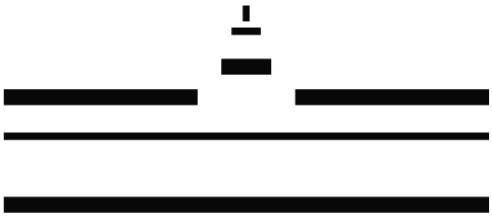

WESTFÄLISCHE
WILHELMS-UNIVERSITÄT
MÜNSTER

Westfälische Wilhelms-Universität Münster
Fachbereich Physik
Institut für Kernphysik

Arbeitsgruppe/Working group Johannes P. Wessels

Diplomarbeit/Diploma thesis

Studies on a di-electron trigger for Upsilon-mesons with the ALICE TRD

Paul Martin Kohn
martinkohn@uni-muenster.de

Münster, 25.04.2014
1.Gutachter: Prof. Dr. Johannes P. Wessels
2.Gutachter: Prof. Dr. Christian Weinheimer

Contents

1 Introduction

"HEP (Modern High Energy Physics) research has been constantly limited by technology, both in the accelerator and detector domains as well as that of computing."[CAR12]
Certainly this fact is valid for all fields of research, the limits of technology have a special meaning concerning the amout of data from HEP experiments.

Therefore it is necassary to keep pushing the limits of technology to improve physical results.

The ALICE (A Large Ion Collider Experiment) experiment is one of the main experiments served by the LHC (Large Hadron Collider). It has the purpose to examine the quark gluon plasma. The LHC is located at CERN (European Organization for Nuclear Research[1]), in the area of Geneva in Switzerland.

Triggering - the selection of interesting particle collisions - is an important task to ensure the physics performance of the experiment without the need of recording bulk data. Starting with the triggered cloud chamber from Patrick Blackett in 1932[2], triggers developed to an indespensable tool in high energy physics.

The trigger discussed in this thesis will be implemented in the environment of the Transition Radiation Detector (TRD) of ALICE, which is assembled in Münster, Germany. The goal of this diploma thesis is to plan and analyse a dielectron trigger for the Upsilon (Υ-particle, a meson composed of one bottom and one anti-bottom quark).
It will include considerations on efficiency, rejection and various other points.

After a short introduction to the goal of this thesis, given in this first chapter, Chapter 2 elucidates the theoretical background of heavy-ion physics, whereupon Chapter 3 treats the experimental situation, especially the system used for this analysis: the trigger system of ALICE. Chapter 4 shows all aspects of the analyses for this thesis, which is followed by a summary.
The appendix includes some additional information and detailed results from the analyses.

[1] CERN is an abbreviation of the french translation:¨Conseil Européen pour la Recherche Nucléaire¨
[2] Awarded with the Nobel Prize in Physics 1948
http://www.nobelprize.org/nobel_prizes/physics/laureates/1948/

2 Theoretical background, the Quark-gluon plasma (QGP)

Since the function of the ALICE experiment is to examine the properties of the quark-gluon plasma, this chapter gives an overview on the theoretical background. Initially an classification of QGP in the standard model is given, the formation of the QGP in context with hadron collisions and the occurrence in the phase diagramm of matter are given, too. The second parts of this chapter describes the measureable signals from the QGP.

2.1 Introduction

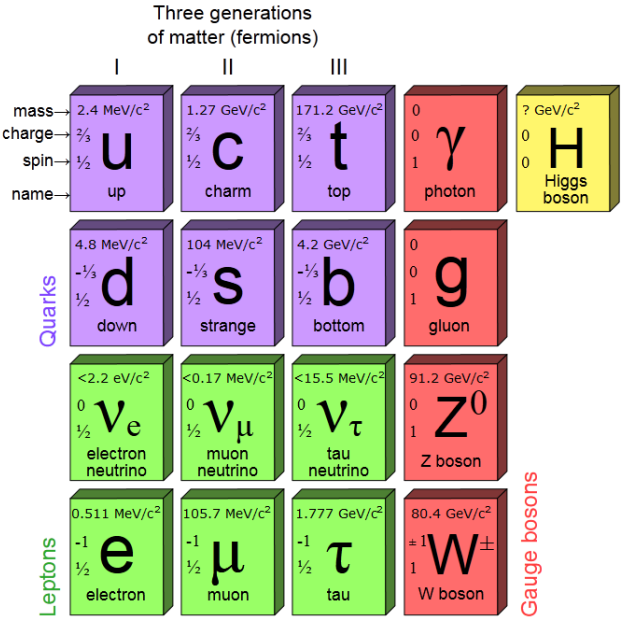

Figure 1: Elementary particles of the Standard Model [wiki2]

The Standard Model of particle physics classifies elementary particles in different categories. The fundamental interactions of the weak, strong and electromagnetical force are mediated by gauge bosons, which represent one particle group. The two other groups are quarks and leptons; both of which are classified as fermions [Pov06].
The Standard Model describes six types of quarks, which are sorted in three families. These six quarks are the up-, down-, charm-, strange-, top- and bottom quarks. Each quark carries a so-called color charge. The theory which describes this physics property is quantum chromodynamics (QCD).
Quarks form particles like mesons, which are quark-antiquark pairs, and baryons like protons and neutrons that are made out of three quarks. Because of color confinement, all particles have to be neutral in color charge. Analogous to color mixing in the RGB (additive Red, Green and Blue) color system, the quarks are assigned a color charge. In these color systems the three colors red, green and blue add up

to white (defined as neutral).
Quarks can carry one of three colors, or the corresponding anticolor for antiquarks. A proton consists of three quarks like all baryons. More specific, it consists of two up- and one down-quark with color charges of red, blue and green. These three colors add to neutral white. A positively charged pion, which is a meson built by one up- and one anti-down quark, might have the color charge blue and anti-blue and is color neutral in this way. It is described through a $SU(3)$[3] gauge symmetry. If one quark is seperated from such a neutral particle, the energy of the gluon field - that binds the quarks together - increases until there is enough energy to produce additional quark-antiquark-pairs. The increase in the energy is faster than a free quark can emerge. These created pairs bind to existing quarks from the neutral particle and also to other newly created quarks, so new combinations arise and new hadrons are formed. Therefore a single quark cannot be isolated.

Gluons are the exchange particles (gauge bosons) of the strong interaction between the quarks. They carry a color and an anticolor, which leads to 8 combinations of net color. They are massless, electric neutral vector gauge bosons. Because of their color charge interactions between gluons are possible. When two quarks exchange a gluon, both quarks change their color charge, according to color conservation.
In a quark-gluon plasma, which is supposed to be one state of the early universe, the quarks and gluons are assumed to be free like electrons and nuclei in a conventional plasma [SaS10].
A QGP can be created experimentally in hadron colliders like the LHC at CERN. Properties of the QGP - discovered through the ALICE experiment - help to get a clearer view on the Standard Model. The matter in the collision has to undergo a phase transition which is described in the next chapter.

[3]Special unitary group - see [SUr82].

2.2 Phase diagram of nuclear matter

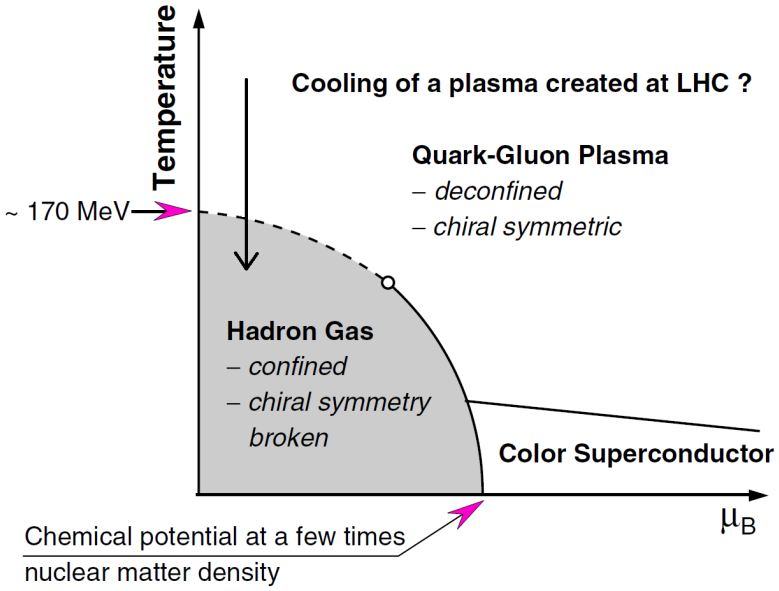

Figure 2: Phase diagramm of the QGP [ALI04](modified)

Figure 2 shows the phase diagram of nuclear matter. The phase diagram contains information about the different states of quark matter and their dependence on temperature and baryo-chemical potential. The baryo-chemical potential is a measurand for the net baryon density [Cou08].
In the shaded area, starting at low temperatures[4] up to medium values and from low to medium chemical potential, conditions allow quarks to form hadronic matter. The hadronic matter (hadron gas) is the vast majority of matter in our universe.
Chiral symmetry breaking - quoted in the phase diagram as a distinction between quark-gluon plasma and hadron gas - means that the corresponding gauge theory of the strong force, quantum chromodynamics, is invariant under chiral symmetry transformation, but the real physical system is not.

At high chemical potential and low temperatures quarks and gluons are acting like a color superconductor, a state which is assumed to exist in the core of compact (neutron) stars (see chapter 6.1.1)[Had01].
A color superconductor is equivalent to the normal superconductor for electrical currents and has different properties than the other states of nuclear matter.

At temperatures above the color superconductor state and at medium chemical potential μ_B the hadron matter is subject to a phase transition to the quark gluon plasma.
This phase diagramm has a critical point, so that at high energies and low μ_B there is no clear phase transition between the QGP phase and hadron gas, like at high pressure and temperature the liquid and gaseous phases of water have no clear transition either.

[4]For our universe approx. 2,73K, derived from the cosmic microwave background.

The proposed trajectory of the hadronisation process of a quark gluon plasma at the LHC is also given in the figure (labeled: "Cooling of a plasma created at LHC?") [Had01] [ALI04].

2.3 Stages of a hadron collision

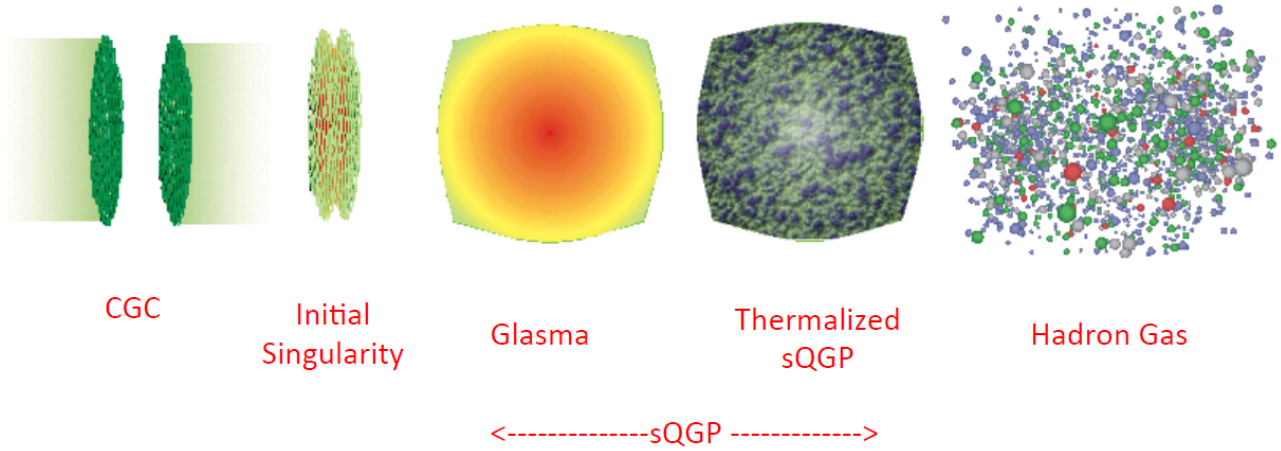

Figure 3: Phases of a heavy ion collision, time ascends from the left to right. [Bas05]

According to the theories proposed in [BrW06][IaV03][McL01][McL12][Nay06] and [Ven08], a heavy ion collision can be divided in various stages (see figure 3).
The color-glass condensate (CGC) is a special type of matter - postulated but not yet proven -, that occurs when atomic nuclei, such as the lead ions used in the LHC, are accelerated to speeds near the speed of light. Accelerated particles are Lorentz contracted, they have the form of thin slices instead of a spherical shape. It is a dense condensate of gluons. Gluons change their position in the nucleus very slowly in comparison to the hadrons. This fact has lead to the word "glass" in the name Color Glass Condensate [IaV03][McL01].

When two nuclei at the state of a CGC collide, they form the initial collision (labeled "initial singularity" in figure 3), which evolves quickly into a Glasma.
Glasma is the state of the collision, appearing shortly after the initial singularity, it is named "Glasma" because it is the successor of the CGC and the precessor of the QGP.
An important fact is that the Glasma is non-equilibrium matter opposed to any kind of quark-gluon plasma. Glasma might have some influence on processes like flow of particles and jet quenching (see next chapter) [Ven08].

sQGP is simple a name for a QGP with strong interaction or strongly coupled particles in contrast to the earlier expectations of weak interacting or pertubative QGP at the LHC (see [Nay06] for further reference).
A hadron gas is created when the energy density of the QGP decreases and the so-called freeze-out of hadrons takes place. Due to the high energy of the created particle the hadron gas expands with time as the QGP did before, too [RaL99].
Particles - generated in this phase - move away from the collision vertex with high velocities and can be detected.

2.4 Probes of the QGP

There are several probes to get information about the collision and the QGP. They are very important due to the fact that direct information is not available. Probes can give information about the QGP properties. Measurements of probes can be compared to theoretical predictions.
The next chapter will give an overview on some types of probes used in the ALICE experiment. The last chapter of this section deals with the quarkonia probes which should be triggered with the ALICE TRD.
One can distinguish between soft probes with a momentum lower than 2 GeV/c and the hard probes above that threshold. Quarkonia mark an exception since they have large masses even at zero momentum; so they are hard probes.
Two categories - quarkonia and jets - of the four probes described in this chapter are hard. The other two categories - photons and di-leptons - can be accounted to the hard and also to the soft regime. Hard probes deliver a better signal to background ratio. Background is being created by all particles that do not come from hard scattering partons e.g. photons from bremsstrahlung.

2.4.1 Photons

Photons in collision experiments are mainly created by particle decays, but direct photons are created in the early moments of the collision and not by decays. They are a result of partonic scattering (prompt photons) or of thermal processes [Pei09].

Initial hard scattering of hadrons: There are also photons produced from scattering of hadrons. They have high transverse momentum p_T and are probes for QCD. They deliver information about particle distribution functions.

Thermal photons: These photons are produced at quark-quark or gluon-quark collisions from parton scattering, via hadronisation processes of the QGP, up to production out of hadron gas. They dominate the photon spectrum at low energies and deliver information on the early states of the QGP.

In lead-lead collisons interactions with the QGP have also to be taken into account:

Jet-photon conversion: Through scattering of jets with the quark-gluon plasma photons are produced.

Jet fragmentation: Photons can occur during the fragmentation of a quark or gluon into a jet. When parton cascades scatter with other partons they produce bremsstrahlung.

Figure 4 shows a spectrum of direct photons with a fit to extract the temperature of the QGP [RIc11][LWe07][Wil12].

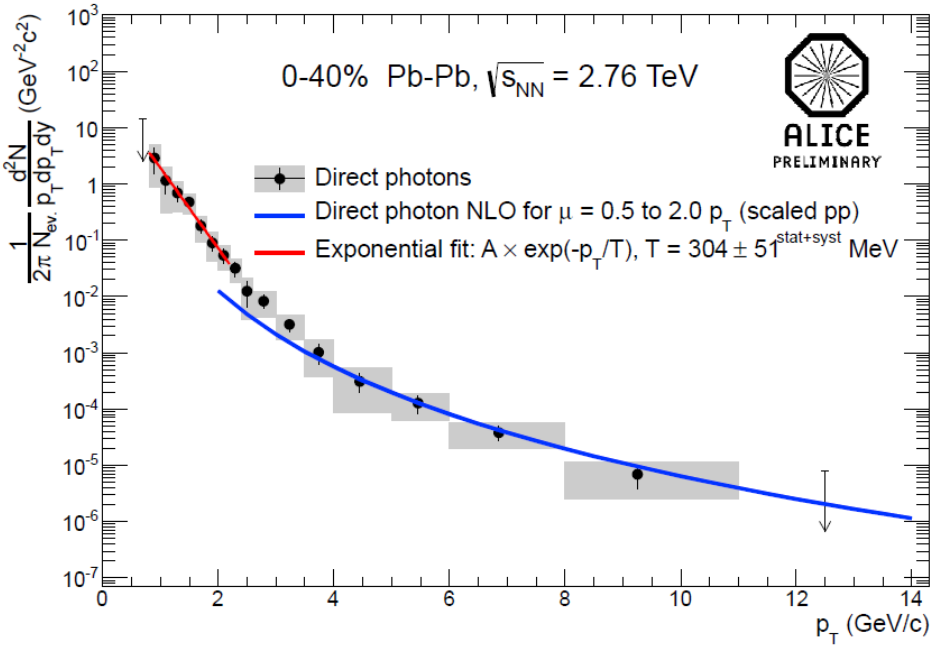

Figure 4: Direct photon spectrum showing the exponential decrease towards higher transverse momentum [Wil12].

2.4.2 Di-leptons

The so-called di-leptons are lepton-antilepton pairs, e.g. electron and positron. Di-lepton pairs are created in all phases of parton collisons, starting from hard processes, which take place when the colliding nuclei hit each other. Nearly all processes that are described via pertubative QCD can be hard. Anyhow, it is common to declare only processes with a transferred momentum greater than 2 GeV as hard processes (some sources set 10 GeV as threshold, see [EIa12]).

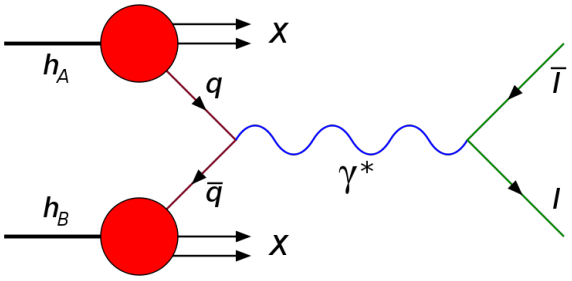

Figure 5: Di-lepton production in the Drell-Yan Process or in the QGP [wiki4].

Figure 5 shows the creation of a di-lepton through a virtual photon generated in a quark-antiquark annihilation. The di-leptons are delivering similiar information about the collision like direct photons. The quark-antiquark interaction is triggered through scattering of two arbitrary hadrons h_A and h_B.

In detail, di-leptons have the following origins:

1. Drell-Yan: In direct hadron-hadron scattering at high energies like in the LHC the interacting quarks form a virtual photon or a Z-boson. These virtual particles deliver the corresponding di-lepton through decay [DYa70].
2. Thermal radiation: Through scattering between partons and via decays di-lepton pairs are produced. They couple weakly to the partons and therefore do not interact. Their information can be measured, for example from the reaction: $\pi^+\pi^- \rightarrow \gamma^* \rightarrow e^+e^-$. The thermal radiation evolves from hadronic and QGP sources.
3. Final state[5] hadron decays: Particles like J/Ψ or Υ[6] can decay into lepton pairs.

[5]See chapter 3.1.
[6]See chapter 2.4.4.

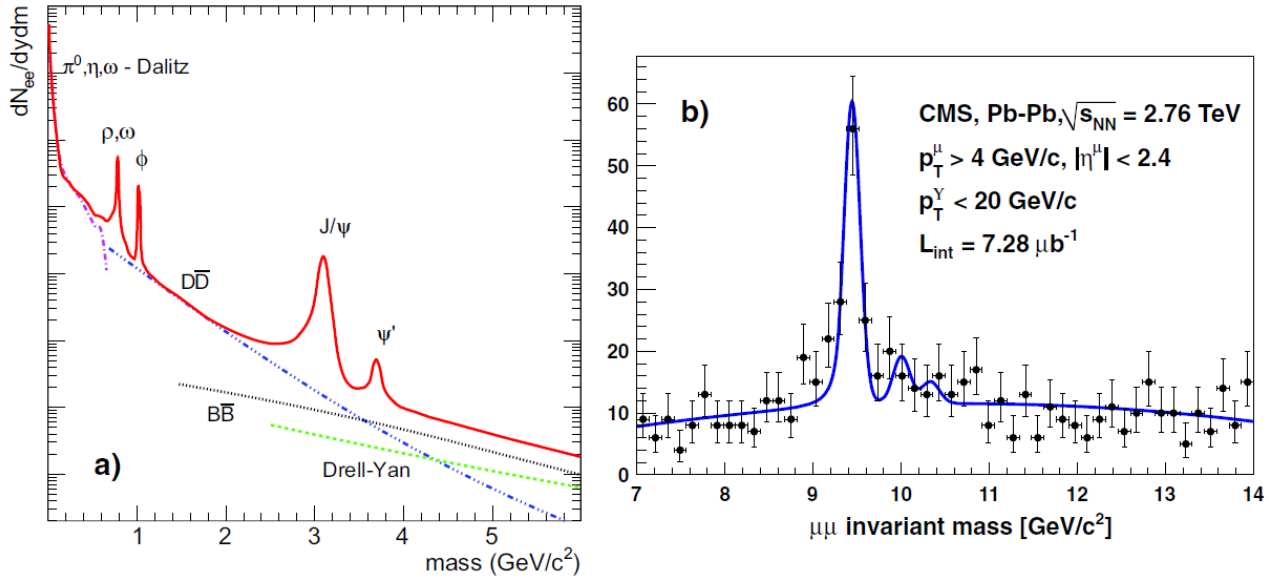

Figure 6: Invariant mass of di-lepton resonances [ADr09][CMS11], pointing out the different energy regimes of dilepton sources like J/Ψ. Counts are given in arbitrary scaling.

Figure 6 shows the invariant mass spectrum of several di-lepton resonances. Resonances deliver through their invariant mass information clear momentum thresholds for daughter particles of the decay.
Dalitz decays are briefly worded three body decays from various sources. The main decay of the π^0 is into two photons, but with 1,2% probability it decays into a electron-positron pair and a photon. The shown ω and η resonances show similar behavior.
All particles with three-body decays have a widely smeared invariant mass. ω and ρ-mesons have also two-body decays with a clear peak in the invariant mass.

$D\overline{D}$ means a process where two charm quarks are created; these charm quarks form a D- and an anti-D-meson. These two D-mesons then further decay in the semileptonic channel, which ends in an electron-positron pair and addional products. The resulting wide invariant mass distribution is obvious. The $B\overline{B}$ process proceeds analogically.

With lower resonance mass, the dilepton production process occurs later in time. Energy density decreases after the initial collison, up to the hadronic freeze out due to expansion. Therefore the high mass resonances deliver information of the early stages of hadron collisions.
As one can see in figure 6, some processes are dominating certain energy regions. At higher energies $B\overline{B}$ and the Drell-Yan Process become more and more the dominating sources. For the signals from quarkonia (J/Ψ and Υ) see chapter after next. Di-lepton pairs are only affected by the electromagnetic force, not the strong force dominating the plasma. This makes di-leptons an ideal base for comparisons with probes that are influenced by the QGP through the strong force or other interactions [EIa12] [Won94]. The comparison of di-leptonic probes to other types is essential

to get a measurement of enhancement or suppression in the yield of some of these probes. The yield is changed through physical properties of the underlying forces in the QGP (comparison of pp and Pb-Pb collisions) [BMS07].

2.4.3 Jets

Particle-jets are created through scattering of nucleons. In these reactions two partons with very high momenta are produced.
Figure 7 shows the creation of these partons in a proton-proton collision. Due to momentum conversation two partons are nearly emitted in opposite direction.

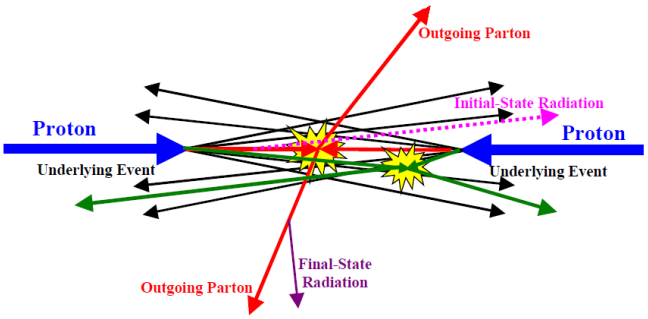

Figure 7: Jet production in a hard scattering process (modified from [RFi01]).

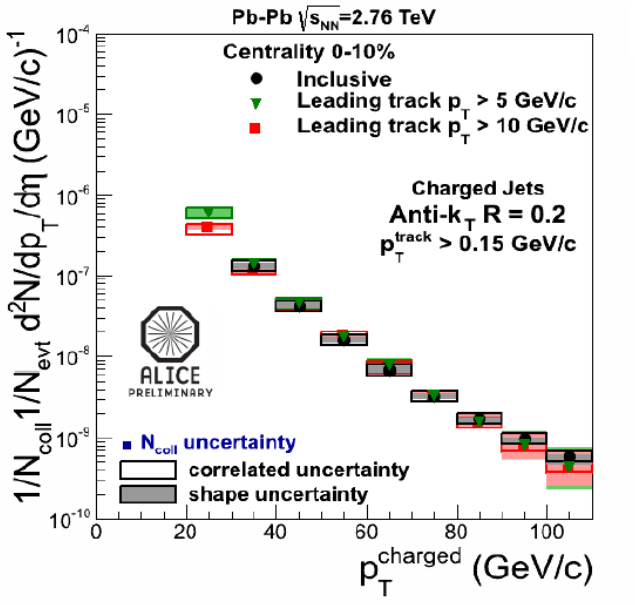

Figure 8: Charged jet spectrum of Pb-Pb collisions [Ver12].

In detail, the source of jets are the bunches of particles, that have been emitted from the initial jet parton. In the experiment it is not directly evident which particles are the underlying event and which particles emerged from the jet parton, especially in ion collisions. Several algorithms can be used to calculate the jet properties on base of geometrical cuts[7] or other variables.
The partons can escape the collision point in pp collisions without further interaction. In ion collisions, a new phenomenon, jet quenching occurs. In this case one or both partons propagate through the QGP.
Since QGP is dense matter, several interaction types are possible. Bremsstrahlung is the most relevant one. Through bremsstrahlung the energy of the jet particle is lowered proportional to the density in the medium. Therefore the number of detected jet particles is reduced when a QGP was created. This is the so called jet quenching, mentioned before.
Measuring jet quenching in relation to pp data and to data of other experiments like RHIC provides useful information about the QGP [Had01].
In figure 8 the raw jet spectrum of Pb-Pb[8] data is shown. Jet momentum was determined through the anti-k_T-jet[9] finding algorithm.

[7] For cuts in general, see chapter 4.4.
[8] Dataset from the LHC, year: 2010.
[9] There are several different algorithm for jet finding available. The anti-k_T-jet finder is based on sequential recombination of particles. See [MZi10].

2.4.4 Quarkonia

Quarkonia particles are mesons composed of a quark and its antiparticle. The most notable examples are the J/ψ for charmonium, based on charm quarks, and Υ for bottomonium, based on bottom quarks. Both are the lightest vector meson representants of their kind. Quarkonia with top quarks are not possible, as they would decay before creation because of the high mass of these quarks. The definition of quarkonia implies pure states of these mesons, therefore it does not refer to mesons with lighter quarks than charm, because these mesons are mixed quantum states. Charmoniums have masses from 2980 MeV up to 4263 MeV. Bottomonium particles have masses in a range from 9390 MeV up to 11019 MeV [PDG12].

Most quarkonia particles in a particle collisions are produced in the initial hard scattering processes and therefore they interact with the QGP medium [ED+04]. When the matter has reached the deconfinement temperature, the charm pairs of charmonia are expected to melt. But some of the quarkonia particle can escape, for example when they exceed a transverse momentum threshold or have only a short way through the QGP [HMü96]. Measurements of quarkonia can be compared to theoretical predictions and among themselves concerning different collision energies or other parameters.

Figure 9 shows the suppression of J/ψ in different measurement series at the SPS experiment at CERN. Measured values of the J/ψ yield are compared to expected values from extrapolated proton-proton data. Around 130-150 participating nucleons, the J/ψ yield is reduced due to losses in the QGP or through other effects, which have not been researched yet. Upsilon-states offer extending tests of predic-

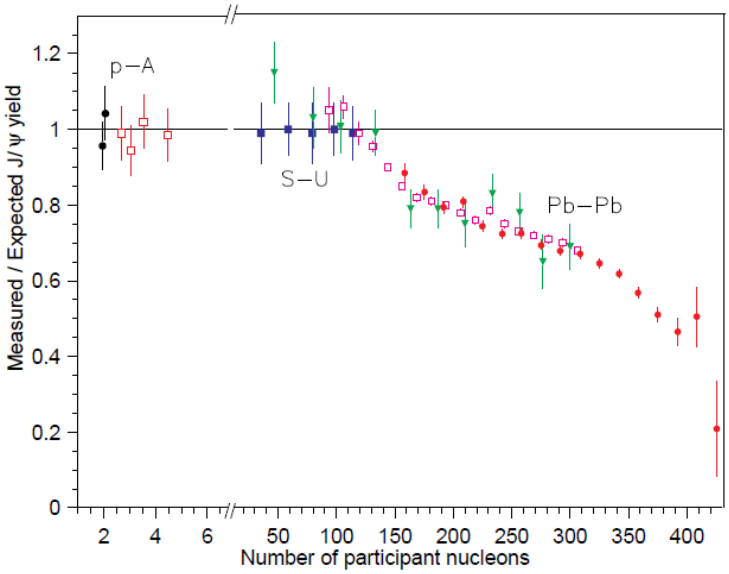

Figure 9: Data from the SPS expriment at CERN (extracted from [Had01]).

tions from QCD, for example current thoughts on the polarisation of these particles depending on different orbital angular momentum [Fac13]. Further they show less losses from recombination than the J/ψ. For the analysis on triggering upsilon-

particles with the ALICE TRD carried out in this thesis, see chapter 4.5.2 and following.

3 The experiment

3.1 The LHC

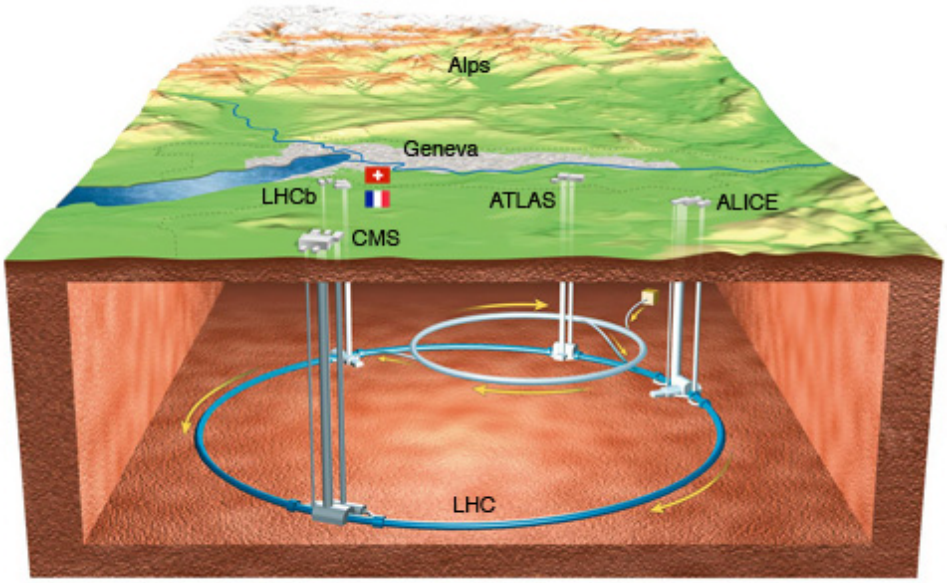

Figure 10: Schematic view of the location of CERN/LHC [lhc08]

The LHC (Large Hadron Collider) is the most complex particle accelerator in our days. CERN[10], a large research center, extends on a small area across France and Switzerland. The collider has the capability to accelerate and collide either protons or lead ions. There is also the option to collide protons with lead ions, which will allow an additional view on the properties of heavy ion collisions. Initial state effects are caused by gluon saturation short before the collision. Final state effects are determined through interactions within the quark-gluon plasma. Due to the fact that ion-proton collisions are free from final state effects, they are a good benchmark for the signatures of the QGP. Proton-proton collisions also allow this benchmarking, but they are also free from initial medium effects, not only from the final state ones. It is planned that the LHC will achieve its design energy of 7 TeV for protons (14 TeV center of mass energy[11]) in 2015. The first idea to build a hadron collider of this size started at a workshop held in March 1984 [CER84]. The LHC is intended to run over the next 10-20 years. Therefore improving the data acquisition to enhance physics performance and simplifying the analyses is a big challenge.

The first collisions in 2009 started at 0.9 TeV center of mass energy increasing to 1.8 TeV the same year. In 2010 and 2011 the collision energy was 7 TeV in the center of mass system with an increase to 8 TeV in 2012.
So far, for Pb-Pb runs a nucleon-nucleon center of mass energy of 2.76 TeV[12] was achieved (3.5 TeV proton beam equivalent). The corresponding nucleon-nucleon

[10] see chapter 1
[11] See 6.1.4 for center of mass energy.
[12] $\sqrt{s_{NN}} = 7\ TeV \cdot \frac{82}{208} = 2.76\ TeV$ for fully ionized $^{208}_{82}Pb$

center of mass energy of 4 TeV proton energy per beam is 3.15 TeV, but instead of this energy in lead-lead, a proton-lead run with 5.02 TeV nucleon-nucleon center of mass was done in 2013.
The asymmetric collision partners cause a shift in rapidity .To exclude effects from this shift the experiment will take p-Pb and Pb-p runs [Ali04]. For details see chapter 6.1.5.

At the LHC there are four big detectors (ALICE, ATLAS, LHCb and CMS) and two smaller ones. Due to the fact that ALICE investigates the QGP, it is mainly designed for lead-lead collisions, whereas the other experiments located at the LHC use mainly proton-proton collisions. But ALICE also analyzes proton-proton collisions.
ATLAS (A Toroidal LHC ApparatuS) and CMS (Compact Muon Solenoid) are the two main multi-purpose experiments of the LHC. Their intention is to detect the Higgs-boson and explore its properties [ATL12][CMS12]. The Higgs-boson is an elementary excitation of the Higgs-field. All other particles have their mass through interaction with the Higgs-field. Detection and precise measurement of the Higgs-boson is one of the last verifications of the so-called Standard Model of particle physics. It is clear that these experiments will provide additional results in new unexplored areas of physics like supersymmetry (an extension of the Standard Model) and extra dimensions [ATL08][CMS08].
In addition to the already mentioned ALICE experiment, ATLAS and CMS are also part of the heavy ion program of the LHC. For the investigation of the QGP and other effects of heavy ion collisions several observables like charged particle multiplicity and hard probes (e.g. jets) are examined [PSt12].

3.2 A Large Ion Collider Experiment (ALICE)

In figure 11 one can see the ALICE experiment, consisting of several detectors. These detectors are arranged cylindrically (the so-called central barrel) around the collision point, where the two particle beams collide. On the right side of figure 11 is the so-called muon arm, which is arranged in the direction of the beam line, starting from the collision point of the two beams.
The different parts of ALICE can be categorized in five different functions [ALI08] [CAL04]:
Starting from the collision point there are three detectors which are mainly used for *particle tracking*; the Inner Tracking System (ITS), the Time-Projection Chamber (TPC) and the Transition Radiation Detector (TRD). In combination with the Time of Fight Detector (TOF), the last two ones are capable of *particle identification*, which is the second function. Furthermore, also ITS delivers information on particle identification.
Photon Spectrometer (PHOS) and Electromagnetic Calorimeter (EMCAL), which are both *electromagnetic calorimeters*, are the third category.
The fourth category is the *muon spectrometer*, which is the muon arm at small angles in reference to the beam pipe. Last and therefore the fifth category are *small reference and trigger detectors* for event characterisation and special purpose detectors like HMPID.
All central barrel detectors are surrounded by a solenoidal magnet with an magnetic field of 0.5 T. The muon arm is an exception, it is partially surrounded by a dipole magnet with a magnetic field of 0.67 T.

ITS is the detector closest to the beamline. ITS consists of six layers of silicon detectors. Because of the decreasing particle rate starting from the interaction vertex, the first two layers are silicon pixel detectors, followed by two layers of silicon drift detectors. Silicon pixel detectors have a better resolution to provide precise track informations whereas silicon strip detectors allow the quantification of energy loss through the analog readout. The previously mentioned tracking capability is one of the main functions of the ITS.
Another important basic function is the measurement of vertices. There are two types of vertices to distinguish between: the primary vertex from the collision which varies from collision to collision and the secondary vertices from charm and hyperon[13] decays.
Another great advantage of the ITS is its high resolution and the capability to measure track properties and information on particle identification (PID) of particles below a momentum of 200 MeV/c^2.
In the last two layers silicon strip detectors with a smaller esolution than the both middle layers are sufficient [CIT99] [ALI08].

The TPC is a gas detector with a volume of 90 m^3. Passing particles ionize gas molecules, which are guided towards the multiwire chambers at the two bases of the cylindrical TPC. Two dimensions of the particle trajectories are directly measured. Via drift time the third dimension (of the particle trajectories) can also be deter-

[13] Hyperons are baryons containing at least one strange-quark, but no charm or bottom quarks [Pov06].

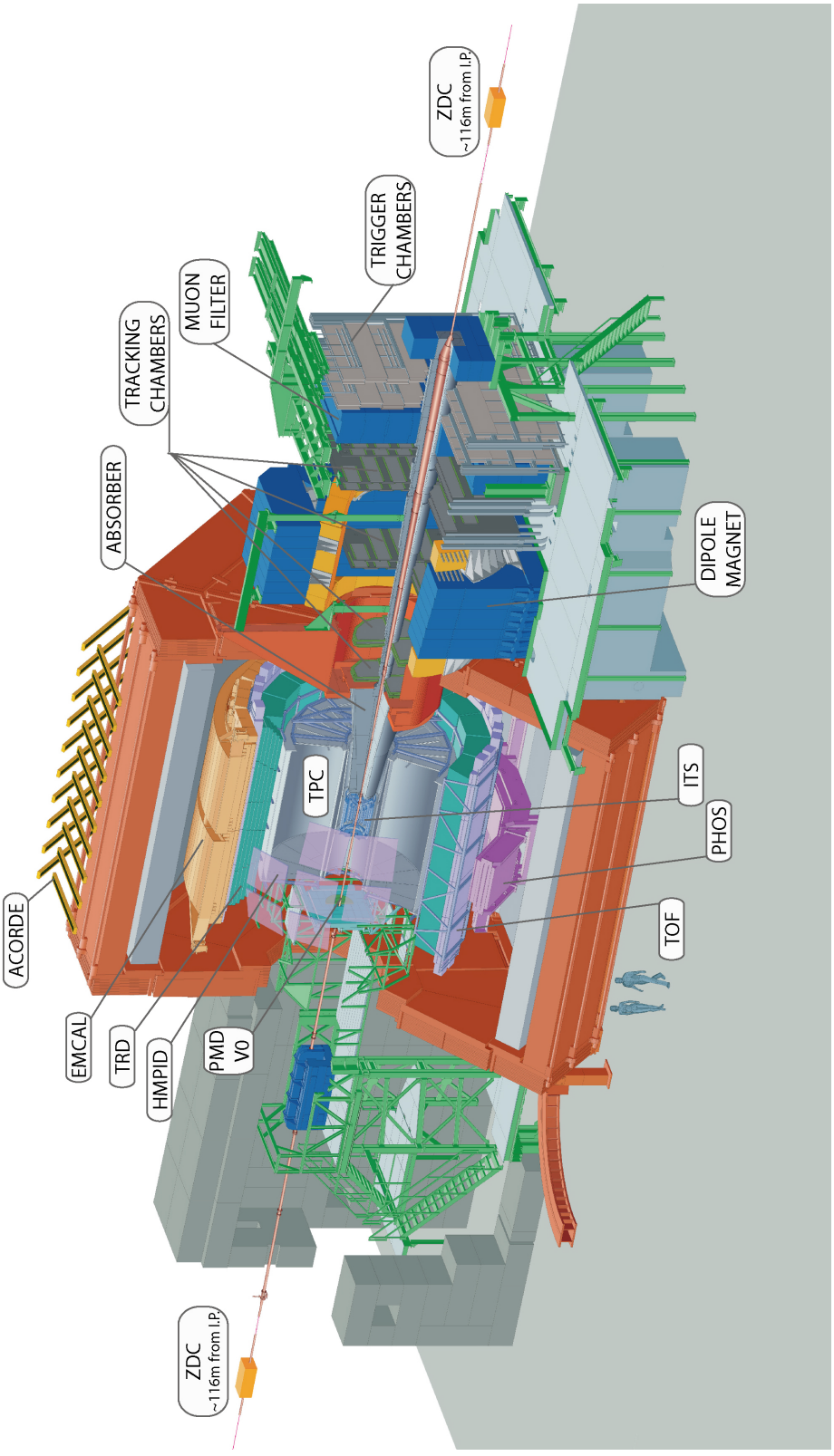

Figure 11: Schematic view of the ALICE experiment with the arrangement of the different detectors [ain12].

mined. Because of this ability the TPC is the main tracking detector of the ALICE experiment. A magnetic field bends tracks of charged particles, which allows to measure the momentum of these particles [CTP00].

Subsequently after the TPC follows the TRD, for detailed information see chapter 3.3.

TOF is mainly used for particle identification. It is also a gaseous detector like TPC and TRD, but it uses Multi-gap Resistive-Plate Chambers (MRPC) instead of MWPC (3.3.3) for a better time resolution. Tests of the MRPC multicell strips have shown that they fulfill a time resolution around 40 ps [ALI08]. The MRPC are a stack of glass plates and electrodes. The ionization by charged particles is amplified by high voltage.
Particles produce different signals in time due to their different velocities, especially these with a low momentum (pions and kaons below 2.5 GeV/c and protons below 4 GeV/c). With information about momentum and track length from tracking detectors it is possible to calculate the mass of the particle [CTO00].

The High-Momentum Particle Identificaton Detector (HMPID) is a Ring Imaging Cherenkov detector, which enhances the PID capability in a momentum range above the main PID detectors ITS, TPC and TOF. It can also detect light nuclei and anti-nuclei created in collisions. [CHM98]

PHOS covers uncharged particles like photons or η mesons and charged particles with the charged particle veto (CPV), a Multi-Wire Proportional Chamber. PHOS is important to examine direct photons from the initial phase of the collision. The measurement is based on the scintillation light from the passage of particles through lead tungstate crystals. For a better effciency the crystals are operated at -25°C, the readout is done with photodiodes [CPH99].
EMCAL is also a calorimeter like PHOS, but its purpose is to quantify the properties of jets. Because of the different function it has a larger acceptance, but a worse energy resolution than PHOS [CEM08].

The MUON spectrometer for measuring muons consists of an absorber, which filters all other particles. The absorber is followed by a tracking system, a large dipole, a second muon filter and trigger chambers. This detector is designed to make detailed measurement of the moun decay channel of quarkonia [CMU99].

3.2.1 Particle identification (PID)

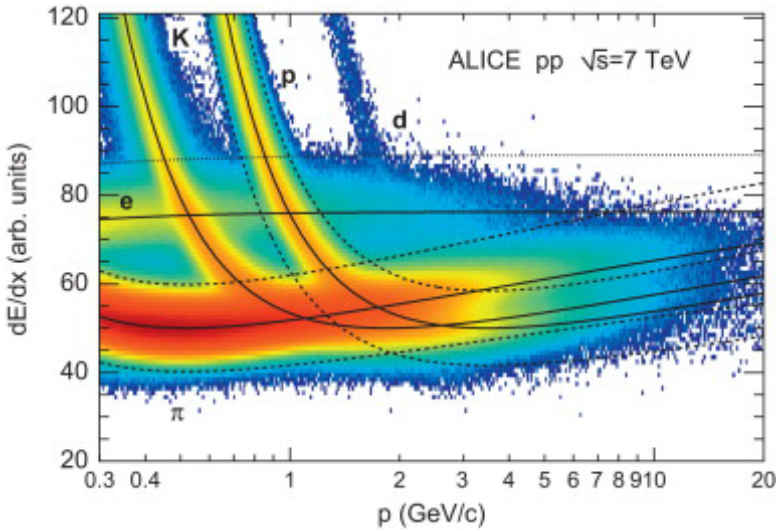

Figure 12: Energy loss of different particle types in ALICE TPC [TPC12]. Color represents the number of counts. Scale starts from white - hich is zero counts - dark blue, light blue to green and yellow. Highest counts are marked red.

The ALICE experiment uses different techniques for particle identification. First one has to distinguish between charged (electrons, protons, pions etc.) and neutral (photons, pions, etc.) particles. Neutral particles are measured in PHOS and EMCAL; furthermore electrons are measured with EMCAL, too. As already mentioned, these two are electromagnetic calorimeters. PHOS includes the already mentioned charged particle veto (CPV) which consists of multiwire chambers, because charged particles can also create cherenkov light in the crystals of calorimeters.
For the identification of charged particles, energy loss in matter is used (ITS, TPC and TRD).
The Bethe-Bloch equation describes the effect theoretically:

$$-\frac{\mathrm{dE}}{\mathrm{dx}} = \frac{4\pi}{m_e c^2}\frac{nz^2}{\beta^2}\left(\frac{e^2}{4\pi\epsilon_0}\right)^2\left[\ln\left(\frac{2m_e c^2\beta^2}{I\cdot(1-\beta^2)}\right)-\beta^2\right]$$

$\beta = v/c$ is the velocity of the particle, n is the electron density in the material and I is the mean excitation potential of the traversed material.
Figure 12 shows the energy loss of different particles in the ALICE TPC as a function of momentum. The solid lines are parameterizations of the Bethe-Bloch curves for the different particle types. To separate particles in a parameter region where the Bethe-Bloch curves overlap, additional information from TOF can be used. A further example is the use of PID from the TRD detector to isolate electrons.
An additional method is the topological PID, which identifies particles when they decay or when photons undergo conversions [Kal11][Pov06].

3.3 Transition Radiation Detector (TRD)

This chapter gives an overview of the Transition Radiation Detector (TRD) of the ALICE experiment.

3.3.1 Transition radiation

Transition radiation is produced when a charged particle passes a boundary between two different dielectric materials. This effect was first discovered and described by Ginsburg and Frank [Gin96].
A simplyfied explanation can be given by a mirror charge model: When a charged particle moves towards the direction of a dielectric medium, it produces a mirror charge with reversed polarity. These two charges compose a variable dipole, which emits electromagnetic radiation.The electron produces transition radiation, the pion does not (in the considered momentum range), because its mass is too big.

The transition radiation depends on the Lorentz-factor :

$$\gamma = \sqrt{1/\left(1 - v^2/c^2\right)} = \sqrt{1 + \left(\frac{p}{m_0 \cdot c}\right)^2}$$

For a particle momentum of e.g. 3 GeV the electron ($m_0 = 0.511$ MeV/c^2 [PDG12]) has a Lorentz-factor of about $\gamma \approx 5870$, a pion (e.g. π^- with $m_0 = 140$ MeV/c^2 [PDG12]) has nevertheless a Lorentz-factor of about $\gamma \approx 21$, which is below the threshold for transition radiation of $\gamma \geq 1000$.

The main property of transition radiation is that it covers an energy range between 2 to 40 keV for a particle with $\gamma \geq 1000$ [PDG12]. The electromagnetic radiation ranges in the energy domain of X-rays. The ALICE TRD is designed to have a low X-ray absorption in the radiator, so $E_{total\ measured} = E_\gamma$ is a valid assumption.

When a particle passes one dielectic boundary, at average 1.45 photons[14] above the threshold are produced. Therefore it is necassary to use several dielectric transitions consecutively.
Figure 13 shows the photon spectra of a single interface and the measurement of a Transition Radiation Detector with 200 foils of Mylar[15].

When the particle's Lorentz-factor is of the order of $\gamma \approx 2000$, these X-rays interact with the gas atoms in the detector. X-rays with lower energy have a smaller conversion probability. For a more detailed theory see [Gin91].

[14] for particles with $\gamma \approx 1000$, and transition radiation photon energy range from 1 to 30 keV [An$^+$11]
[15] A polyester made of polyethylene terephthalate (PET).

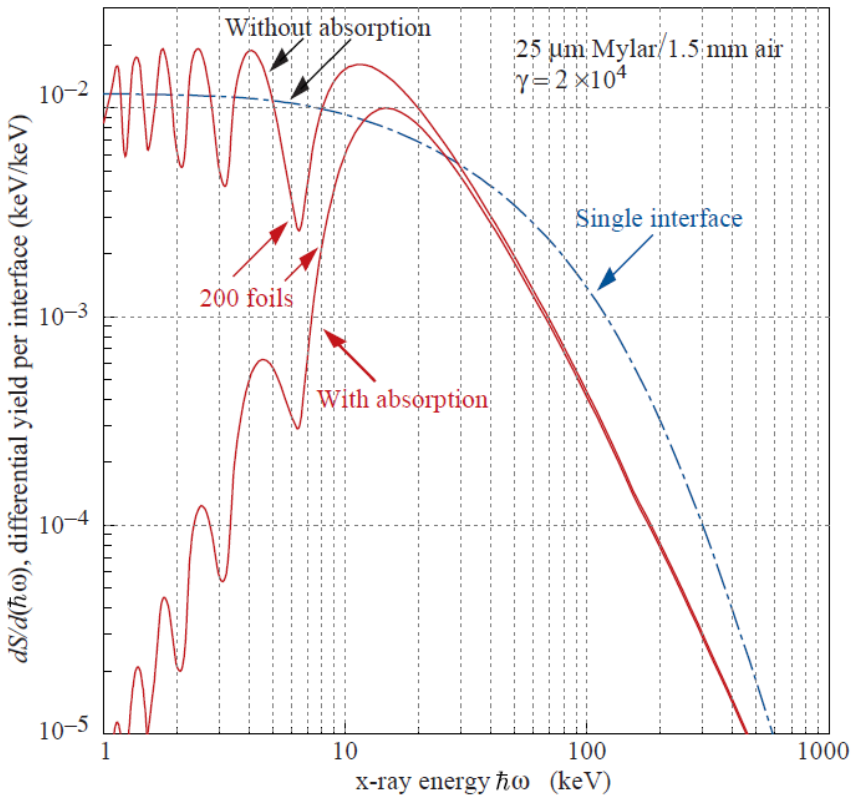

Figure 13: Transition radiation spectra of a single interface and a 200 foils detector. The measurement of the detector also includes absorption effects of the radiator itself in one spectrum [PDG12].

3.3.2 Detector design

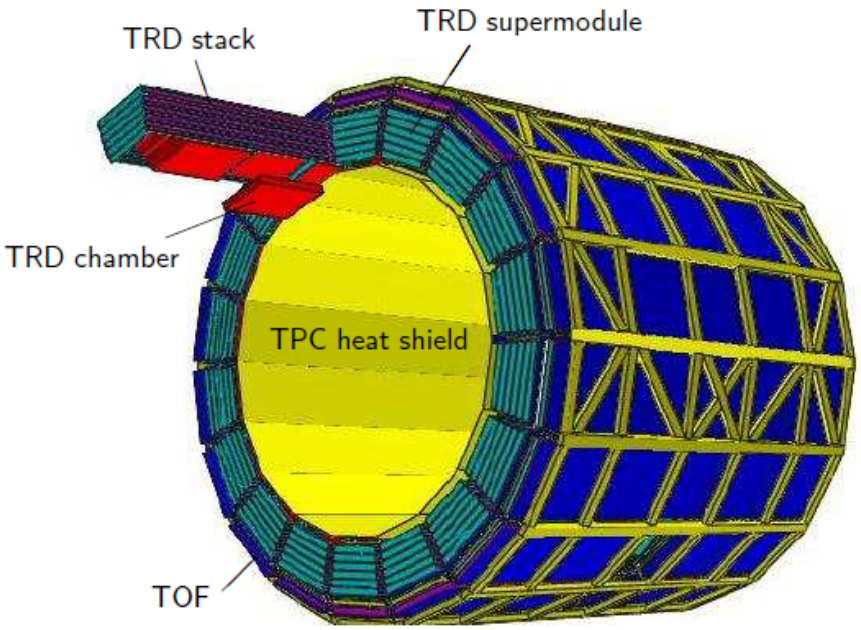

Figure 14: Structure of the TRD frame and supermodules around the TPC detector [ALI08]

The main function of the TRD is particle identification (PID), more precisely to distinguish electrons and pions above 1 GeV/c. The TRD consists of 522 chambers[16] which are assembled in 18 supermodules with 30 or 24 chambers each. The detector chambers are organized in five stacks (0 - 4) in z-direction and in six layers (0 - 5) in radial direction in each supermodule (figure 14). Figure 15 shows the main working principle of the TRD detector. Each chamber is constructed of different layers, starting with the radiator volume, constituted of synthetic fibres and foam. These materials have many interfaces where transition radiation can emerge. The radiator volume is followed by a drift region which is again followed by a multiwire proportional chamber (MWPC). The MWPC consists of anode and cathode wires and copper pads for the signal readout (see also 3.3.3).
The readout pads are mounted on a carbon fibre back panel, which carries the detector electronics on the other side.

[16]The TRD was designed for 540 chambers, but three sectors do not have a central stack. This is done to reduce material budget in front of the PHOS detector. A version with four supermodules with a PHOS hole is also possible; this will result in 514 chambers in total.

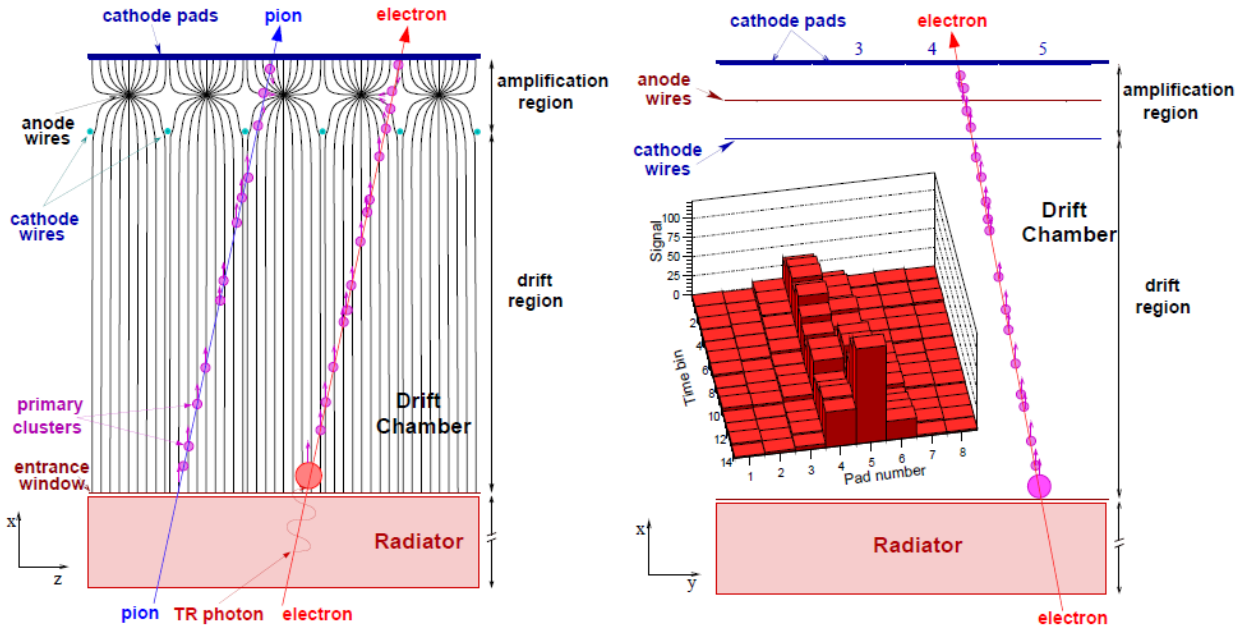

Figure 15: Working principle of the ALICE TRD chambers [ALI08].

3.3.3 Signal generation

In figure 15 two different particle tracks passing the detector volume are shown. The transition radiation photon, created in the radiator by an electron, more specific the electromagnetic field of the photon can be seen following the track of the electron whereas the pion does not create transition radiation photons. For the properties of transition radiation see chapter 3.3.1.

After passing the radiator, particles enter the drift region, where they ionize gas molecules all along their way. Transition radiation photons are absorped shortly after they move into the drift region. For this photo-absortion process a gas with high atomic number like Xe, Kr or Ar is required (see figure. 16) [ALI01]. For the ALICE TRD a mixture of 85% Xe and 15% CO_2 is used for measurement, for testing purpose a mixture of 85% Ar and 15% CO_2 is appropriated. The CO_2 functions as a quenching gas which reduces avalanches from electrons with high energies from the cathodes.

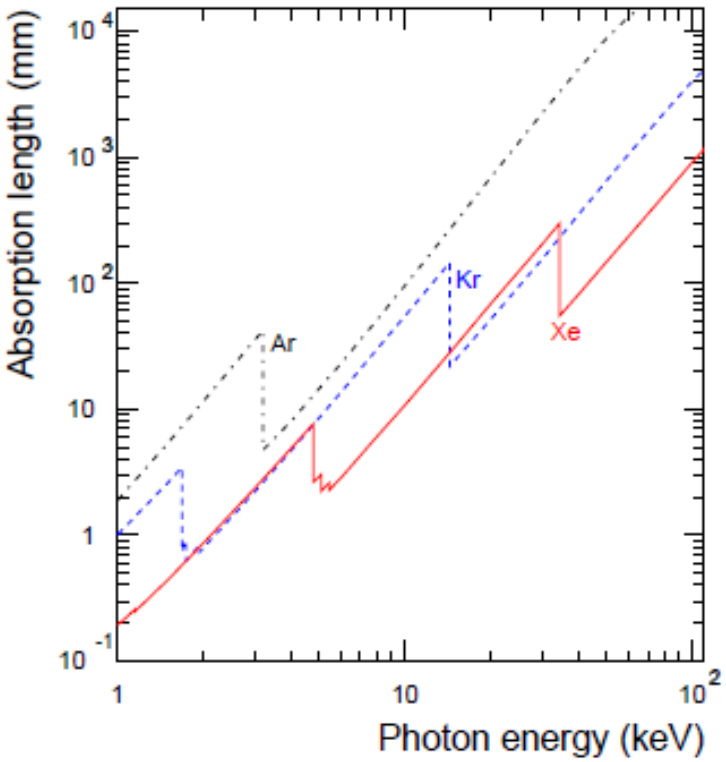

Figure 16: Average absorption length of X-rays in Xe, Ar and Kr [ALI01].

The ionization process produces electron clusters and gas ions, which are positively charged. The electrons drift towards the amplification region. Due to the field intensity in the amplication region, electron clusters are boosted to energies which can induce secondary gas ionization. The wire geometry of the amplification region is shown in figure 17.
Figure 17 shows this avalanche process. Gas atoms, which are ionized in the amplification region, move towards the cathode and induce therefore a positive signal on the pad plane which is measured [FSa76][ALI01].
The striking difference to transition radiation free tracks from particles like pions is the fact that the transition radiation also creates gas ionization, in which electrons are emitted. The cross-section for transition radiation in xenon is smaller than the cross-section for electrons and ions but the TR photons are completely absorped.
The right part of figure 15 shows the measured signal of an electron in discrete time bins and cathode pads. Each so-called time bin is 100 ns long. Figure 19 presents the signal of an electron with and without transition radiation and the signal of one muon, all with a momentum of 2 GeV/c.
The electron without transition radiation is measured with a detector without radiator. All three signals show a peak at about 0,5 μs. This results from different accelerations of electrons created between anode wires and cathode pads in the amplification region. Then, without transition radiation the signal is nearly constant for 1.75 μs, whereas the signal with transition radiation shows an increase with a maximum at the end of the drift time (at 2,3 μs). When the signal ends, the voltage shows an exponential decrease, which is caused by the ion tail from the slow moving

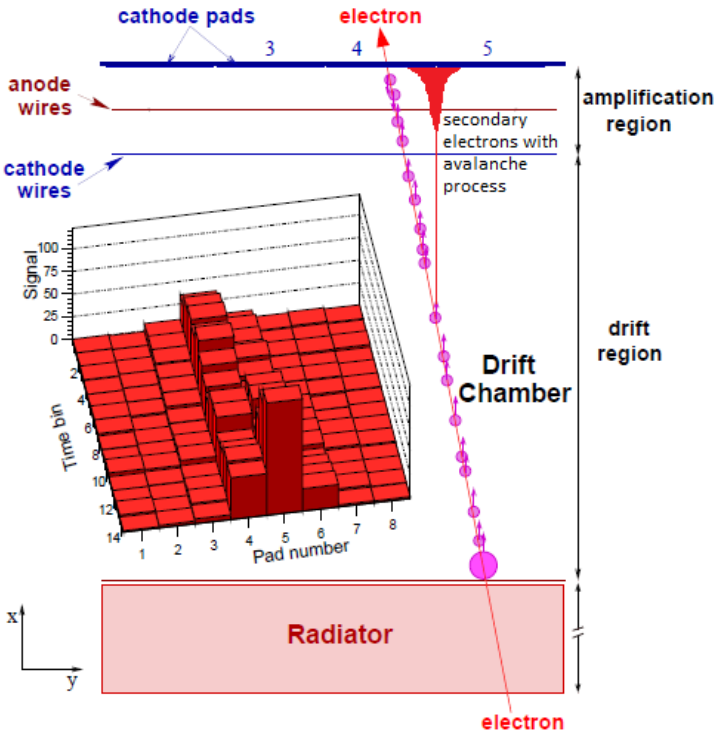

Figure 17: Functional principle of the ALICE TRD multiwire chamber [ALI08](modified).

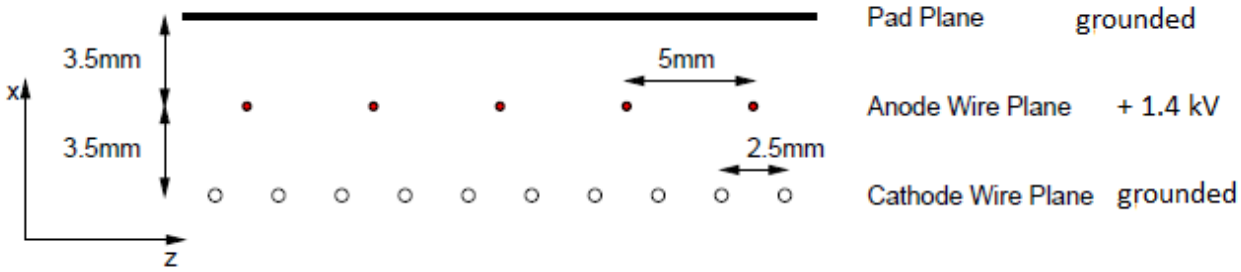

Figure 18: Geometry of the ALICE TRD multiwire chamber [ALI01](modified).

gas ions and signal shaping in the electronics (PASA see 3.3.4).
Through the different signal shapes with and without the transition radiation the TRD is able to distinguish between electrons and other charged particles. The pulse height of the signal is proportional to the strength of the ionization [ALI01][ALI08].

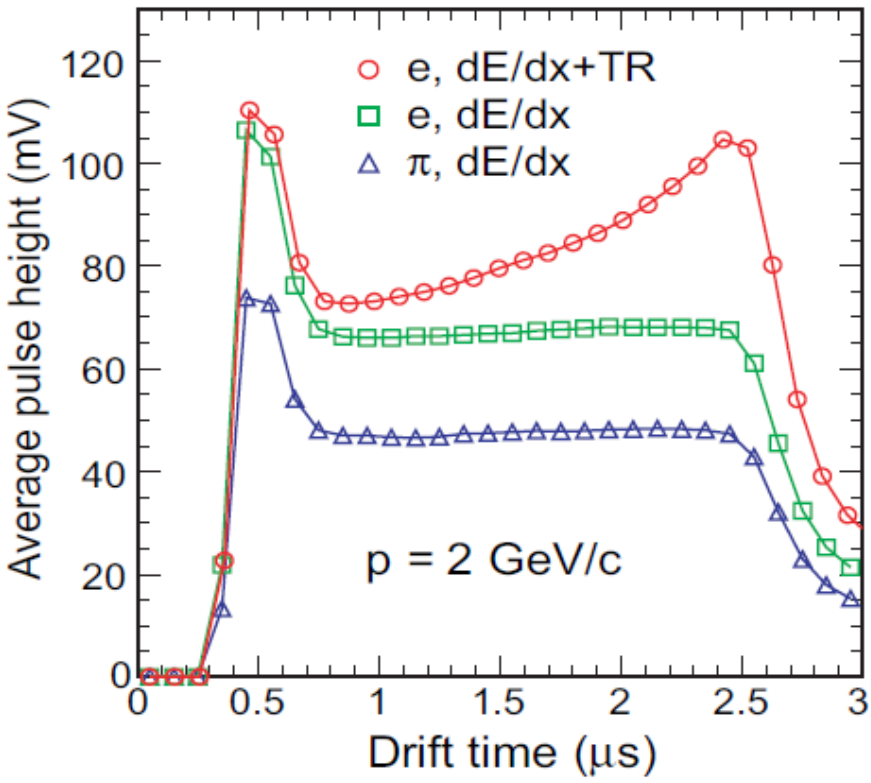

Figure 19: Different signals in ALICE TRD. Red circles show the electron signal with transition radiation, the green boxes the electron signal without transition radiation. The blue triangles show the signal from a pion for comparision [ALI08].

3.3.4 Front end electronics

The front end electronics (FEE) is composed of readout boards (ROBs), optical readout interface (ORI) and detector control system (DCS) boards. They all have different functions for detector control and data readout.

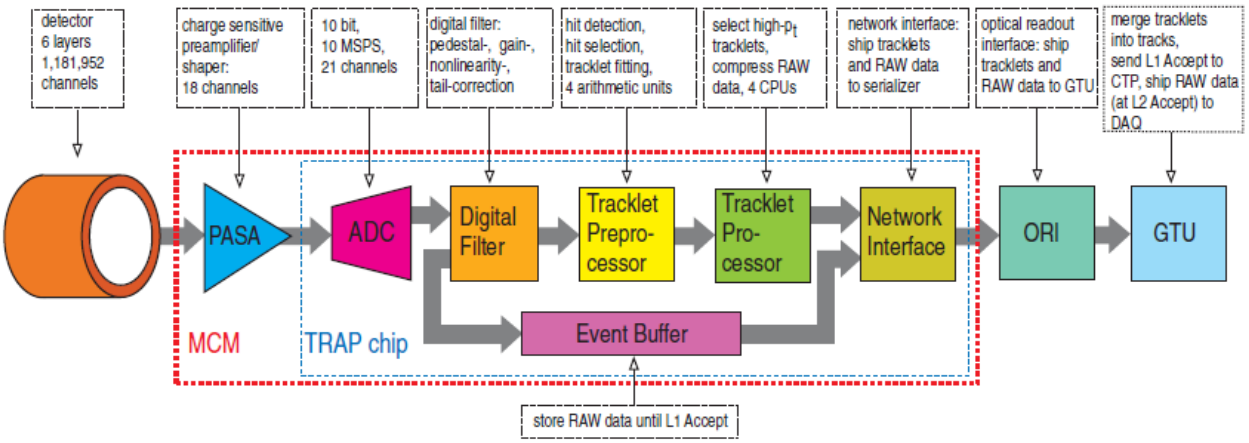

Figure 20: Schematic illustration of measurement and data processing of one TRD channel. For the definition of the trigger level L1 accept see Chapter 3.4.3 [An+11].

Figure 20 shows the processing of data in the FEE for one single channel. To reduce power consumption, the electronics is only activated after a signal from a pretrigger - the so-called wakeup - (see 3.4.3) is received.
The TRD has 1,124,928 [17] channels in total. This number of channels corresponds to a number of approx. 22 mio. pixel in sense of data, because in each channel 20 discrete time bins are being measured [And13].

Figure 21 shows a MCM (Multichip Module[18]) on the right side, which operates 18 channels. The left side of Figure 21 shows a ROB (Read Out Board) on which the MCMs are integrated into the detector. A Multichip Module consists of two parts, the PASA and the TRAP (TRAcklet Processor) chip. The PASA (Preamplifier and Shaper) is used for the first processing of the signal from the readout pads. As its name implies, the signal is amplified and shaped by this component.
The TRAP chip is more complex than the PASA, as one can see in Figure 20. The first part consists of a 10 Mhz analog-digital converter. It converts the preprocessed signal from the PASA and prepares it for digital filtering (orange part in figure 21) in the next step. After filtering, data is processed to the event buffer (lilac), where it is stored until further trigger decisions on the one hand and on the other hand, the filtered signal is processed by a tracklet preprocessor (yellow) and a tracklet processor (green). Tracklets are short track fragments, calculated from information of only one layer. The particle's momentum is calculated based on the tracklet's angle in reference to the detector plane. When the tracklets are merged into a track, the momentum can be used for trigger decision in combination with the PID (Particle

[17] For a configuration with 15 full supermodules and 3 supermoduls without stack 2. The configuration of 14 full and 4 supermodules without stack 2 result in 1,114,560 (Calculation based on [Ali01]).
[18] Capitalization indicates the letters used for abbreviation.

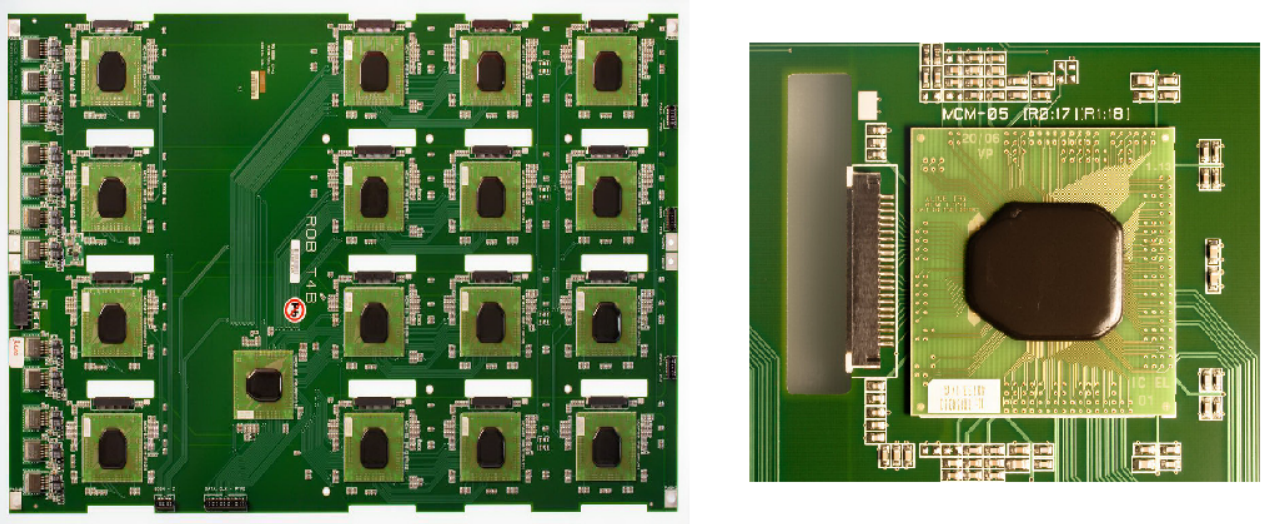

Figure 21: Left side: a ROB with 16 MCMs and one so-called boardmerger chip, which has special functions for data readout and communication between the MCMs.
Right side: a single MCM with a connector for the 18 readout channels [UHe13].

Identification) value.
The event buffer and the tracklet preprocessor run with the same speed, whereas the tracklet processor and the network interface (olive) use a faster speed due to more complex calculations in the tracklet processor and due to raw data throughput in the network interface.

Data from each half-chamber of the TRD is gathered from several MCMs at the optical readout interface (ORI). An extra electronic modul (turquoise/light green in figure 20) is dedicated to the purpose of sending data over a glass fiber to the Global Tracking Unit (GTU, cyan).
In the GTU a matching algorithm of the several tracklets to tracks and further filtering and triggering is being executed. A schematic view of the tracking algorithms of the GTU is given in figure 22.

DCS boards (detector control system) control several parts of the TRD detector. All configuration and monitoring of the FEE is done with the DCS board. For example the calculation parameters for tracklet building are being set on the MCMs through the board. It is a ARM[19] based computer, running a small linux operating system. It has various in- and outputs, e.g. analog inputs for monitoring the low voltage supply and a multi-purpose ethernet interface. [ALI01] [ALI08]

[19] A RISC based CPU from ARM Limited (http://www.arm.com/).

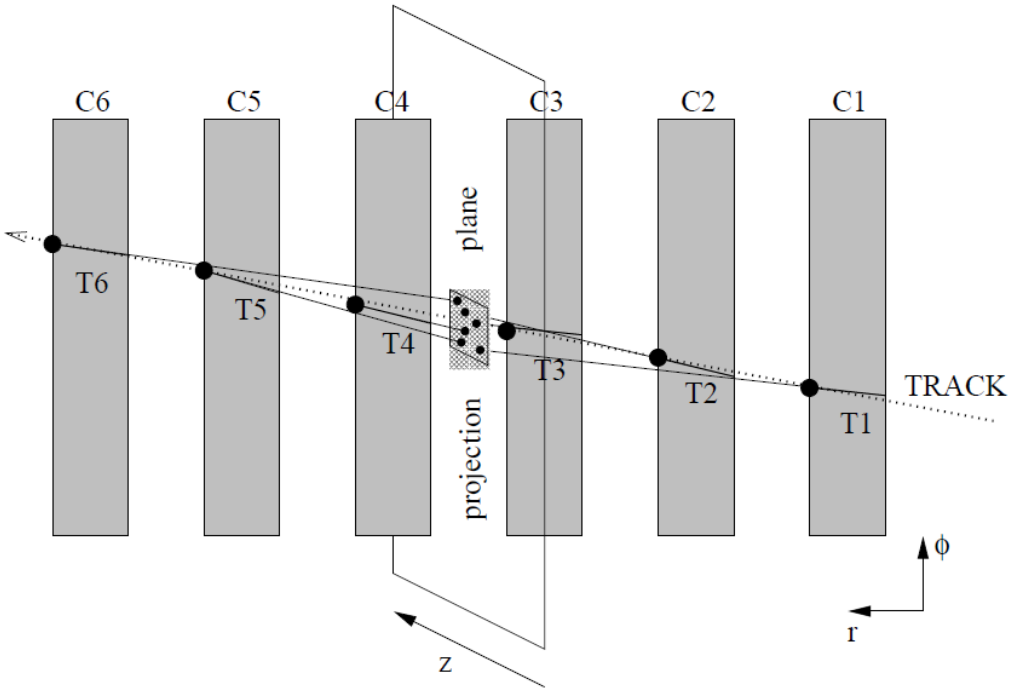

Figure 22: Track-matching algorithm of GTU [ALI01]

3.4 Trigger

Due to the high luminosity[20] of the LHC, there are more collisions than the data acquisition and storage systems could manage either in capacity or of data flow. For example: the DAQ (data acquisition) of ALICE has to manage a flow of 1.25 GB/s ([ALI08]), which will be easily exceeded in the future. Furthermore a rate of 1.2 PB/year of new mass storage is required.[21]
The selectivity of a trigger is defined as following:

$$\text{selectivity of trigger} = \frac{\text{trigger rate}}{\text{event rate}} = \frac{10^{-2}\,\text{Hz}}{10^{9}\,\text{Hz}} = 10^{-11}$$

The values are the expected values for the Higgs search at CERN [VLi04]. Concerning the two points of limitation in data flow and the low number of the relevant physical events, a selection mechanism: the trigger is needed.

In ALICE, the trigger for event selection based on centrality class of the event (central or peripheral collions between the hadrons) runs at a frequency of about 40 Hz. The muon arm can run with a trigger rate of 1 KHz.
To take account of all requested trigger classes for the different physical processes, a single trigger class can be downscaled to record only every nth event. In summary, it can be stated that an efficient trigger helps to reduce the data rate and allows to

[20] Luminosity L is a relativistic invariant factor between cross section and interactions per second: $\frac{dR}{dt} = L \times \sigma$
[21] [KAa08] table 6.5

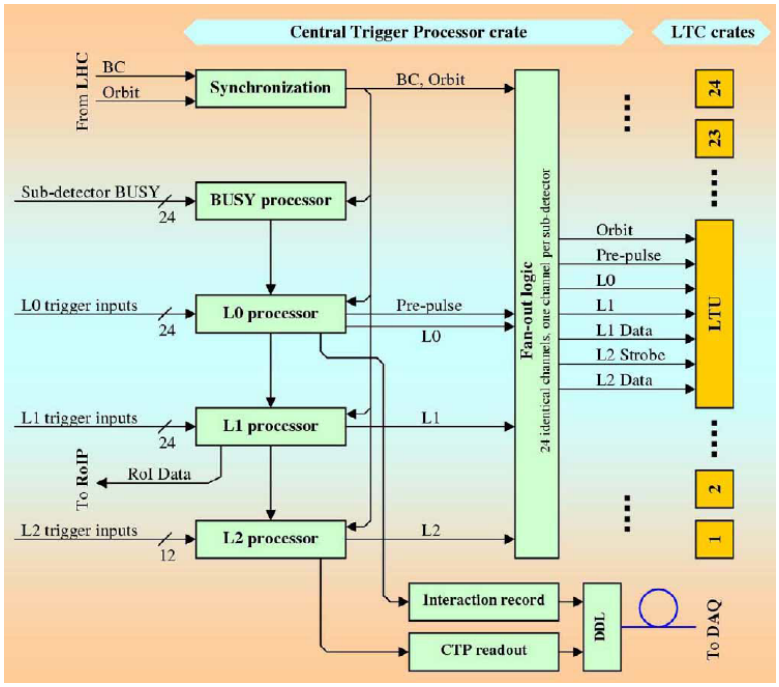

Figure 23: Trigger implementation in the Central Trigger Processor [Ev+05].

record the needed data only.
It is necessary that no fragments of important data is lost. This has to be implemented in the design of the trigger. To take care of these challenges in physics there are different methods of triggering in use.
There are two main types, integrated trigger on the one side and high-level trigger on the other. For very large amounts of data and complex detector systems like ALICE at LHC, several triggers of different types can be combined. These trigger mechanisms can be very complex. Figure 23 shows the implementation of the three different trigger levels at the ALICE experiment.

One must also consider that most triggers work hierarchically, which has the consequence that rejected events at low trigger levels are not available for higher trigger levels. But this enhances the available processing time per event at higher trigger levels.
The differences between integrated and high level trigger are presented in the next two chapters.

3.4.1 Integrated triggers

This trigger type uses mainly specialized FPGAs (field-programmable gate array) or other microelectronics. They have the advantage to have short latencies and are also called hardware or low level trigger. Because of the short latencies they can step in at the level of signal processing or readout. They can process a high rate of events, because of the short time needed to process a single event. A disadvantage is the limitation in the complexity of algorithms and calculations.

3.4.2 High level triggers

High level triggers are typically large High Performance Computer (HPC) clusters, which have larger latencies but are capable of managing complex calculations and filtering. In a high-level trigger full events are reconstructed. With the use of commodity hardware it is possible to construct cheap but flexible trigger systems [VLi04]. An example is the HLT of the ALICE experiment (3.4.3).

3.4.3 Trigger environment and data processing of the TRD

In ALICE there are five different levels of triggers defined: pretrigger, level-0 (L0) , level-1 (L1), level-2 (L2) and the HLT. The CTP (Central Trigger Processor) allows to collect 24 different level-0, 24 level-1 and 12 level-2 trigger inputs from the various ALICE detectors. The different levels correspond to different time windows, which are needed for the readout of the detector electronics. They fulfil the different requirements of the detector properties; the timing of ALICE TRD is presented in figure 24 [ALI08] [CAL04].
The CTP also generates the L0, L1 and L2 signal for further readout and manages signals from the Data Acquisation (DAQ) chain or the Past-Future Protection [MBo08]. The Past-Future Protection avoids event mixing, e.g. when the pauses between collisions are shorter than the drift time of detectors, which will lead to false signals. All these functions of the CTP are realised in hardware and can be customized to fit the several different trigger requirements. The concrete implementation and specification is summarized in the so-called trigger classes.
The TRD needs an additional wake-up signal, the so-called pretrigger[22], generated by T0, V0 and TOF. It has the function to activate the TRD electronics from standby. Because of its high power consumption the electronics can not be continuously active. When a pretrigger is sent, the TRD front end electronic is activated for further trigger decisions and data readout. After the electronics have been activated and a level-0 has been sent, the readout is started (see figure 24). First the readout

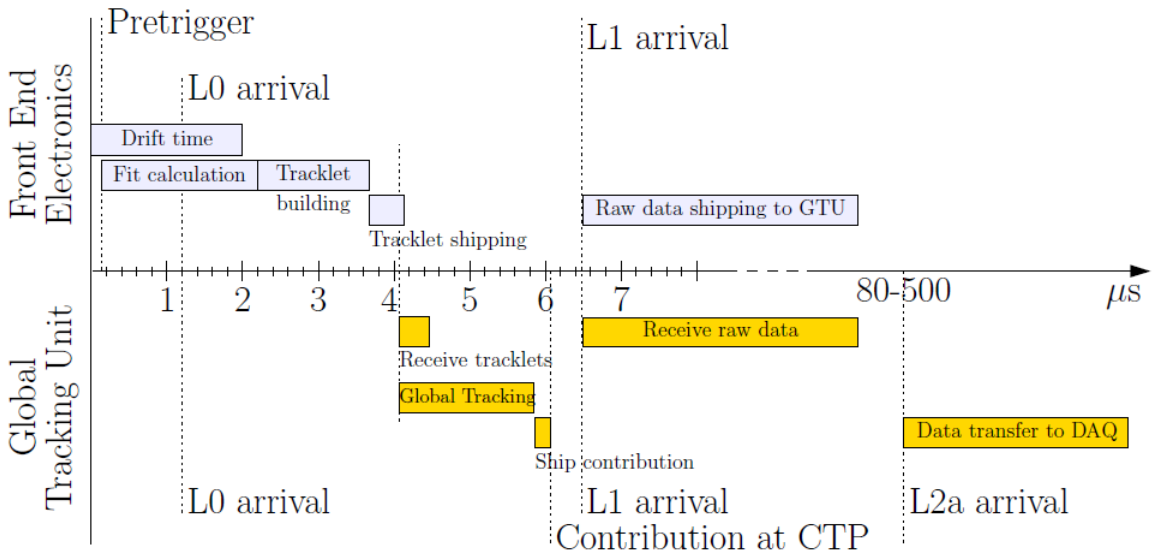

Figure 24: Timings in ALICE TRD Frond End Electronic and Global Tracking Unit [jkl11].

sends tracklets (which are generated in the MCMs of the front end electronic) over the optical links to the GTU (Global Tracking Unit).

[22]The trigger system of the TRD will be updated, the current status until sommer 2013 is decripted here. For information about the new Level Minus 1 Trigger LM1, see:
https://indico.cern.ch/getFile.py/access?contribId=2&resId=1&materialId=slides&confId=263376

The generation of the tracklets in the MCMs takes less than 4 µs. At the arrival of level-1 trigger the full raw data it sent from the MCMs to the GTU.

At the end of one trigger cycle, the GTU sends raw data to the DAQ system (see 3.4.5) when level-2 is accepted. Fast detectors like SPD, EMCAL and PHOS contribute to the level-0 trigger. Slower detectors like EMCAL (has also fast triggers) and ZDC (Zero Degree Calorimeter) contribute to the level-1 trigger. After the readout of TPC, the level-2 trigger, the event is accepted and recorded or declined. After that, data is also transmitted to the HLT (High Level Trigger) which can take further studies on a reconstructed event. The HLT is a multipurpose off-the-shelf computer cluster with the following functions: trigger decisions, selection of partial events with useful information and the compression of data without or with loss of information. The HLT runs currently only lossless data compression and it takes no trigger decisions [ALI08].

The TRD features four different tracklet/track-based trigger types:

1. high transverse[23] momentum (p_T) jet
2. single high p_T particle
3. single high p_T electron
4. di-electron: calculated invariant mass[24] from e^- and e^+

[23]Transverse means: all components of the vector perpendicular to the beam axis.
[24]for invariant mass see 6.1.2

3.4.4 Design of an electron trigger with the TRD

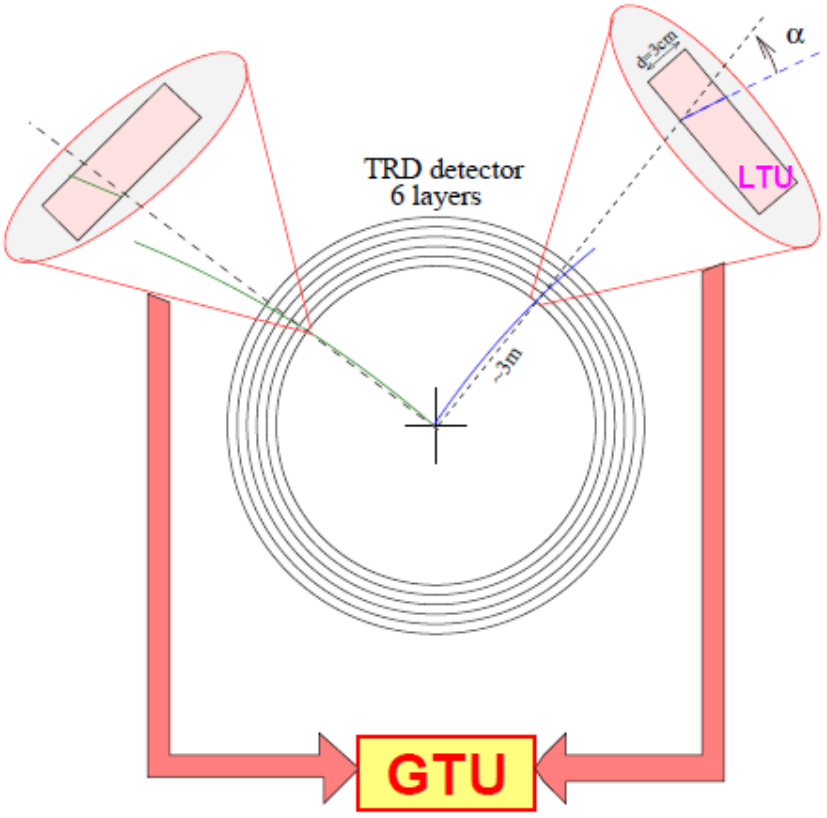

Figure 25: Di-electron trigger in an idealized ALICE TRD [ALI01].

3.4.4.1 Conceptual Design

A di-electron trigger with the TRD can be implemented with the following steps [ALI01]:

1. The TRD FEE calculates local track segments in each detector chamber.
2. Cuts on the tracklets concerning p_t can be applied.
3. Calculation of the PID takes place in the front end electronics based on lookup tables.
4. Data is transfered to the GTU (filtered tracklets only).
5. Trigger decision on the base of number of tracklets and p_t is executed.
6. PID is calculated in GTU on base of the PID done in the FED.
7. Number of positive and negative track candidates is evaluated.
8. Two-particle relations as invariant mass can be calculated.
9. Trigger is sent to the Central Trigger Processor.

This chapter will give an overview which parameters and cuts can be modified in each step. Therefore they have to be an object of check and verification.

3.4.4.2 Useful parameters for improving trigger performance

The first three steps are configured in the FED and can therefore be changed with new software settings. The changes have to take into account that the detector performance apart from this special trigger is not affected.

The data transfer to the GTU is relevant as it limits the rate of transmitted data and will be an issue when the interaction rate of the LHC is improved after the long shutdown in 2016 (see [LoI12]).

The trigger decision on cuts like number of tracklets, PID, momentum, etc. is the main point to be analyzed here. It can be tested from the simulation's point of view and can then implemented in the configuration of the GTU. Points 5 and 6 will be investigated concerning the Υ-meson trigger in this thesis.
This also applies to the following points 7 and 8. The transfer to the CTP should not affect the trigger performance unless not all trigger requests will be accepted. For fair use of the available bandwidth some trigger classes can be downscaled[25] to avoid too much deadtime[26] for the other classes.

3.4.4.3 Divergences in the trigger signal

There are four main sources for errors and signal contamination in the TRD trigger implementation ([ALI01]).

1. Wrong PID, which leads to an electron track, but is actually caused by a pion.
2. Fake tracks and tracklets e.g. from two particle tracks that are relatively close to each other.
3. Tracks and tracklets caused by so-called late conversions, which occur after the TPC, so that it can not be detected from the signal in the TPC.
4. Detector effects like dead regions, etc.
5. Contamination from background.

3.4.4.4 Attempts of solving the divergences

Points 1, 2 and 4 seem to be reducible through different cuts and software optimisation in the FED and GTU. Detection of late conversions will require a new tracking filter [ALI01] .

[25] Only every nth request is accepted.
[26] Deadtime arises from the time for detector readout.

3.4.5 Data acquisition and storage in the ALICE experiment

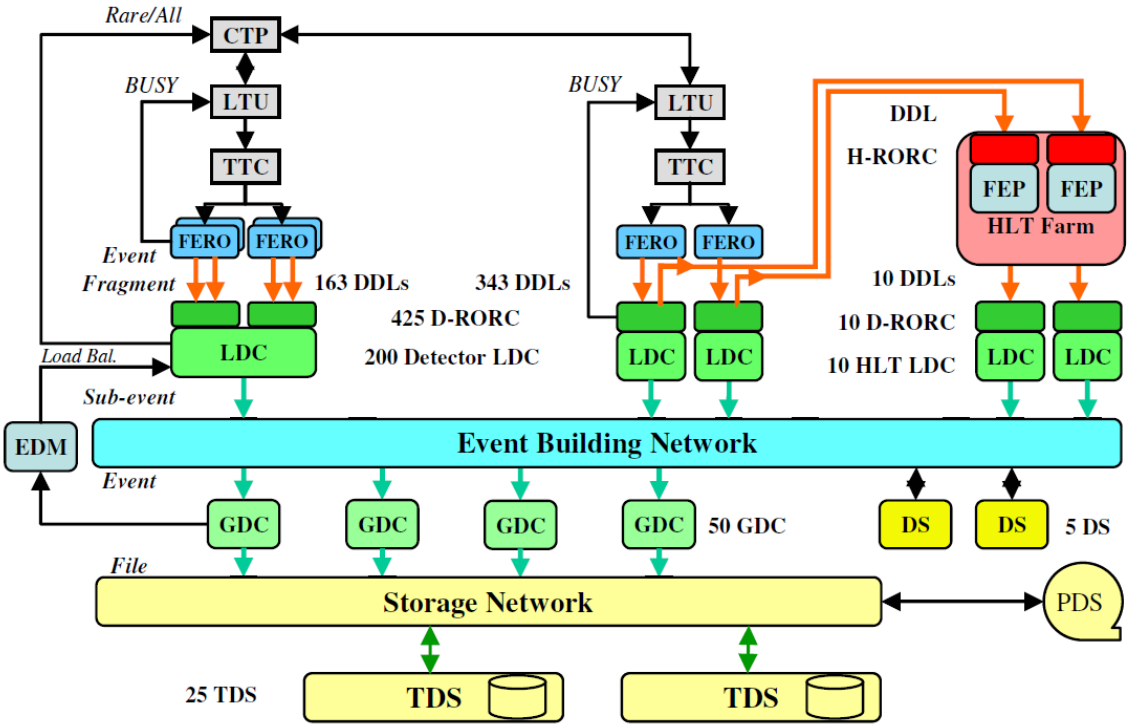

Figure 26: Working principle of the ALICE DAQ System [DAQ06].

After a positive decision from the CTP (Central Trigger Processor), the Local Trigger Units (LTUs) gives a signal to the Timing, Trigger and Control System (TTC), which activates the Front End Read-Outs (FEROs) of the different detectors.

The FEROs send their event fragments over the DDL (Detector Data Link) to dedicated PCs, the Local Data Concentrators (LDCs). All detectors use the same DDL protocol, which reduces the complexity of the ALICE DAQ system.
The High Level Trigger (HLT) obtains its input from a copy of LDC's data and uses the DDL system, too. After processing in the HLT, events are sent to the LDCs.
All LDCs from the different detectors and the HLT ship the processed subevents to the Global Data Concentrators (GDCs). These GDCs generate a complete event from the subevents out of LDCs and transfer it to the Storage Network, where it can be stored on harddisks or tape for analysis. The EDM (Event-Destination Manager) controls the distribution of load on the GDCs.

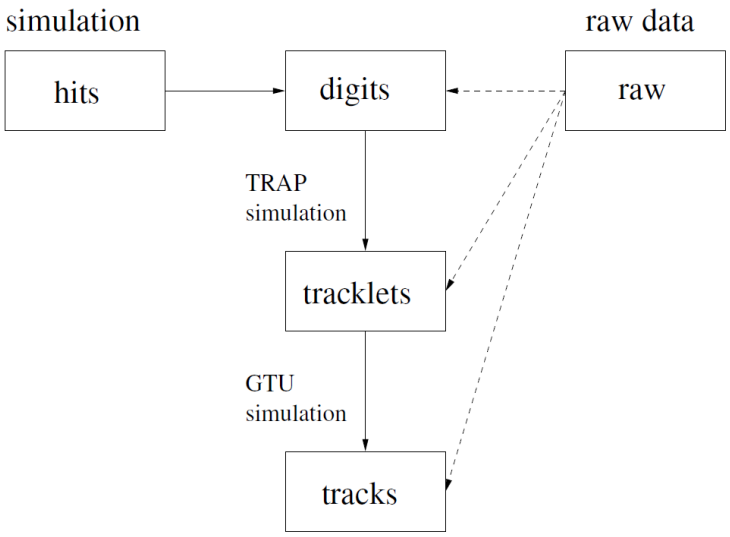

Figure 27: Structure of raw and Monte Carlo data [jkl11].

4 Analysis

For all analyses in this diploma thesis the AliRoot framework has been used.[27] It has the ability to handle simulation, data reconstruction and analysis for the ALICE experiment. Written in the programming language C++, it makes extensive use of object-oriented programming techniques.
Figure 27 shows the steps of online emulation on the TRD through the AliRoot framework. There are two options to start with; the base of all analysis can either be simulation- or raw-data from measured collisions.
Monte Carlo data includes full information about the particles from event generators. The raw data consists of the measured values in the different detectors like the ADC values per channel in the TRD. These are the digits which can be extracted, but raw data includes calculated tracklets and tracks from the dedicated detector electronics. On basis of the digits, the tracklets are calculated via TRAP (see chapter 3.3.4) simulation software. Then on base of the tracklets, the tracks are created via GTU simulation software.

[27] http://aliweb.cern.ch/Offline/

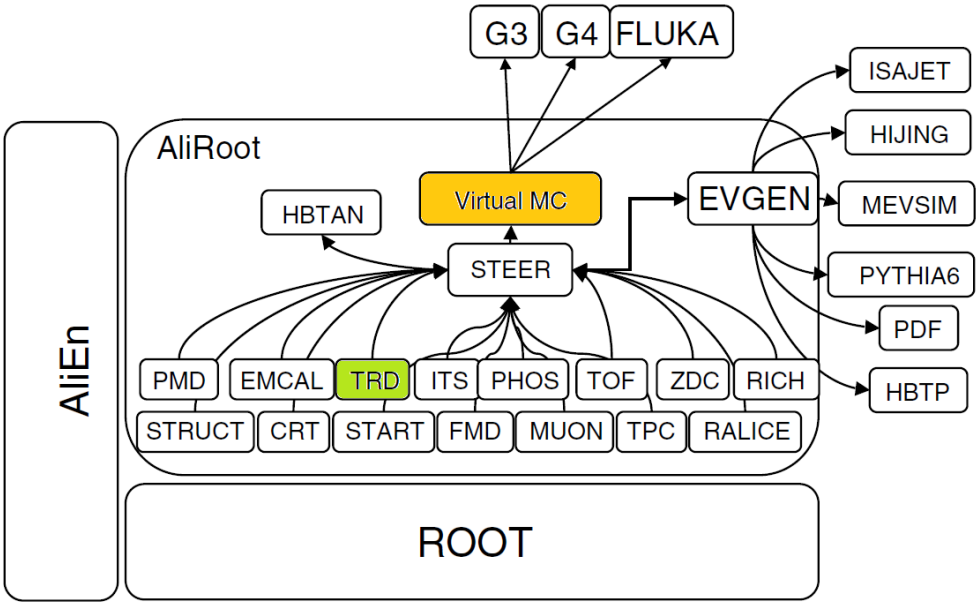

Figure 28: Structure of the AliRoot framework [ALI04]

4.1 Simulation with the AliRoot framework

This chapter will give a short overview of the internal implementation of simulations within AliRoot.
The development of AliRoot started in 1998 to cope the data challenges of the Large Hadron Collider (LHC), that was being planned at that time. It should use object-oriented paradigms instead of the old procedural design of FORTRAN based frameworks. [ALI04]
The ROOT framework is the base of data processing for the AliRoot framework which copes all specific needs of the ALICE experiment. Figure 28 shows the internal structure of AliRoot with the main moduls AliEn for the support of distributed computing; ROOT as base for general data i/o , handling of histogram classes for visualisation.
It further includes the AliRoot module - containing the support for detector und experiment relevant information - and interfaces to the event generators (on the right side) and to the detector simulation tools (on top corner).
The STEER module is the central part of AliRoot. For detailed information on AliRoot see [ALI07]. For details on the different functions, the source files of aliroot are the best origin[28].

The first step in simulating hadron collisions is the Monte Carlo event generator. The Monte Carlo Method[29] was proposed by Stanislaw M. Ulam and Nicholas Metropolis in 1949 [MUl49].
Monte Carlo algorithms use random samples to calculate numerical problems. Prominent simulation modules are PYTHIA and the build-in classes of AliRoot, AliGen-

[28]For work simplification it is recommend to generate a web based documentation with tools like doxygen (http://www.stack.nl/~dimitri/doxygen/ - 11.04.2014).
[29]Named after the Monte Carlo Casino.

Param and AliGenBox. An other event generator for the simulation of heavy-ion collisions is HIJING.
Simulations can show some issues. It is not guaranteed that the simulation shows the same results as the measurements. Different generators show furthermore different results. But with constrained parameters and settings analogous to the theoretical theories, simulation can be fitted to experimental data. But on the other hand it is easy to use setups of generators to generate samples with a higher quantity of physical signals. It is also possible to tune event generators on base of real data from the experiment to have a better mapping [ALI04] [PZS11].

The next important step is the propagation of generated particles and the calculation of the detector response on this particles. This is done with the GEANT3 framework. Newer frameworks available in AliRoot are GEANT4 and FLUKA. The first task in particle tracking is to calculate the track of the particle and the crossing points with the various detectors as defined in the geometry module of AliRoot. After searching for the interaction points between particle and detector, the signal from the detector for each particle is calculated.
Subsequently on calculating the detector signals, the data is formatted and converted to the format used in the experiment's data acquisition chain. To speed up the simulation it is also possible to use pre-calculated parametrizations for signal generation in the detectors [ALI04].
Information on the structural data of the ALICE experiment and its detectors is implemented in AliRoot.

Reconstruction of the generated simulation data is done in the same way as the reconstruction of measured data. The hits in the various detectors are combined to tracks and are saved in ESD (Event Summary Data) and/or AOD (Analysis Object Data) files [ALI07].

4.2 Analysis with the AliRoot framework

Analysis on physical issues can either be done locally, on the Alice Grid or on other large computing clusters. The Grid[30] is a world-wide net of computing clusters which can also handle the large amount of data needed for analyses.
To run an analysis, two elements are required: first the steering macro and second the analysis task macro with a header file.
The steering macro sets the AliRoot/Root environment on the Grid and the required libraries. After initialising the AliAnalysisManager, which coordinates the analysis, access to events is initialized. Events can be accessed as ESD, AOD or Monte Carlo data. The classes are AliESDInputHandler, ALiAODInputHandler for data and AliMCEventHandler for Monte Carlo simulations.
The following list shows the points which are moreover necessary for running a analysis.

```
// Create task
gRoot->Load("AliMCComparisonTrack.cxx++g");
gRoot->Load("AliTRDComparisonTask.cxx++g");
AliAnalysisTask *task = new AliTRDComparisonTask("
    AliTRDComparisonTask");

// Add task
mgr->AddTask(task);

// Create containers for input/output
AliAnalysisDataContainer* cinput = mgr->
    GetCommonInputContainer();
AliAnalysisDataContainer* coutput =
mgr->CreateContainer("coutput", TList::Class(),
AliAnalysisManager::kOutputContainer, "
    AliTRDComparisonHist.root");

        // Connect input/output
mgr->ConnectInput(task, 0, cinput);
mgr->ConnectOutput(task, 1, coutput);
```

The macros are loaded first and the task is declared and added to the analysis manager. Several different tasks can be combined. In the next step assignments of input and output slots are made. The input container is automatically connected to the matching data format. Histograms and other data types can be written in the output container.

The analysis task macro consists of three parts. In the beginning *UserCreateOutputObjects* is being executed. All output histograms, etc. are declared within this function. *UserExec* is carried out for each event and contains the main analysis functions. All variables of tracks and others are accessed here. In the *Terminate*

[30] http://alien.cern.ch - 30.04.2013

function output data is written to file. The event based running of analysis allows simple parallelization on large datasets.

4.3 Trigger terms of reference

Some definitions for measureable parameters of a trigger are defined as following. All definitions are based on particle numbers as the corresponding variables. They can also be calculated on a base of events or tracks.

1. **Trigger efficiency** is defined as (figure 29 shows an example):

$$\text{trigger efficiency} = \frac{\text{particles found by trigger}}{\text{particles in reference sample}}$$

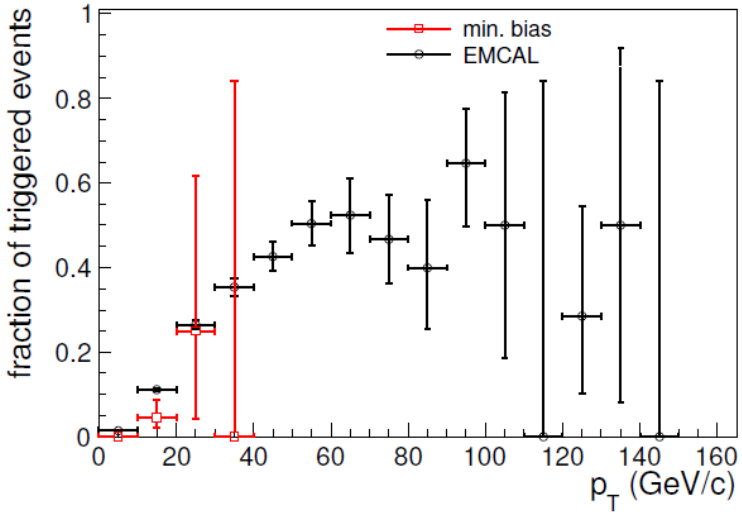

Figure 29: Example for trigger efficiency: here the efficiency for the TRD jet trigger is given on base on minimum bias (see footnote 39) events (red) and on an EMCAL triggered sample (black). The minimum bias sample is limited in statistics at higher p_T [jkl11].

It must be admitted that the trigger efficiency can depend on parameters like the transverse momentum (see figure 30). It shows an arbitrary jet spectrum and the trigger rate. Detector effects can avoid efficient tracking of particles at low p_T, which then cannot be triggered. The trigger efficiency presented in figure 30 is very low at low p_T and increases after passing a threshold in p_T at around 22 GeV/c.

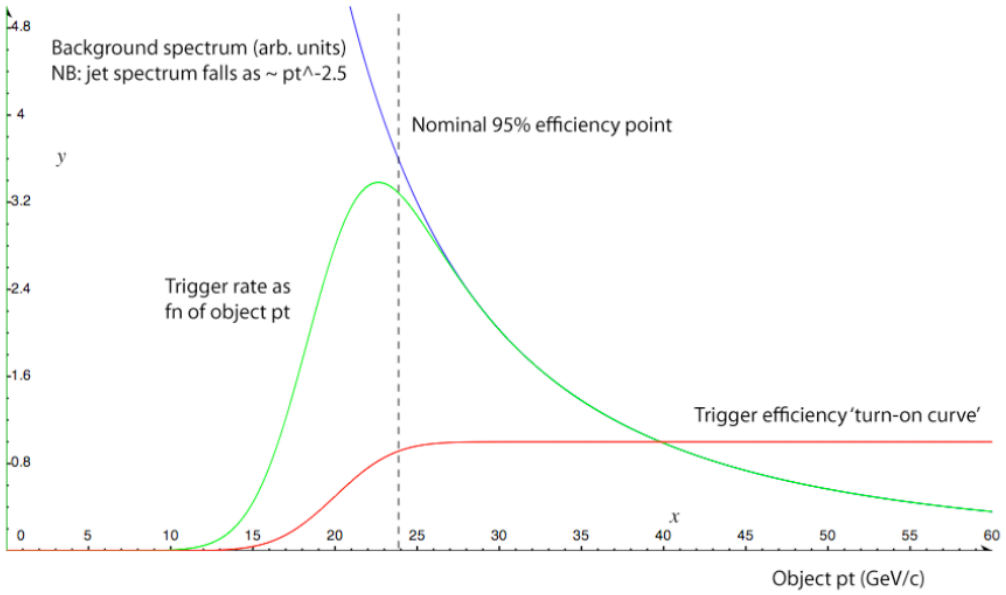

Figure 30: Example of trigger efficiency for a jet trigger, depending on p_T. [New13](NB: The slope of the jet spectrum is not correct for ALICE in the figure, current results show a power law dependence of p_T^{-5} [Ver12])

2. The **(geometrical) acceptance** of a detector can be evaluted as:

$$\text{detector acceptance} = \frac{\text{particles found by detector}}{\text{particles in reference sample}}$$

This geometrical acceptance is relevant for the TRD, because only 13 supermodules out of 18 are installed[31]. The geometrical acceptance must not cover the total space around the collision point to archive good results, because particles may occur preferentially in certain areas of the η / ϕ space (see chapter 6.1.6 for the coordinate system).

3. With the detector acceptance, the total **trigger acceptance** can be defined. It considers both the geometrical acceptance as also the intrinsic efficiency from the detection mechanismen.

$$\text{trigger acceptance} = \text{detector acceptance} \cdot \text{trigger efficiency}$$

4. **Rejection of particles on which are triggered** gives a number for falsely rejected events, which are verified from the simulation as triggerable. This means false negative decisions.

$$\text{trigger rejection (false negative)} = \frac{\text{number of falsely rejected particles}}{\text{particles in reference sample}}$$

[31] From 2012-01-25 on.

5. Another main parameter is the **selectivity of a trigger** which was given already in chapter 3.4:

$$\text{selectivity of trigger} = \frac{\text{trigger rate}}{\text{event rate}}$$

6. The **purity of a trigger** is defined as:

$$\text{purity of trigger} = \frac{\text{number of "useful" events}}{\text{number of triggered events}}$$

   The definition of "useful" must then be given explicitly.

7. An additional useful term in connection with the TRD is the **pion rejection factor**[gun03] defined as :

$$\text{pion rejection factor} = \frac{1}{P_{\pi \to e}}$$

   Whereas the probability for a misidentified pion $P_{\pi \to e}$ is:

$$P_{\pi \to e} = \frac{\text{number of pions with an electron probability in the range between x and 1}}{\text{number of pions}}$$

   As one can see in the previous equation the pion rejection can be only defined with a defined electron efficiency x. Usually the 90%-electron efficiency-threshold is used. The same definition can be used for the background rejection. It is clear that most definitions can only be derived from simulation or a reference sample. A reference sample can be obtained with an additional detector with well known properties.

4.4 Thresholds/cuts for analysis

For the selection of interesting parts of large data sets, filtering via thresholds on measurands is common use. These are the so called cuts which have already been mentioned earlier.
The complexity of cuts varies over a wide range: from a simple yes-no condition whether there is a detected signal up to cuts on invariant mass, which are calculated for one or more particles using energy and momentum.

Geometrical cuts can avoid effects from detector boundaries. A mentionable example is the limit of the TRD in the η-space. For the choice of feasible cut values, statistical considerations also have to be recognized. Too restrictive cuts reduce the amount of data points unnecessarily. On the level of Monte Carlo data, parameter of particles are exact. When cutting on measured parameters, uncertainties might influence the trigger threshold.
For the analysis on ESD tracks, a specific class - AliESDtrackCuts - steers the cuts. Some settings which were used:

```
trackcut1->SetEtaRange(-0.8,0.8);
trackcut1->SetPtRange(1.,1e30);

trackcut1->SetMaxDCAToVertexXY(0.05);
trackcut1->SetMaxDCAToVertexZ(0.5);

trackcut1->SetAcceptKinkDaughters(kFALSE);
trackcut1->SetRequireTPCRefit(kTRUE);

trackcut1->SetMinNClustersTPC(70);
trackcut1->SetMaxChi2PerClusterTPC(4);
```

SetEtaRange and SetPtRange accept only tracks within the given range, selection of momentum and pseudorapidity.
The next two functions ensure the quality of tracks based on the distance to the collision vertex in the XY plane and Z direction. DCA is an abbreviation for distance of closest approach. Large amounts of particles from interactions with dectector material and tracks from decays have a large DCA.

After this the track is checked for kinks; a kink occurs when the particle undergoes a collision or a decay. SetRequireTPCRefit also affects particle tracking. The tracking has three steps; in the third, the refit is used to calculate the particle-vertex, hereby the TPC information is used.

The next function - SetMinNClustersTPC - causes a selection on TPC clusters; more clusters are a stronger signal. Finally SetMinNClustersTPC divides the χ^2 deviation of the track - compared to the TPC signal (clusters) - by the number of clusters, so track and signal quality are combined here.

4.5 Upsilon-meson trigger

4.5.1 The Upsilon-meson

The upsilon-meson (Υ) is a particle made of one bottom quark and of one anti-bottom quark. Its mass amounts to 9460.30±0.26 MeV. Table 1 shows the three leptonic di-particle decays of Υ-mesons. Further it has 37 known hadronic decays [PDG06]. The trigger, which is presented here, should trigger when an Υ decays into two electrons. For further information about the Υ see chapter 2.4.2 about the di-lepton probes of the QGP.

mode	fraction of total known decays
$\tau^+\tau^-$	$(2.67^{+0.14}_{-0.16})\%$
e^+e^-	$(2.38 \pm 0.11)\%$
$\mu^+\mu^-$	$(2.48 \pm 0.05)\%$

Table 1: Different Υ decays [PDG06]

4.5.2 Expected signal from Upsilon

Figure 31 shows the signal from Υ-resonances in pp and Pb-Pb data from the CMS experiment. A similar result is expected for the ALICE experiment, but with lower statistics.
The comparison of figure 31 a) and b) shows the suppression of the three Υ-states in Pb-Pb. The Υ-1S state is suppressed due to the fact that it is a state after the decay from the excited states 2S and 3S [CMS11].

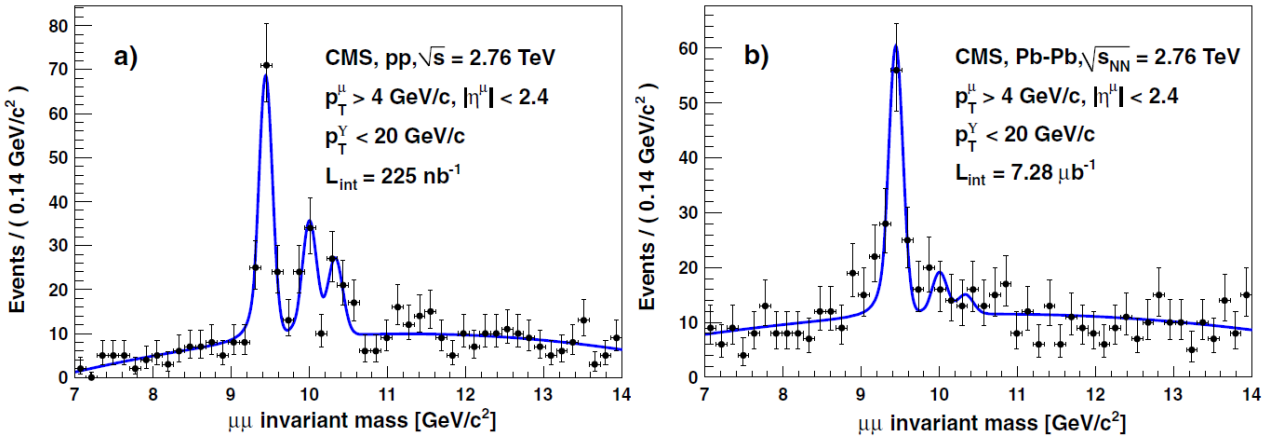

Figure 31: Invariant mass spectrum in pp and Pb-Pb data around the Υ-resonances [CMS11].

4.5.3 First analysis

For a first start the offline efficiency of Υ containing events is determined[32]. It has the function to show whether the simulation[33] shows the expected results and it is a base for further calculation.
Using simulations has the advantage to understand the detector and to avoid errors from effects like detector problems, background effects, etc., before analyzing real measured data.

4.5.3.1 Verification of the simulation parameters

AliRoot uses parametrizations from theory and older experiments in the class AliGenParam, so one has to note that all other parameters like cross-section etc. - if crucial - must be verified with extra investigation.
This chapter will give a short explanation of the different simulation parameters at first and then the invariant mass results from the Υ simulation.
The modified simulation parameters of the next chapters will be given more explicitly in each stage.
The settings for the particle generator in Config.C of AliRoot Simulation are:

```
AliGenParam *gener = new AliGenParam(1,AliGenMUONlib::
    kUpsilon, "Flat");
      gener->SetPhiRange(0,360);
      gener->SetYRange(-1.0,1.0);
      gener->SetPtRange(0,20);
      gener->SetOrigin(0,0,0);
      gener->SetForceDecay(kDiElectron);
```

The corresponding parametrizations of "AliGenMUONlib::kUpsilon" are shown in figure 32. There are approx. 40 parametrizations for each p_T and rapidity available. In the example the "Flat" distribution is selected. For some other selected parametrizations, see appendix 6.2.1. With the selection of kUpsilonP, Υ-2S-states and with kUpsilonPP 3S-states can be simulated. All three particles can be simulated with kUpsilonFamily as a mixed sample.

Without specified parametrization, AliRoot uses YUpsilon and PtUpsilon by default. The flat distributions have the advantage to deliver higher statistics at higher p_T values, whereas the standard distribution nearly does not have events above 10 GeV/c.
The ϕ and y range are set to the given parameter. SetPtRange sets the p_T range of the generated Υ-particles, not of the decay particles. SetOrigin sets the origin of the particles to the collision vertex (0,0,0). The unit of the p_T-range is given in GeV/c and the vertex parameter are in cm [34]. In the real experiment the vertex fluctuates a bit around this point. The parameter SetForceDecay forces the event generator

[32]For the local simulations there were used: Triad 1: AliRoot trunk-2012-02-21, build against ROOT v5-30-05 and GEANT v1-12(specially marked) Triad 2: Root v5-34-08 Geant v1-15a and Aliroot v5-04-Rev-01

[33]The recommended AliRoot macros from the source macros/Config.C and test/gun/*(for rec.C and sim.C) of the appropriated AliRoot version are used.

[34]Further units are degrees for angles and GeV for momentum and energy values. These details are only valid for AliSimulation.

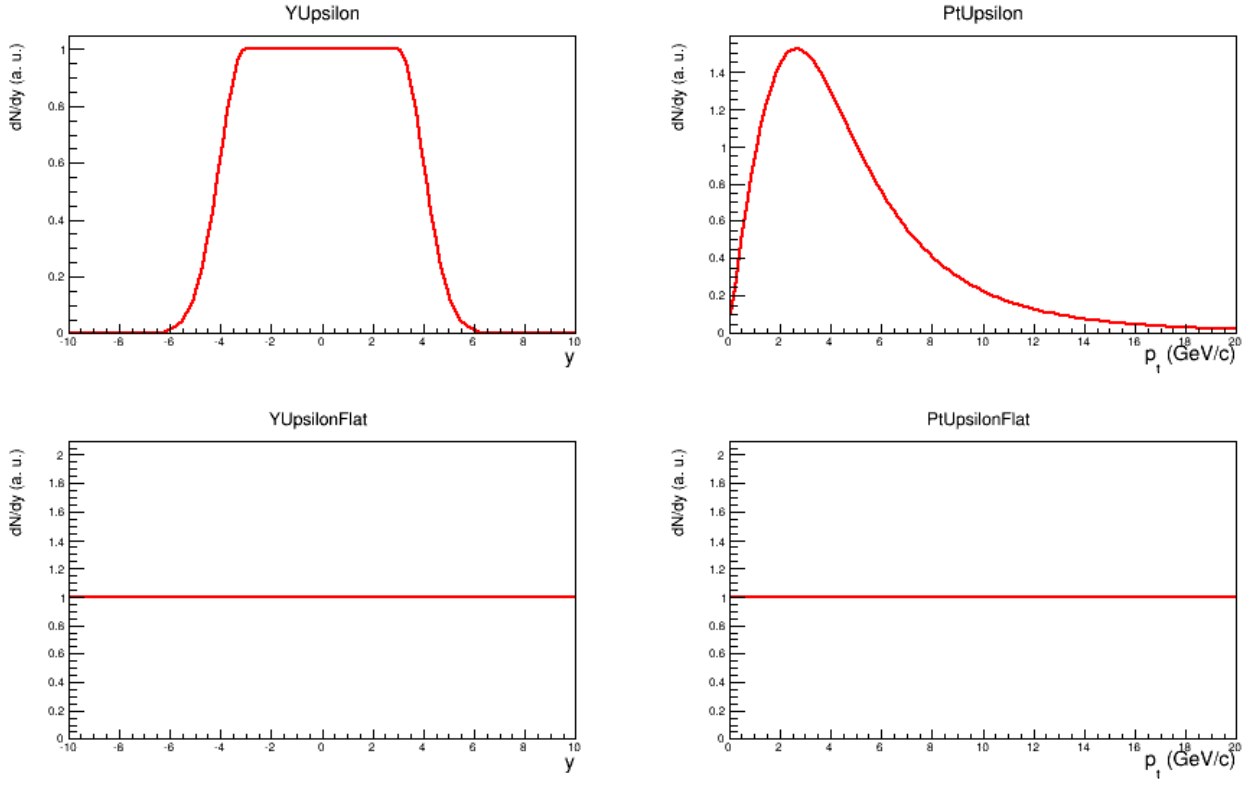

Figure 32: Parametrizations from the class AliGenMUONlib used by AliGenParam.

to let the Υ-particles decay to di-electron pairs. In nature, the dominating decay of Upsilon is another one (see chapter 4.5.1). The class ALiGenMC from which AliGenParam inherits, also supports cuts on the child particles formed through the decay (e.g. the functions: SetChildMomentumRange, SetChildPtRange ...).

Figure 33 shows the invariant mass plot of a simulation containing only one Υ per event. The invariant mass is calculated from Monte Carlo data, so no cuts are used. It becomes apparent that the simulation parameters are appropriate, the invariant mass of the Υ-meson is reproduced in the given error range.

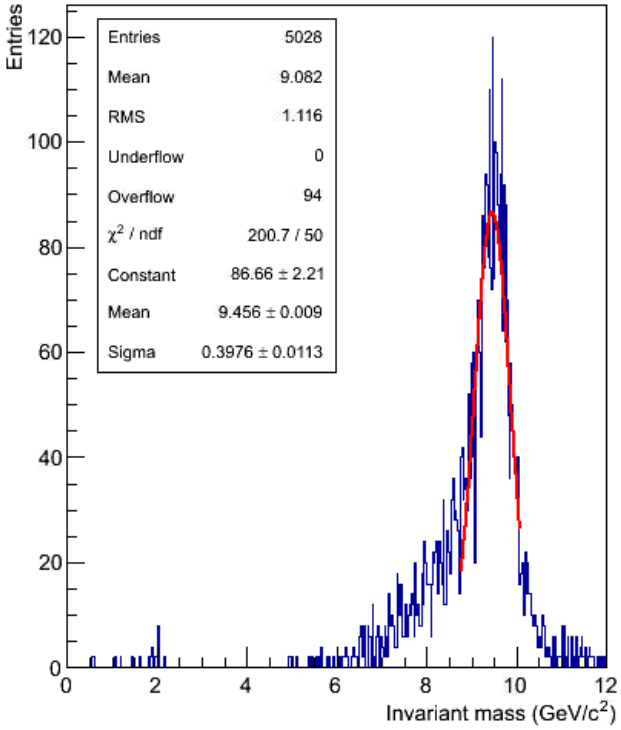

Figure 33: Simulation of approx. 10000 upsilon-particles in the ground state 1S. (MC = Monte Carlo data)

Table 2 shows the result of the invariant mass of the three Υ-states. The invariant mass plots for the higher states 2S und 3S can be found in figure 34 and 35.

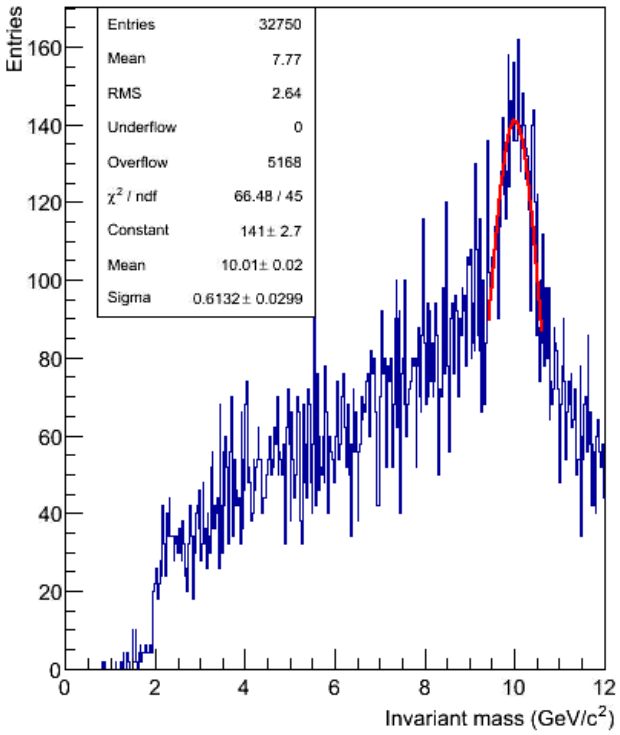

Figure 34: Simulation of approx. 10000 Υ-2S particles. (MC)

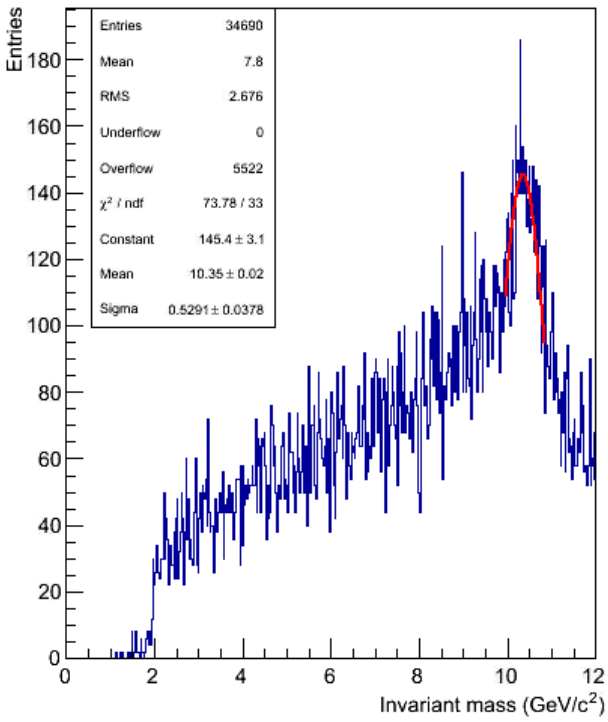

Figure 35: Simulation of approx. 10000 Υ-3S particles. (MC)

	Reference (MeV)	Value (MeV)
1S	9460.30±0.26	9456±9
2S	10023.26±0.31	10010±20
3S	10355.2±0.5	10350±20

Table 2: Masses of Υ-mesons in comparison to invariant mass from simulation [PDG12]

Unfortunately the invariant mass spectrum of a combined simulation with all three different Υ-1S, 2S and 3S can not resolve the single peaks. Background and non optimal mass/tracking resolution smears the three signals to one indistinguishable peak. The high background in the simulation of 2S and 3S has the reason in the higher number of simulated particles in one event (10 versus 1).

4.5.3.2 Variation of the eta parameter

The ALICE TRD covers the range in η (pseudorapidity) from -0.8 up to 0.8. Υ-particles are expected to be measured over the whole η-range, for example also at forward rapidity in the muon arm.

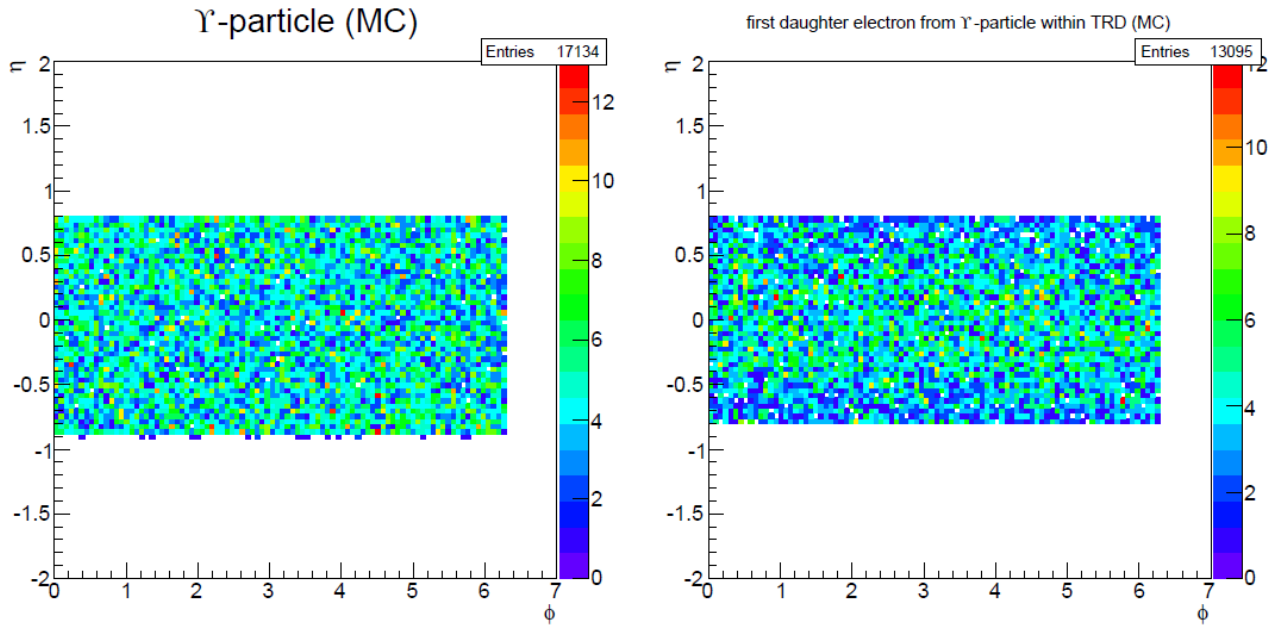

Figure 36: Simulation of 20000 Υ-particles with y=[-1.,1.] filtered to TRD solid angle of η=[-0.8,0.8]. (MC)

Figure 36 shows the distribution of the simulated Υ-particles and the resulting electron daughter particle. By comparison of the number of entries one can easily recognise, that $\approx 24\%$ of the Υ-particles within the η-range of the TRD cannot be measured. This is due to a shift in η of the decay products.

Via the functions SetChildYRange and SetChildThetaRange it is possible to constrain daughter particles in a measurable range within the TRD, see appendix 6.2.2 for result. It is important to note that the value SetChildCuts is being set, otherwise the settings are ignored by AliRoot.

4.5.3.3 Variation of the phi parameter

Figure 37 shows the number of tracks that cause a reference from the TRD. The plots show electron tracks from Υ-particles. The left plot shows the full TRD and the right plot the actual[35] existing configuration of 13 supermodules. The assumption is, that approx. 13/18 of total particles generated can be tracked with the current TRD. The factor of 13/18 needs to be considered due to the PHOS holes of TRD which are easily visible in fig. 37. A missing stack causes 1/5 less tracks. Further aspects like different chamber size will not be considered here. The expectation is:

$$\frac{12.8}{17.4} = 73,6\%$$

and the result (number of tracks) is:

$$\frac{13977}{18975} = 73,7\%$$

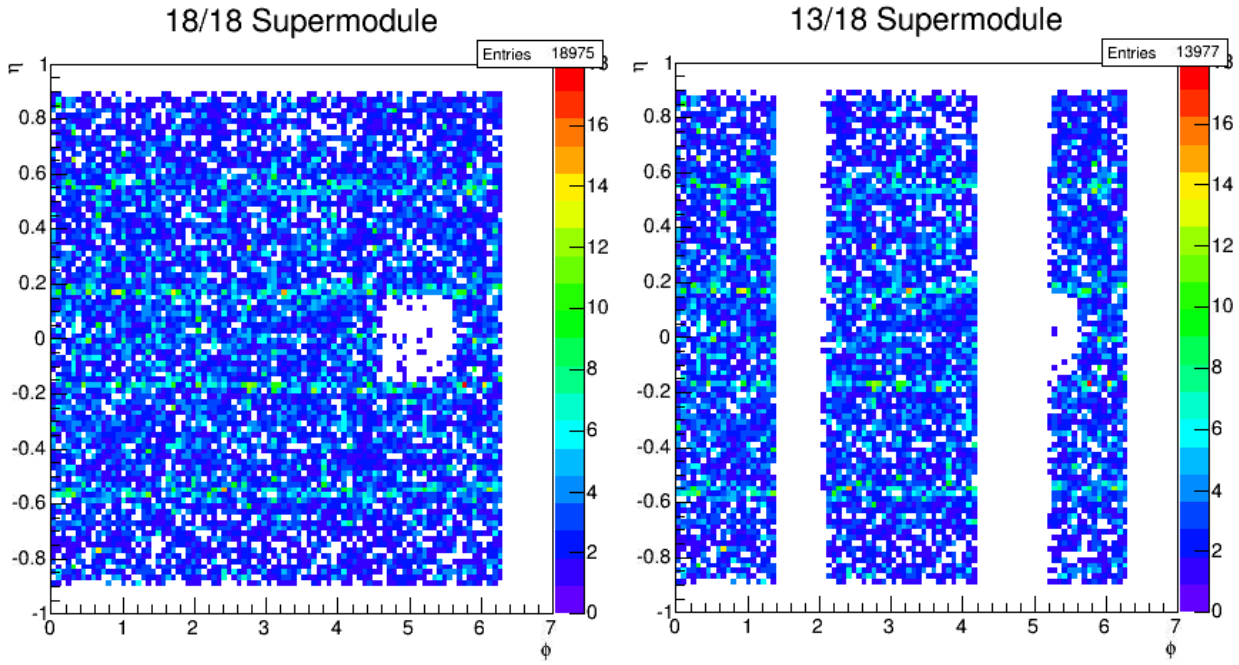

Figure 37: Electron tracks from upsilon with TRD reference.
Cuts (exclusive): $p_t < 0.5\,\mathrm{GeV/c},\ \eta > 0.9$ (MC)

It is verified on the simulation side that the factor of approx. 13/18 can be used as long as no combinatorical effects between the two leptons of one decay are taken into account. Also the dead zones between the different stacks can be seen as horizontal lines with less statictics in figure 36.

[35] December 2013

4.5.3.4 Influence of cuts on leptons from the upsilon-decay

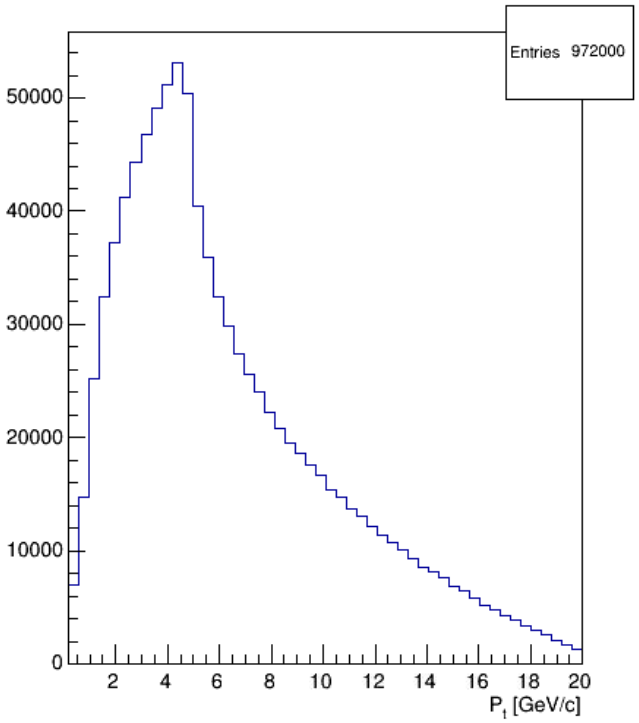

Figure 38: Electron and positron tracks from Υ-meson (MC)

Figure 38 shows the distribution of transverse momentum of leptons from Υ-decay. A peak between 2 GeV/c and 7 GeV/c contains a large part of all tracks.
A cut around these values in data shall deliver acceptable results with the rejection of low p_t background.

4.5.3.5 Influence of tracklet numbers

As described in the theory section, in each layer of the TRD short track fragments - the tracklets - are being calculated. Figure 39 shows how much tracklets the ESD-tracks have attached. Tracks with zero tracklets might be out of the TRD acceptance but are created from other detectors. A large amount of tracks have six tracklets. There are also some with four and five tracklets, so that enough data is available for GTU tracks. Then in the plot on the right side the numbers for GTU-tracks can be found. The GTU needs at least four tracklets to calculate a track, so only tracks with four, five and six tracklets are being taken into account here.

Cutting on six tracklets per track for signal filtering in data might be an idea to increase quality of the track sample. But an AliESDtrack has not nescessarily the tracklets attached. There are some tracks with zero tracklets, see bottom of figure 39. These tracks with zero, one, two and three tracklets only have a matching AliESDTrdTrack, which is not exspected on the number of tracklets stored. The number of tracklets is available through the AliESDTrdTrack class. This might be only an issue of simulation data and can be checked by comparing AliESDTrdTracks and AliESDtracks in real data.

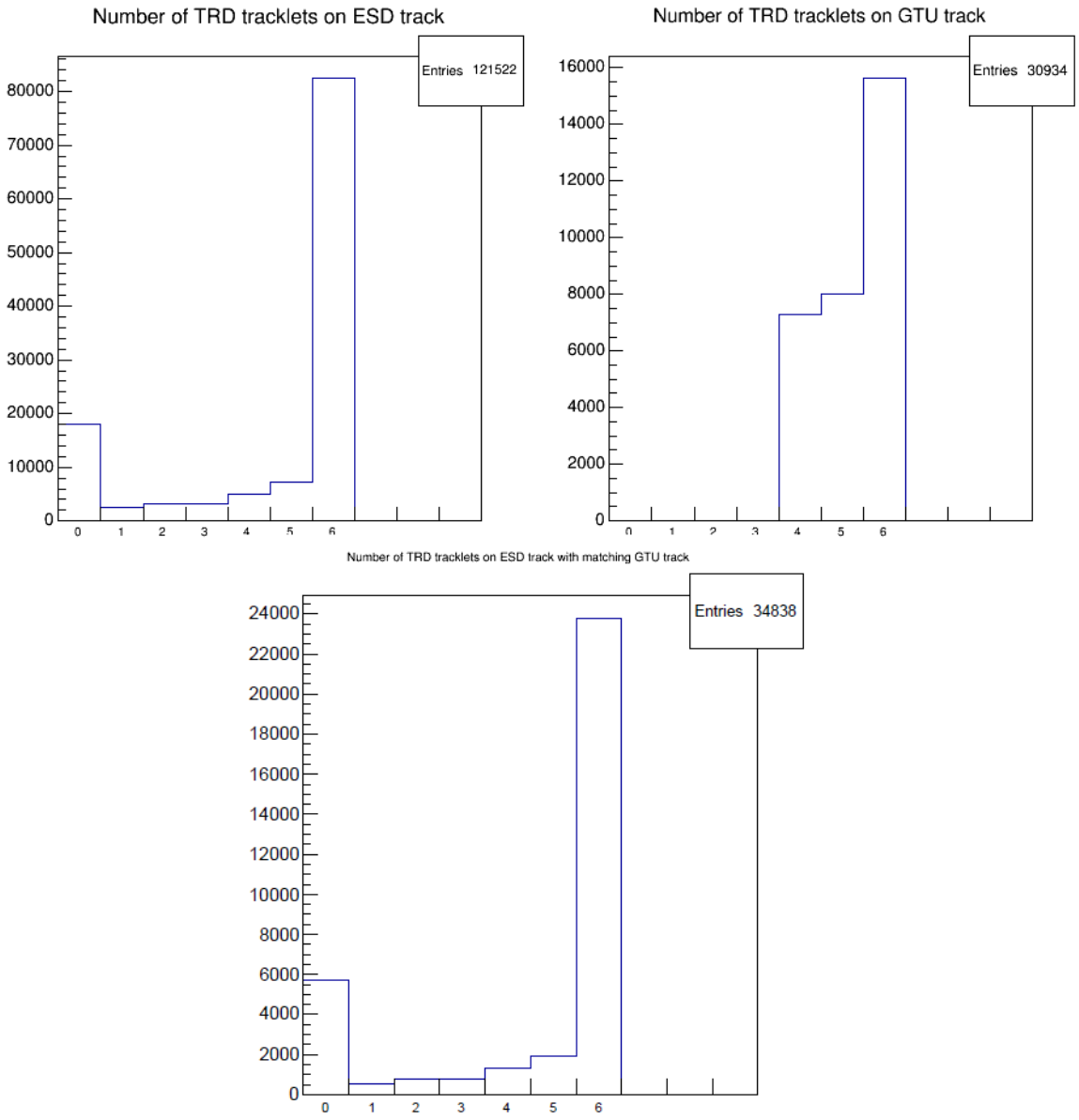

Figure 39: Simulation of approx. 200,000 Υ up to 100 GeV, no cuts (MC).

4.5.4 Correlations of decay products

Geometrical correlations between several particles are being frequently used in collider physics. Evaluating decay products or patterns based on momentum or energy conservation can become visible this way.
Taking the structure of the TRD and the trigger system down to the GTU into account, geometrical correlations can be exploited for data processing. Since the electron and positron have reverse charge, the most effects from deflection of the magnet field in the TRD experiment should be balanced.
Figure 40 shows the correlation between two decay leptons in the ϕ-dimension. Due to a p_T cut the number of tracked upsilon-particles is reduced. No further cuts on the vertex of the tracks are used.

The right graph illustrates that the two leptons are emitted back to back in direction of the ϕ-coordinate due to momentum conservation. The left graph shows the deviation from the expected 180 degrees angle between the two leptons. The deviation is calculated in units of TRD supermodules.
If one particle (electron) is detected in one supermodule, the second one (positron) is expected to be measured in the opposite supermodule or in one of its direct neighbours[36]. Table 3 and 4 show then the number of detectable Υ-mesons. When the cuts do not require the strict 180 degrees arrangement, a widening of one or two supermodules difference is allowed.

The results lead to a first suggestion for trigger settings with the TRD:

- usage of back to back correlation
- p_T cut: exclusion of electrons above approx. 5 GeV/c

Δ Supermodule	Number	Percentage
$\pm$ 0	21749	27.6
$\pm$ 1	41208	52.4
$\pm$ 2	50692	54.4

Table 3: Number of detectable MC tracks with a cut on back to back configuration. "Δ supermodule" refers to a deviation from 180 degrees.

Δ Supermodule	Number	Percentage
$\pm$ 0	1117	9.3
$\pm$ 1	3111	25.8
$\pm$ 2	4746	39.3

Table 4: Number of detectable MC tracks with a cut on back to back configuration, here with pp background. "Δ supermodule" refers to a deviation from 180 degrees.

For further settings of the simulations with background see chapter 4.8.1. As shown in figure 41 the peak is smeared out and the background is enlarged, but the result

[36] One example: An electron from a possible upsilon-decay is measured in supermodule 00, the second one will be in supermodule 09 or in 08 or 10 (see picture: 6.2.4).

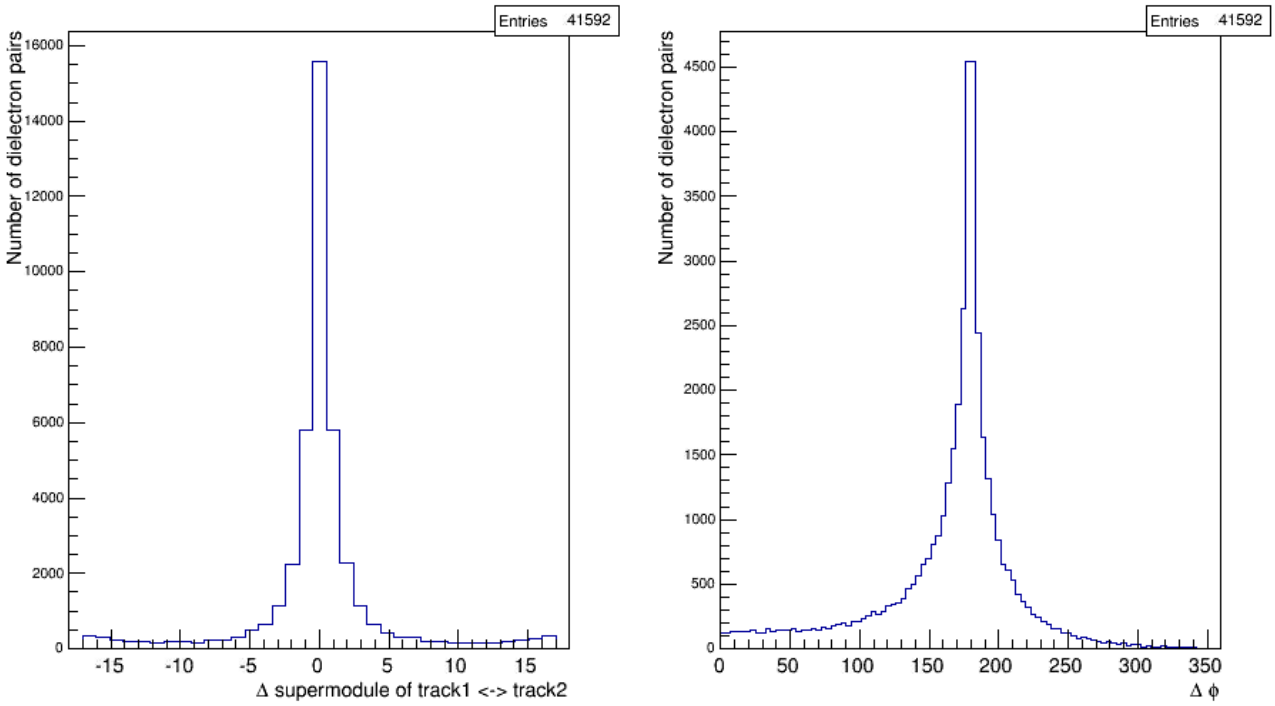

Figure 40: Simulation of 486,000 Υ (y=[-1.,1.]). Cuts (exclusive): $p_t > 5.0\,\mathrm{GeV/c}$ (MC). "Δ supermodule" refers to a deviation from 180 degrees.

remains the same. In Pb-Pb data the background is expected to be even more enhanced in comparison to pp data.

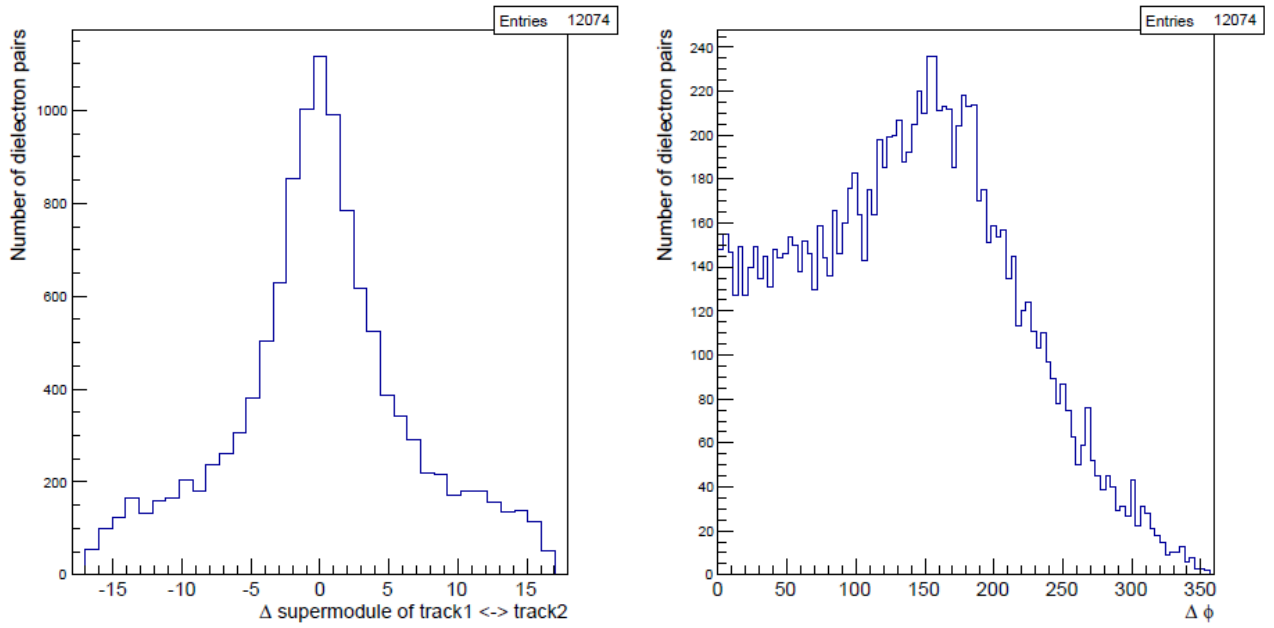

Figure 41: Simulation of 200,000 Υ (y=[-1.,1.]). Cuts (exclusive): $p_t > 5.0\,\mathrm{GeV/c}$ (MC) with pp background. "Δ supermodule" refers to a deviation from 180 degrees.

All considerations of back to back emittance are only exactly valid if the Υ has low transverse momentum. If a meson has higher momentum, the decay looks like a v-

shape with smaller angle values than 180 degrees in ϕ. Figure 42 and 43 display the context between the momentum of the Υ-particle and the angle between the decay leptons. The comparison of both figures shows the impact of cuts in η. Figure 42 has no cuts in η direction. Figure 43 displays a simulation with constrained tracks to $\eta = [-0.8, 0.8]$. The space without signal from 0 to 10 GeV is caused from the TRD acceptance.
An extended simulation up to 100 GeV momentum of the Υ-meson is plotted in figure 44. The same simulation with cuts for leptons and the Υ with $\eta = [-0.8, 0.8]$ is presented in figure 45. Further an interesting effect, namely a shift in low p_T is visible in figure 45. This is caused by a different signal for p_T, which is not taken from the original meson, but rather the sum of both decay leptons.
Generally it was found that a cut range (inclusive) of $\Delta\phi = [0, 0.5]$ (corresponding to approx 0 up to 30 degrees) seems to be sufficient for a momentum (p_T) above 60 GeV, see figure (45). In the intermediate range of $p_T = [30, 60]$ a linear function for the maximum threshold is used. It starts with a $\Delta\phi \approx 1$ at 30 GeV and ends with $\Delta\phi = 0.5$ at 60 GeV. Therefore in figure 46 only the p_T-range $[0, 30]$ GeV is selected. For the p_T-range from 0 up to 30 GeV the signal will be selected through two exponential functions as low and high threshold. For the high threshold an additional constant is required for fitting. They are laid out in figure 47 and the parameters are printed in table 5.
The data points for fitting are selected manually in steps of 5 GeV, see appendix 6.2.5 for the values. The functions are then fitted with the minuit[37] function of root.

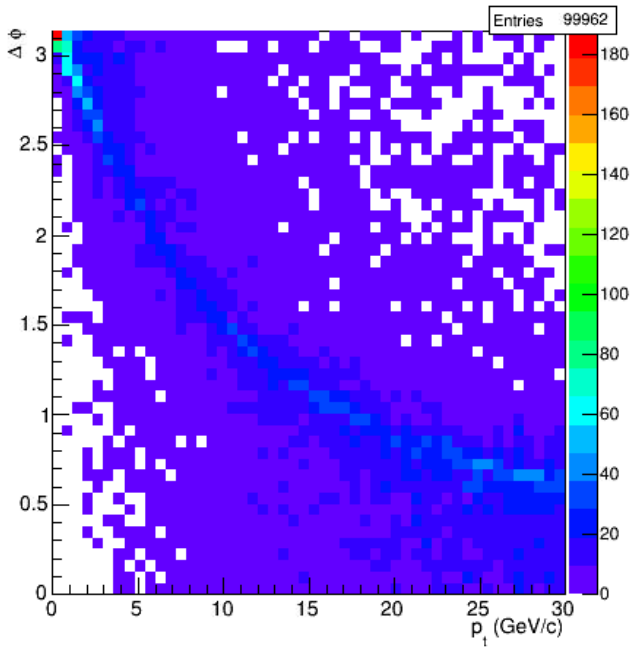

Figure 42: Simulation of 200,000 Υ-particles, no cuts applied, up to 30 GeV.

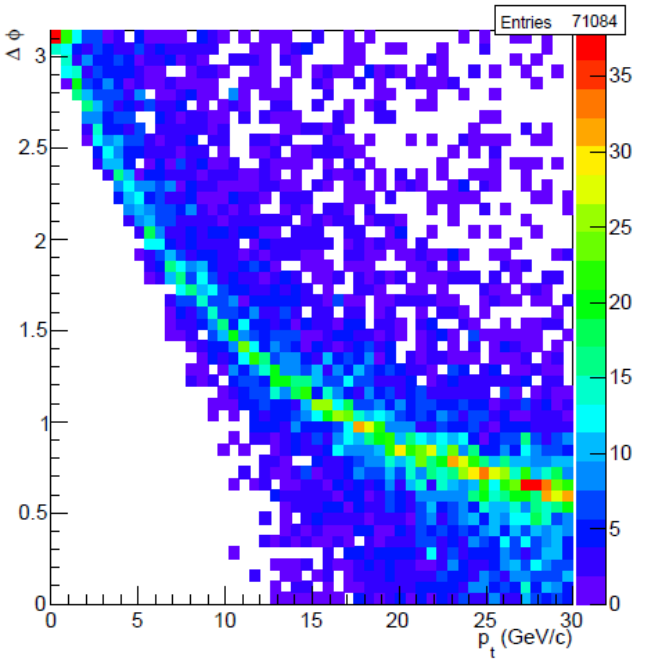

Figure 43: Same data as in figure 42, but cuts on Υ and decay lepton in $\eta = [-0.8, 0.8]$ (inclusive).

[37] A numerical minimization software included in root.

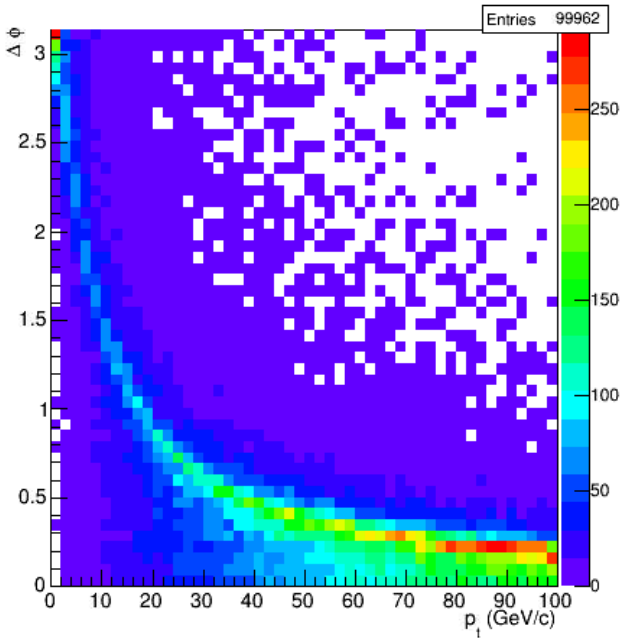

Figure 44: Simulation of 200,000 Υ-particles, no cuts applied, up to 100 GeV.

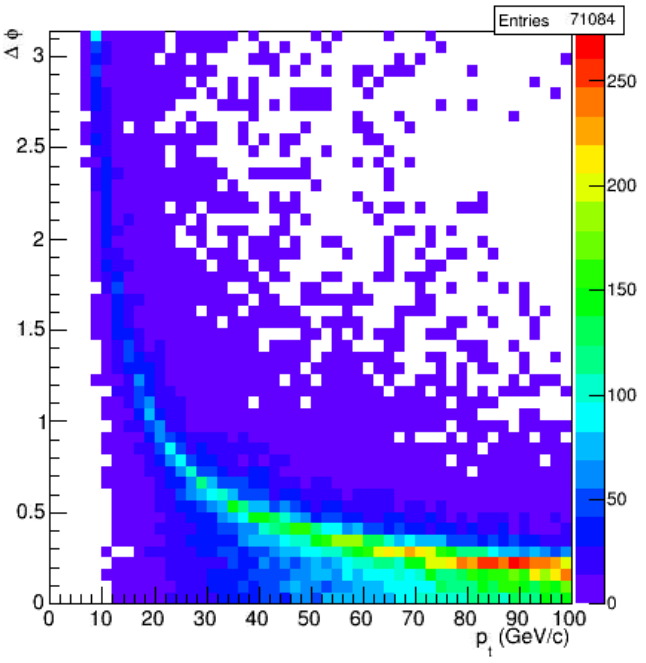

Figure 45: Cuts on Υ and decay lepton in $\eta = [-0.8, 0.8]$ (inclusive). Momentum added from the two decay particles.

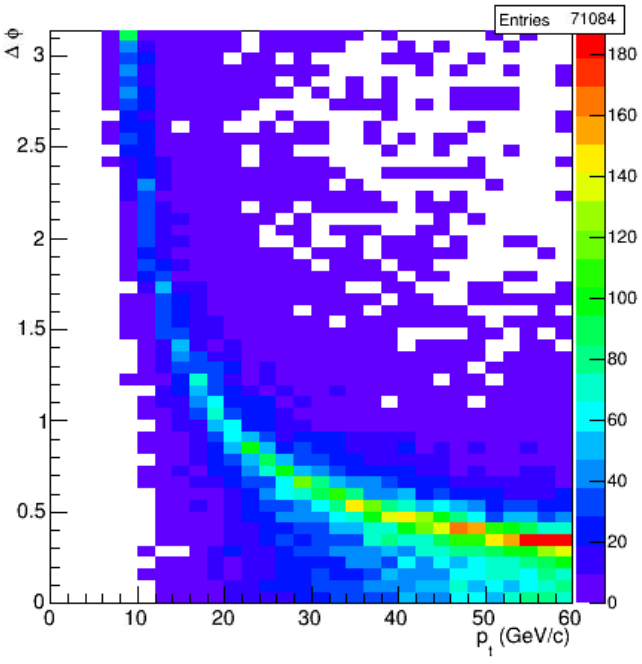

Figure 46: Simulation of 200,000 Υ-particles, no cuts applied, up to 100 GeV.

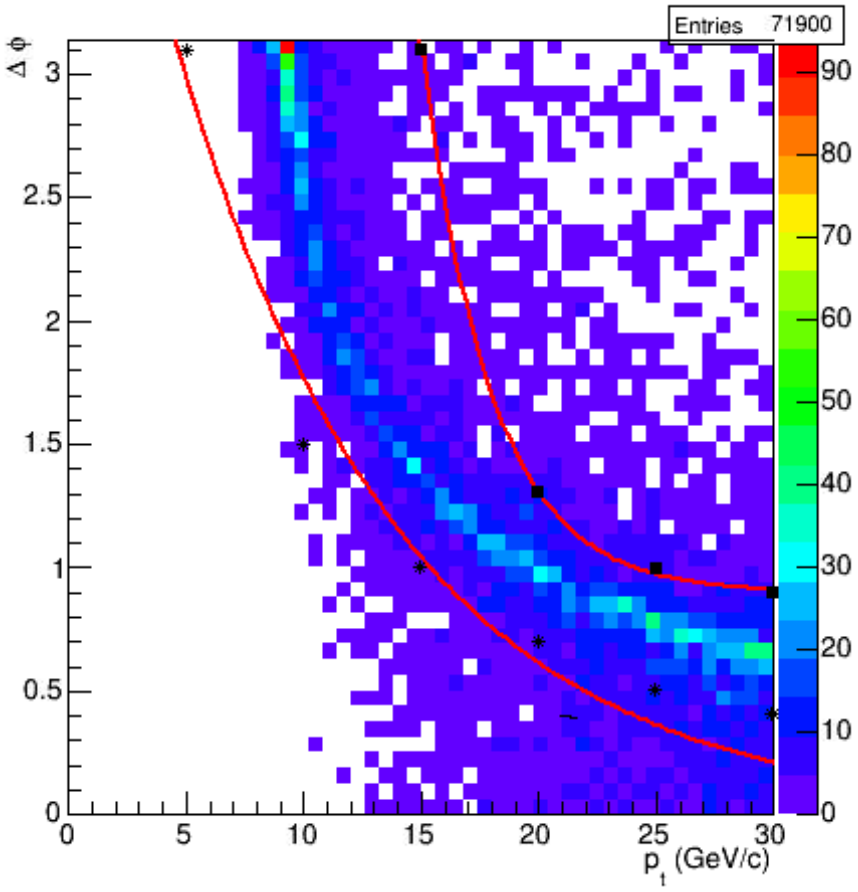

Figure 47: Cuts on Υ and decay lepton in $\eta = [-0.8, 0.8]$ (inclusive). Cut functions as red lines. Data points as black squares (high threshold) and black stars (low threshold).

cut range and function	high threshold parameter	value	low threshold parameter	value
$p_T = [0, 30]$ f(x) = exp(p0+p1*x)+p2	p0 p1 p2	5.938 -0.343 0.905	p0 p1 p2	1.612 -0.105 -
$p_T = [30, 60]$ f(x)=c+m*x	c m	1.336 -0.0140	c m	0 0
$p_T = [60, \infty]$ f(x)=c	c	0.5	c	0

Table 5: Properties of cut functions.

Figures 48 and 49 show two different overlapping distributions. It becomes clear that Υ-2S (figure 48, colored) and Υ-3S (figure 49, also colored) have nearly the same pattern in p_T versus $\Delta\phi$ distribution as Υ-1S . Their invariant mass has a small difference to the Υ-1S, they can also be selected with this filter function.

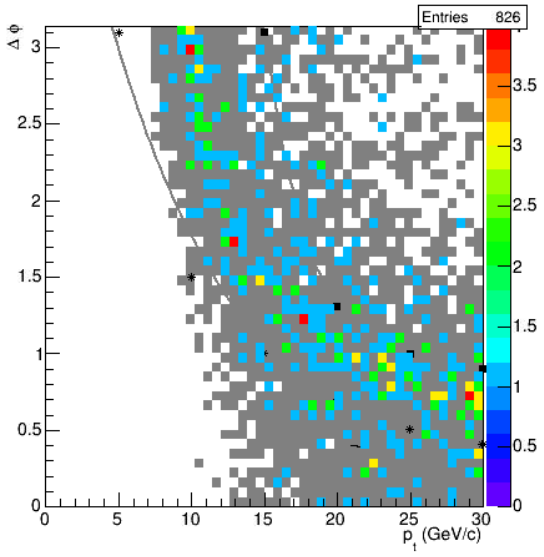

Figure 48: A simulation of 20000 Υ-2S particles (with color palette). The gray background is the distribution from the 1S-state. The visible black dots are the data points for the fitting functions.

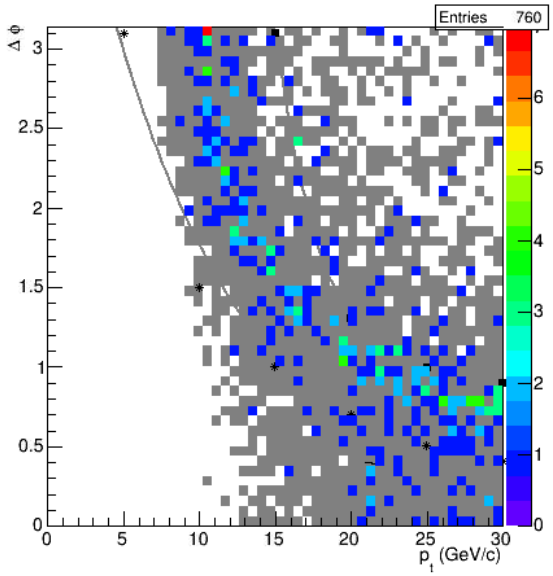

Figure 49: A simulation of 20000 Υ-3S particles (with color palette). The gray background is the distribution from the 1S-state. The visible black dots are the data points for the fitting functions.

Moreover, the distribution in η-space is interesting. Figure 50 refers to two daughter particles from a Υ-decay. The p_T-sum from these two particles is plotted on the x-axis. Because of this sum, the entries start at a minimum of 7 GeV. The difference of η from particle 1 minus η from particle 2 is shown on the y-axis the difference. A cut on the eta difference between the particles of $\eta = [-1, 1]$ might exclude uncorrelated particles.

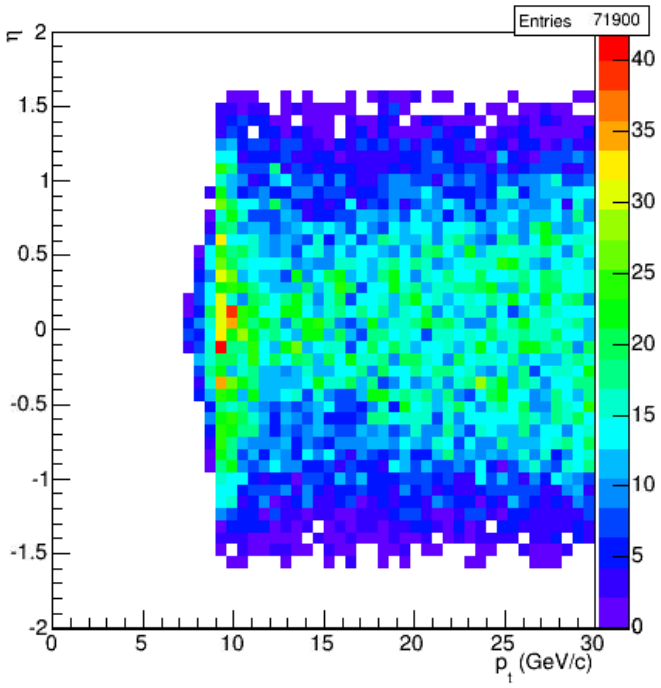

Figure 50: Difference in η between the two particles from a Υ-decay plotted versus the sum of p_T from these both daughter particles.

4.6 Efficiency

In the first place the significant parameters of the two simulation datasets will be given. The 30 GeV and the 100 GeV sample are both generated via the already described AliGenParam class with flat Υ distribution. Apart from the different values in p_T, the following parameters are interesting: For the 30 GeV simulation, an inclusive cut on the upsilon for $y(\eta) = [-0.8, 0.8]$ was used. This was also used for the 100 GeV simulation. The 100 GeV includes an additional inclusive cut for the decay leptons of $\theta = [45, 135]$ degrees, which represents the TRD acceptance. A 100 GeV simulation with a cut of $\eta = [-0.8, 0.8]$ on the decay leptons has no signal larger than 40 GeV, see 6.2.6. For both simulations SetPhiRange(0,360), SetOrigin(0,0,0) and of course SetForceDecay(kDiElectron) were used.
Figure 51 and 52 show the efficiency of tracking the decay particles from Υ. Both tracks from the decay are expected to have a signal in ALICE in general, an ESD track. This is shown on the left top side. The efficiency for GTU tracks is shown an the right top side. For this, both tracks need a signal from the Global Tracking Unit of the TRD. It is stored in the data class AliESDTrdTrack. Both efficiency plots only include tracks with $\eta < 0.8$. The TRD detector has a pseudorapidity coverage of $\eta = [-0.9, 0.9]$, so potential effects from detector boundaries are avoided with this η-cut. On the right bottom side, the distribution of the Monte Carlo particles is displayed. The left bottom side show the efficiency with a condition of at least five tracklets on both ESD tracks as a cross-check. As described in chapter 4.5.3.5, GTU tracks are created with a minimum of four tracklets per track.

With higher transverse momentum of the Υ-mesons, the electrons/positrons have also higher momentum. Tracks with higher momentum are then easier to measure. Other results [VUL04] concerning the efficiency within the TRD acceptance show also only an efficiency of around 40 %. One reason for the low efficiency is that not necessarily both tracks are within the TRD geometrical acceptance, see chapter 6.2.2. Higher transverse momentum tracks have also a better tracking efficiency.

From comparison of the two GTU efficiency plots one will note that the efficiency is lower at 30 GeV than at 100 GeV. This is due to a parameter in the reconstruction of the data. The function rec.SetFractionFriends() has a default value of 0.04, in the 100 GeV it was set to 1. This value steers the storing of AliGTUtracks in the AliESDfriends.root file. That the value of GTU efficiency is still lower even with the corrected parameters might be an issue of the GTU simulation itself or other parameters which are not documented. The TRD was simulated with all 18 supermodules but of course there is a small fraction of data which is lost due to geometrical acceptance (dead zones and PHOS-hole; see chapter 4.5.3.3).

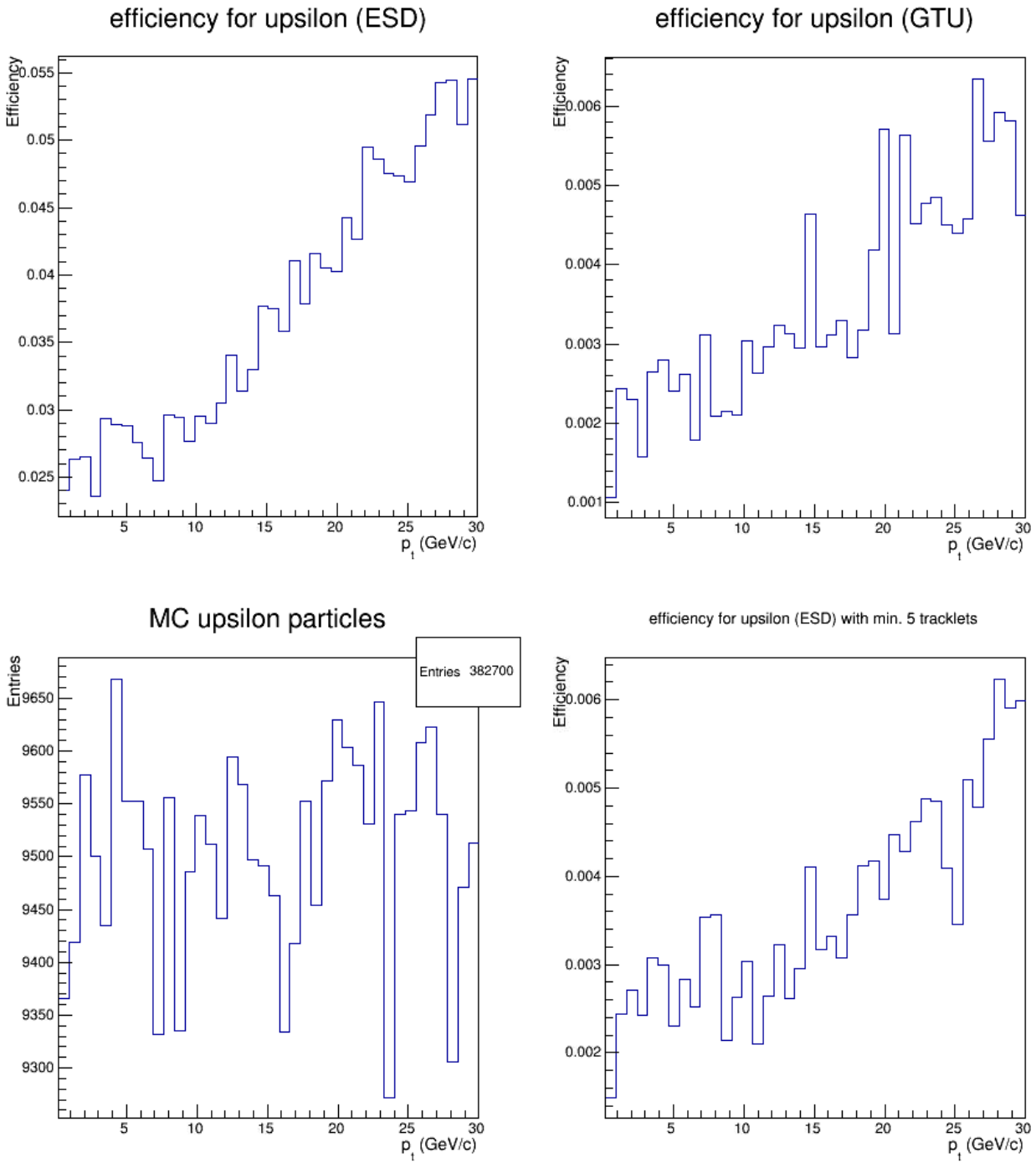

Figure 51: Efficiency of the Monte Carlo generated Υ-particles up to 30 GeV (bottom left), which are nearly uniformly distributed. The efficiency for at least five tracklets per ESD-track is presented on the bottom right plot. The left top diagramm shows the reconstructed tracks in ESD; the right top side the tracks accepted from the TRD (in the GTU).

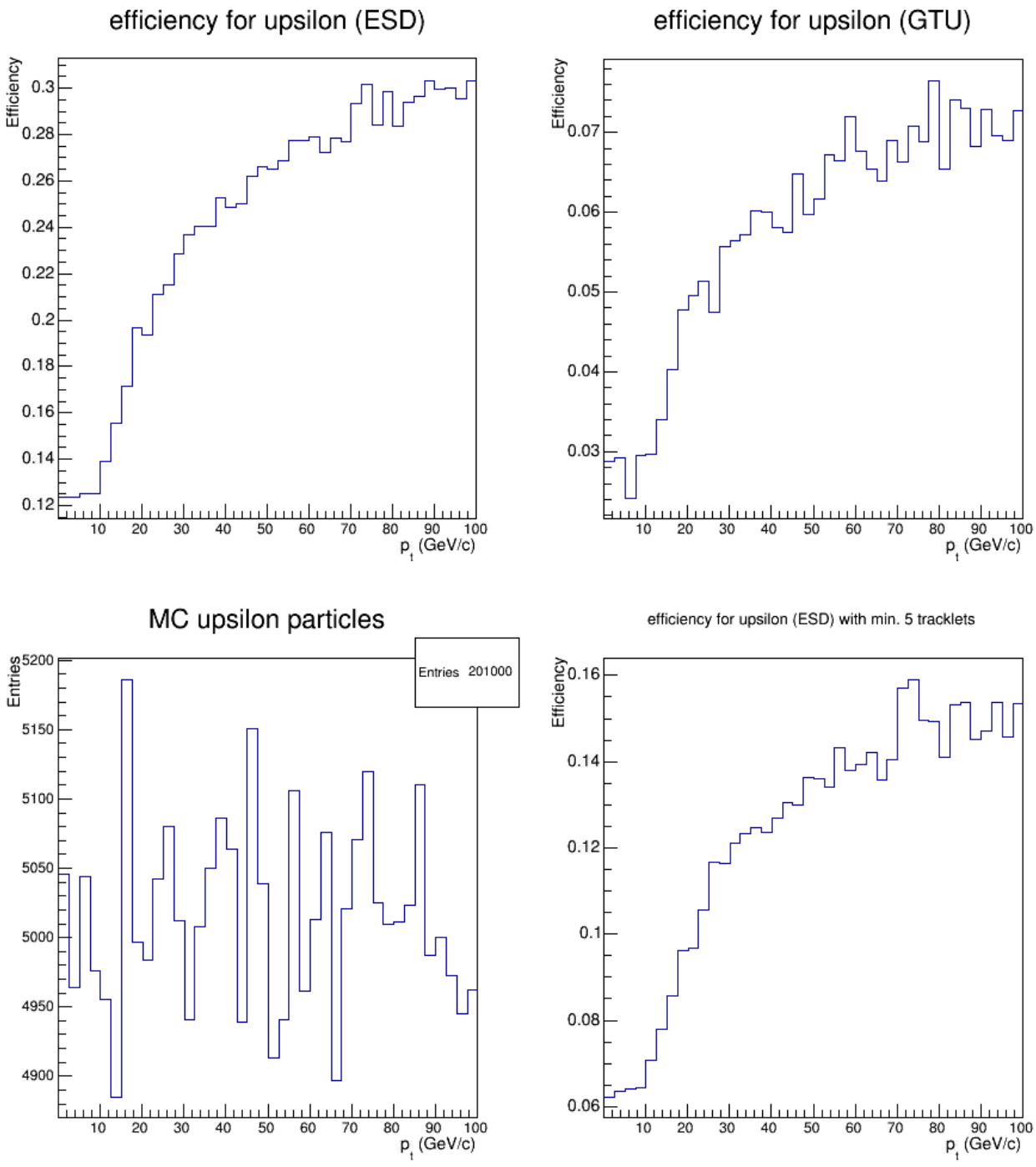

Figure 52: Efficiency of the Monte Carlo generated Υ-particles up to 100 GeV (bottom left), which are nearly uniformly distributed. The efficiency for at least five tracklets per ESD-track is presented on the bottom right plot. The left top diagramm shows the reconstructed tracks in ESD; the right top side the tracks accepted from the TRD (in the GTU).

4.7 Acceptance

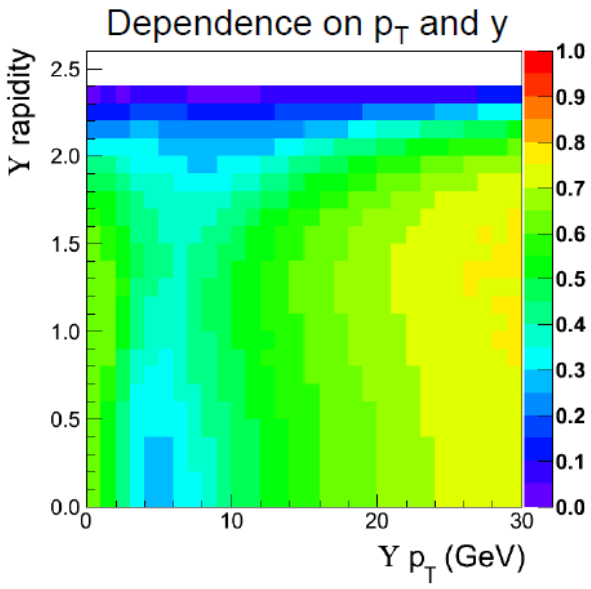

Figure 53: Acceptance for Υ-mesons from the CMS experiment with muon decay channel [Mat10][Mat11].

In figure 53 a measurement of the CMS experiment is shown. This data uses the muon decay and not the electron decay of the Υ. As the plot covers a p_T-range up to 30 GeV/c for comparison, the simulation is also extended to this range. A second simulation includes a p_T-range up to 100 GeV/c. In the CMS example the distribution is given in rapidity y plotted against p_T. Therefore for comparision the distribution concerning the rapidity is presented here. For further comparison the distribution concerning pseusorapidiy η is given in the appendix, too. For all distributions the Monte Carlo information for η/y and p_T from the decayed Υ-particle is used. Further are the ESD and GTU tracks filtered for $\eta = [-0.8, 0.8]$ (inclusive). For the simulation parameters see the chapter before.
The results from the y-distribution are presented in figure 54 and 55. For each of the two simulations, the distribution of the Monte Carlo-Υ-particle is shown in the plot at the bottom. On the top left side of the figures, the acceptance for Υ with two ESD-tracks is shown. Last but not least the acceptance distribution for Υ-mesons with two GTU-tracks is displayed on the right top of the figures. It is to note, that each data point also represents the efficiency for Υ-mesons at the concrete y/p_T data pair.
In this chapter the distribution in units of rapidity is discussed. In appendix 6.2.3 the acceptance distribution is shown in units of pseudorapitiy, which leads to no significant difference. The distribution in figure 54 follows the measurement from the CMS experiment. The acceptance is higher towards lower rapidity and higher towards higher transverse momentum. There is not enough data for a convincing statistic in the 30 GeV simulation. For this issue with the acceptance from GTU tracks see the chapter before, but the shape of acceptance is not influenced; it follows the pattern in ESD tracks described before.

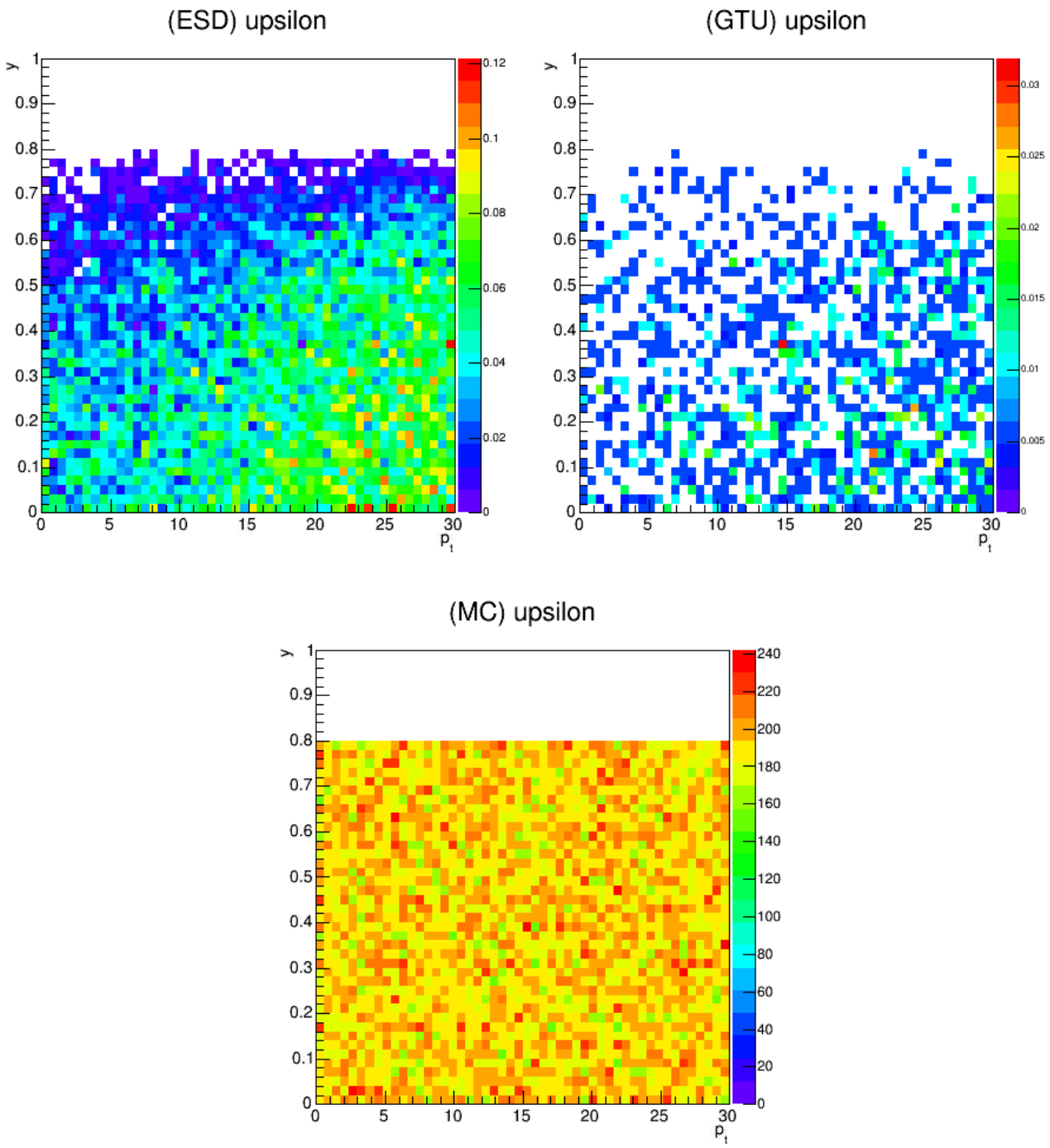

Figure 54: Acceptance for Υ-mesons - rapidity distribution - from a simulation up to 30 GeV p_T. The left plot shows the acceptance for Υ-mesons when the two decay tracks are existing ESD tracks. The right side shows the same for two GTU tracks from the decay. The bottom plot shows the simulated Monte Carlo Υ distribution. Cuts on all particles: $y = [-0.8, 0.8]$ (inclusive).

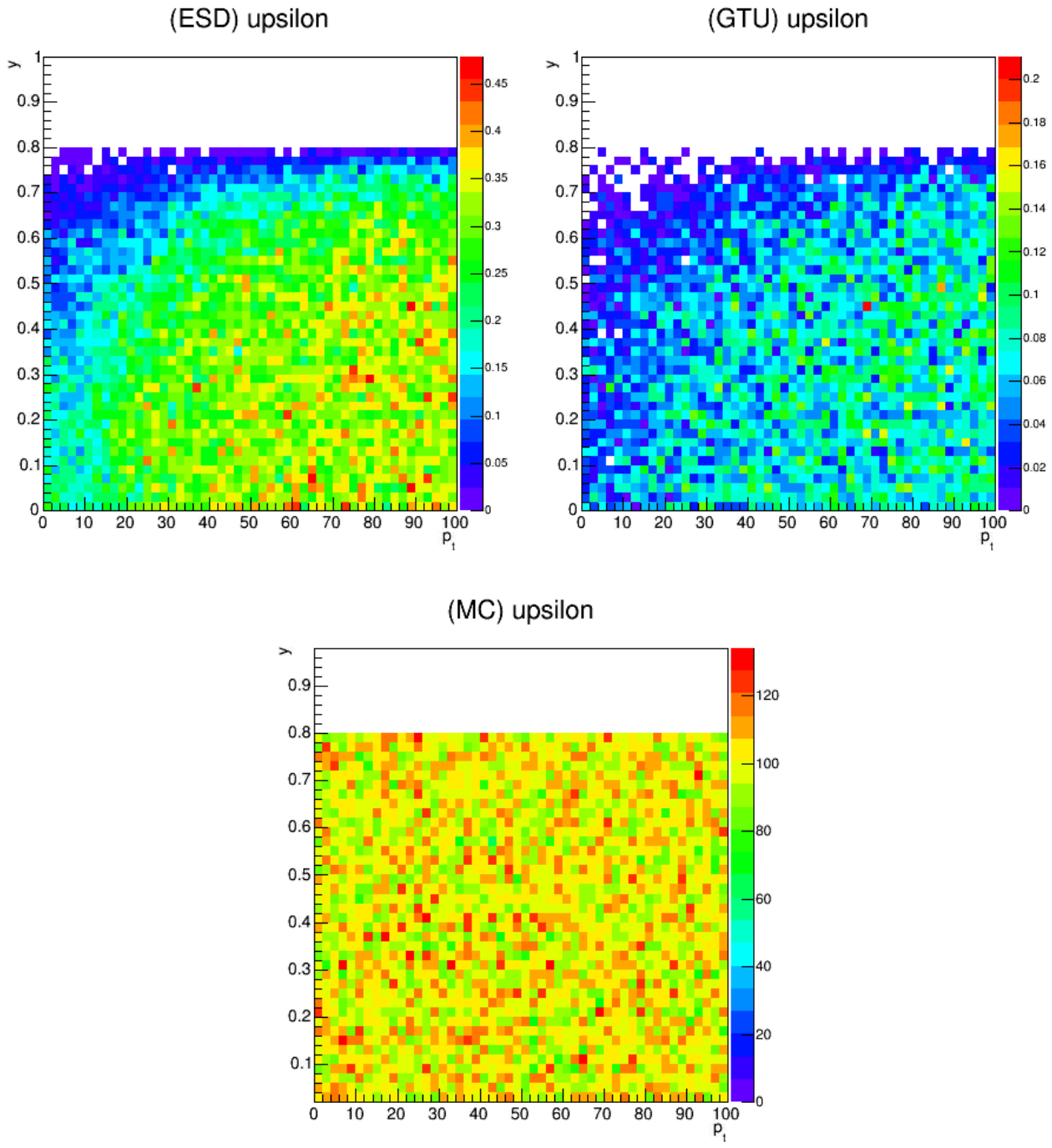

Figure 55: Acceptance for Υ-mesons - rapidity distribution - from simulation up to 100 GeV p_T. The left plot shows the acceptance for Υ-mesons when the two decay tracks are existing ESD tracks. The right side shows the same for two GTU tracks from the decay. The bottom plot shows the simulated Monte Carlo Υ distribution. Cuts on all particles: $y = [-0.8, 0.8]$ (inclusive).

4.8 Background in simulated pp and Pb-Pb collisions

As already mentioned in chapter 2.4, the background originates from various sources. The resulting particles are uncorrelated and correlated, depending on the source, making the distinction between signal and background even more complicated. In this chapter a description of background sources and methodes to filter data will be given.

The simplest approach for the separation of signals from the background is to fit data and background with mathematical functions. Another simple method is the subtraction of the "like-sign" background, see chapter 4.8.2. If like-sign subtraction is not sufficient, methods like event mixing are required.
For event mixing, pairs with different signs are taken from two different events. This way, the particles are surely uncorrelated. For statistical accuracy, data from more than two events can be used [CrB97]. But before the detailed analysis of background is presented, the next chapter summarizes the simulation settings for pp and Pb-Pb events.

4.8.1 Simulation of pp and Pb-Pb events

The already mentioned Pythia tool is used for the simulation of pp collisions. The development was started in 1978. Pythia can model high energy collisions between electrons and positrons or protons and antiprotons. The Aliroot class AliGenPythia is the steering interface. If not specified in the next chapter, the following settings are used:

```
AliGenPythia *py = new AliGenPythia(-1);
    py->SetMomentumRange(0,999999);
    py->SetThetaRange(0., 180.);
    py->SetYRange(-12,12);
    py->SetPtRange(0,1000);
    py->SetProcess(kPyMb);
    py->SetEnergyCMS(14000.);
    py->SetOrigin(0, 0, 0);
    py->SetSigma(0, 0, 5.3);
    py->SetCutVertexZ(1.);
    py->SetTrackingFlag(1);
    py->SetProjectile("p", 1, 1);
    py->SetTarget("p", 1, 1);
```

Setting -1 as parameter for AliGenPythia allows the Pythia generator to simulate as much particles as needed for the pp collision. The momentum range is also not constrained to vary this value on the particles. The functions SetThetaRange, SetYRange and SetPtRange allow further restrictions of the θ parameter, pseudo-rapidity (η) [38] and transverse momentum p_T.
SetProcess modifies the internal parameters - for example jets - or in this case background events with no special bias. SetEnergyCMS sets the LHC beam energy in

[38] See chapter 6.1.3

the Center of Mass System (CMS). The collision vertex is set through SetOrigin, which is smeared in direction of the z-axis through SetSigma. The smearing is also possible in the x- and y-direction. SetCutVertex filters secondary particles from decays near the vertex. The next function enables the particle tracking which can be disabled if only the particle production is required. The last two functions set the collision particles.
The Heavy Ion Jet INteraction Generator (HIJING, also written Hijing in AliRoot) was developed for the simulation of proton-proton, proton-atom and atom-atom collider events. The relevant settings Hijing are the following:

```
AliGenHijing *gener = new AliGenHijing(-1);
gener->SetImpactParameterRange(0., 5.);
gener->SetEnergyCMS(5500.);
gener->SetProjectile("A", 208, 82);
gener->SetTarget("A", 208, 82);
gener->KeepFullEvent();
gener->SetJetQuenching(1);
gener->SetSpectators(0);
gener->SetSelectAll(0);
```

The settings of the impact parameter are given in fm. This parameter describes the distance between the nucleons in the x-y plane. SetEnergyCMS is the same parameter as in Pythia. The functions SetTarget and SetProjectile require the following syntax: ("A" , 208 , 82) which means in detail: Label for proton p or nucleus A, the atomic mass and proton number. KeepFullEvent preserves the family relationships of simulated particles. With SetJetQuenching the jet quenching of the QGP can be enabled or disabled. Non interacting nucleons from the colliding lead atoms are ignored through SetSpectators(0). Kinematic selection with SetSelectAll offers a kinematic cut to reduce the calculation time.

The Υ-particle signal generated by AliGenParam is added through the function AliGenCocktail. This way an arbitrary number of particle generators can be mixed:

```
AliGenCocktail *newgener = new AliGenCocktail();
newgener->AddGenerator(genhi, "Hijing", 1);
newgener->AddGenerator(genpa, "extra upsilon", 1);
```

4.8.2 Like-sign background

Like-sign means the combination of pairs of particles with the same signed charge. Un-like-sign then means of course the combination of particles with opposite charge. Decay signals for example consist of an electron and a positron, so the condition is fulfilled. Pure electron pairs can be then used for an estimate of the background. Mixing an Υ decay to electron/positron with only one minimum bias[39] event enhances the background in the invariant mass spectrum. Figure 56 shows a simulation

[39] The parameter b is the impact parameter which can be up to the sum of the radii of the colliding nucleons 1 and 2. Minimum bias collisions are all collisions starting from $b = 0$, up to $b = R_1 + R_2$. If b is zero, both nuclei collide on their full plane. Is $b = R_1 + R_2$, the nuclei only touch at their margins.

with mixed events. For comparison to unmixed events, refer to figure 33.
For the simulation of the background, proton-proton collisions from Pythia were used. For a full listing of the relevant parameters see 4.8.1.

Like-sign background subtraction has no effect when correlated processes are present. In nucleus-nucleus reactions, decays from the B meson decay are relevant. In pp collisions the number of semileptonic decays from open[40]-bottom and open-charm mesons are less significant and the like-sign background is sufficient. In the next chapters the like-sign background on p-Pb data is shown also. Figure 57 shows the like-sign background from a Hijing simulation with settings as described in chapter 4.8.1. One event needed about 5h CPU time[41] to complete simulation and reconstruction of data.

[40] Open states originate from the breakup of bottonium and charmonium mesons into pairs of mesons. The bottom/charm quarks are split and form new mesons with lighter quarks.

[41] The time the processor is active, idle time (waiting for data or other processes) is not included.

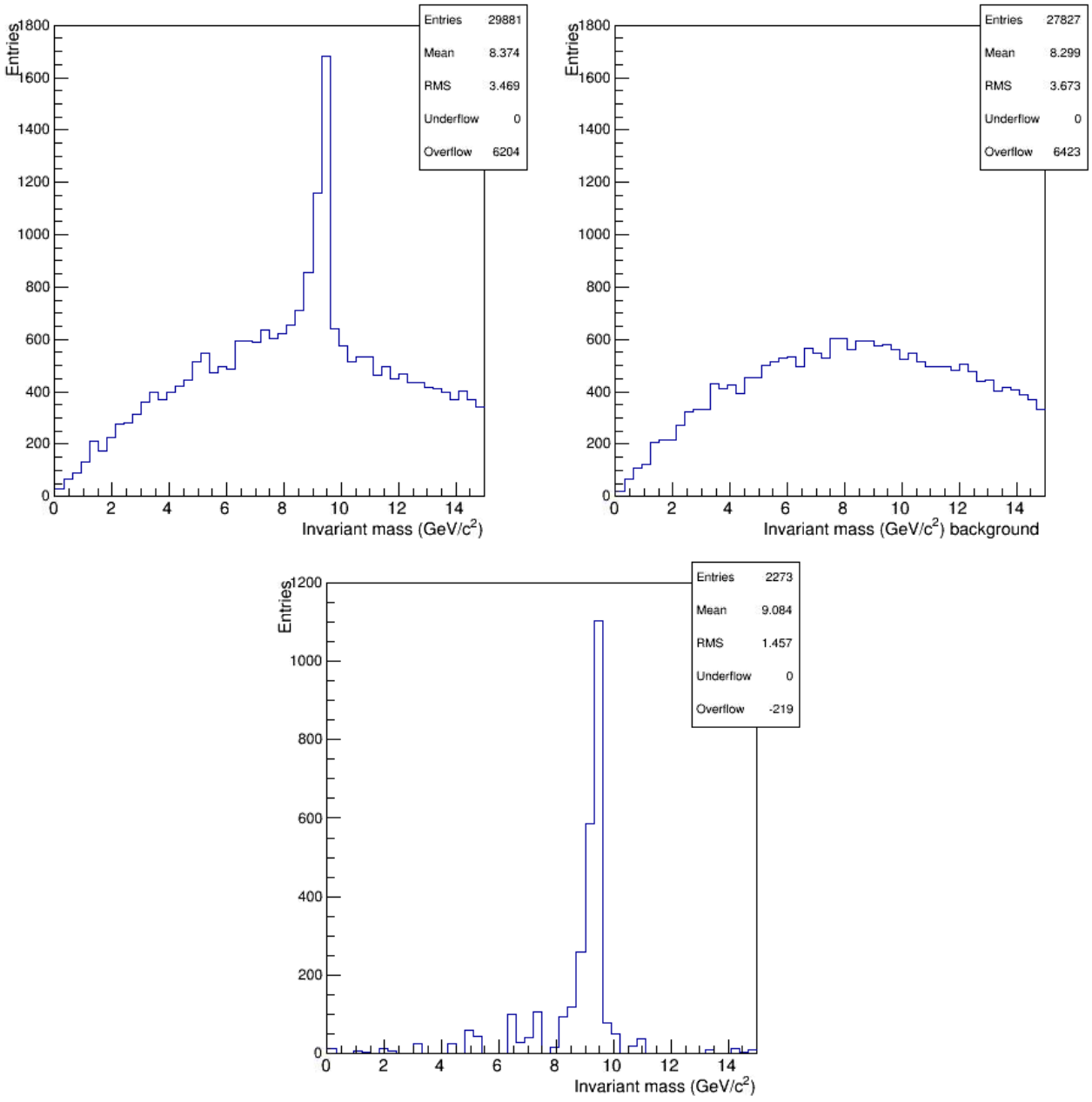

Figure 56: Simulation of 200,000 Υ with pp background, high loss due to cuts. The left side shows the total invariant mass spectrum. Right side shows the like-sign background. Bottom shows the invariant mass spectrum with substracted background. $3\,\mathbf{GeV} < p_T < 7\,\mathbf{GeV}$ was used for lepton tracks.

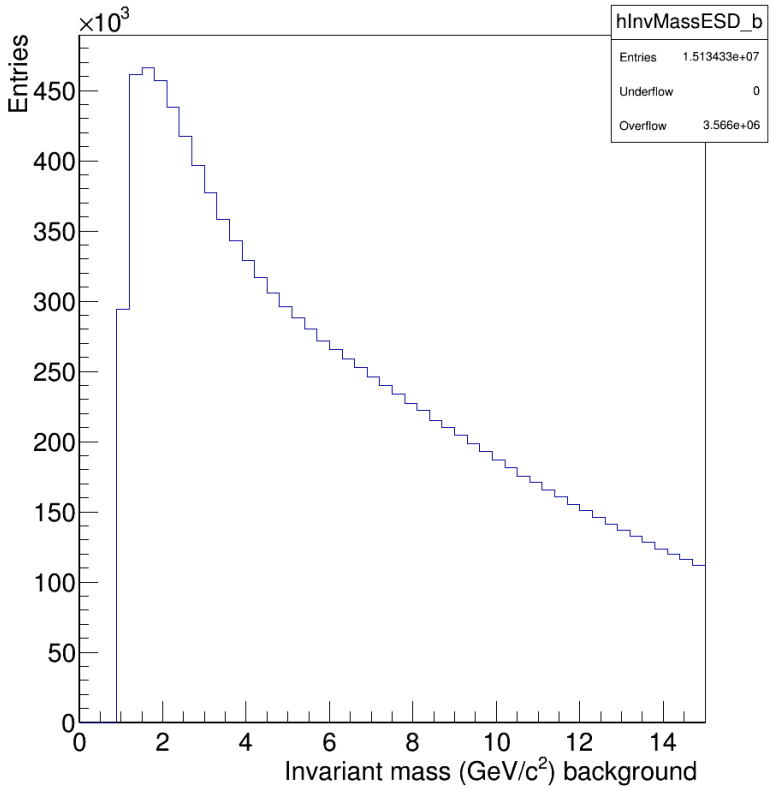

Figure 57: Like-sign background from Pb-Pb simulation with Hijing, 300 events with full tracking. Cut off of invariant mass smaller 1 GeV. Also cut on $\eta = [-0.8, 0.8]$ (inclusive).

4.9 Analysis on real data

ALICE generates at least 1 PB[42] of data per year; to manage this amount, data is stored decentralized. Large computer clusters around the world are organized in the already mentioned ALICE Grid (see chapter 4.2).
The Grid has to store data and to provide computing capacity. Raw data is reconstructed on the Grid. Further large Monte Carlo simulations can be run on the Grid.
The details of steering and running the Grid are complicated, therefore only parts affecting the user analyses are given here. The access to the Grid is based on user certificates. Aliensh, a shell equivalent, allows navigating through data sets and other tasks. Monalisa[43], a web based tool, grants the simple tracking of jobs and output of jobs. The output can then be downloaded to the local computer for further processing and evaluation. All ways of output in Root (class TList, class TNtuple, histograms, etc.) are supported.

4.9.1 Analysis with Alien AliRoot plug-in

The analysis should be based on a local analysis structure (AliAnalysisTaskSE or related) with input and output slots for the AliAnalysisManager.

The Alien plug-in then encloses the analysis and makes it executable. The example used here is derived from the runEMCalJetAnalysis.C[44] macro. As an analogon to the local analysis, an AliAnalysisManager is created, which adds a data source from ESD, AOD or Monte Carlo files.
Before setting the analysis task, it might be useful to initiate other tasks, e.g. AliPhysicsSelectionTask for the selection on additional parameters, which filters unwanted events. The initialization is the same as in the local case. Even more than one user analysis task can be run at one data selection. This is also done in large - so-called - trains, which go through data sets with several user tasks at once.

Another step is different from local analysis; before the run is started, the Alien connection has to be initialized. This is done through:

```
AliAnalysisGrid *plugin = CreateAlienHandler(uniqueName,
    gridDir, gridMode, runNumbers, pattern, additionalCXXs,
     additionalHs, maxFilesPerWorker, workerTTL, isMC);
mgr->SetGridHandler(plugin);
```

CreateAlienHandler is a function which creates a new AliAnalysisAlien instance and passes a set of parameters to it. The variable uniqueName is simply a name for identification, gridDir is the main directory of the requested data set. The next parameter runNumbers provides the selected runs with a naming pattern given in

[42] See: http://aliceinfo.cern.ch/Public/en/Chapter2/Chap2_DAQ.html (15.02.2014), increasing with collider energy and luminosity.
[43] http://alimonitor.cern.ch/ - 17.02.2014
[44] http://git.cern.ch/pubweb/AliRoot.git/blob/refs/heads/master:
/PWGJE/EMCALJetTasks/macros/runEMCalJetAnalysis.C - 20.02.2014

the next variable. The inclusion of additional *.cxx and *.h[45] files can also be passed to the plug-in. The settings maxFilesPerWorker and workerTTL depend on the users quota of computing resources and can be adjusted for datasets. The boolean value isMC enables the Monte Carlo data handler.

[45] C++ source code and header files.

4.9.2 Physical selection parameter

In this analysis the invariant mass spectrum of di-electron pairs is presented. For probing the background also a like-sign invariant mass spectrum is generated. For analysis on ESD data, at first an AliESDtrackCuts filter can be initialized to exclude tracks with wrong properties as described in chapter 4.4. In AOD data the cuts need to be done manually. In a for-loop over all like- und un-like-sign pairs, cuts are being made.
Concerning the cuts there occur some differences in the ESD and AOD data format. Through the function of AliAODtrack->GetMostProbablePID()=0 only electrons and positrons are selected. In ESD data the function is AliESDTrack->GetPID(). With the Charge() function, which is the same for ESD and AOD, pairs of like-sign and un-like-sign can be matched. Before the invariant mass is calculated on both tracks of a pair η and p_T cuts are being done. For plots which make use of the back-to-back correlation of track pairs in ϕ, a cut in the ϕ variable is carried out. It is divided into three parts, as posited in chapter 4.5.4. It calculates at first the difference in ϕ between a particle pair. After this the sum of the particle's momentum is used to select a case of the three different treated parts. For details on the cut functions see table 5 in chapter 4.5.4. The source code of the function is the following:

```
bool AliTRDUpsilonTask::FilterMomentum(Double_t pT1,
   Double_t pT2,Double_t phi1,Double_t phi2) {
Double_t diff = phi1 - phi2;
        if (diff>3.141)
        {
          Double_t x=diff;
          diff = 3.141-(x-3.141);
        }
        else
        {          //change nothing in this case  }
         Double_t pTsum = pT1+pT2;

         if(pTsum < 30)
           {if ( (diff>( exp(1.612-0.105*pTsum) )) && (diff
               < (exp( 5.938-0.343*pTsum )+0.905 )) )
               { return 1;}else{return 0;}}

         if((pTsum>30)&&(pTsum<60))
           {if (diff<(1.336-(0.0140*pTsum)))
               { return 1;}else{return 0;}
           }

         if(pTsum>60)
           {if (diff<0.5)
               { return 1;}else{ return 0;}
           }}
```

The invariant mass is described in the appendix, see chapter 6.1.2; in Root it can be calculated from two particles in the following way. There exists a class for four-momentum-vectors in Root, the TLorentzvector class. If a TLorentzvector is filled with energy and momentum (see the following code sample), the magnitude of the vector gives the invariant mass. The separate values are from particle number 1 and particle number 2, which are like-sign or un-like-sign pairs in this analysis.

```
TLorentzVector v;
v.SetE(E1 + E2);
v.SetPx(px1 + px2);
v.SetPy(py1 + py2);
v.SetPz(pz1 + pz2);
Double_t invMass = v.Mag();   // calculating invariant mass
    .
```

4.9.3 Analysis on the LHC13f dataset (di-electron)

For the analysis p-Pb data was chosen because of a lower background than at Pb-Pb and for the good availability of datasets with GTU information. In the AOD data the class AliESDtrdTracks is not included. The shift in rapidity for p-Pb collisions, which is described in chapter 6.1.5, is not significant here, the used cuts only refer to a difference in rapidity and not to absolute values. Only the analysis with the last iteration of cuts is presented here. It took some unsuccessful attempts to find the cut settings and also the dataset. Any general cuts, applied to all particles, were not set, only the invariant mass was skipped if smaller 1 GeV/c^2. Surely only electrons through PID information were selected. For this analysis only run number 197388 from the LHC13f dataset was used. Figure 58 shows that the $\Delta\phi$ distribution from the cut yields the proper results. All data is within the given boundaries.

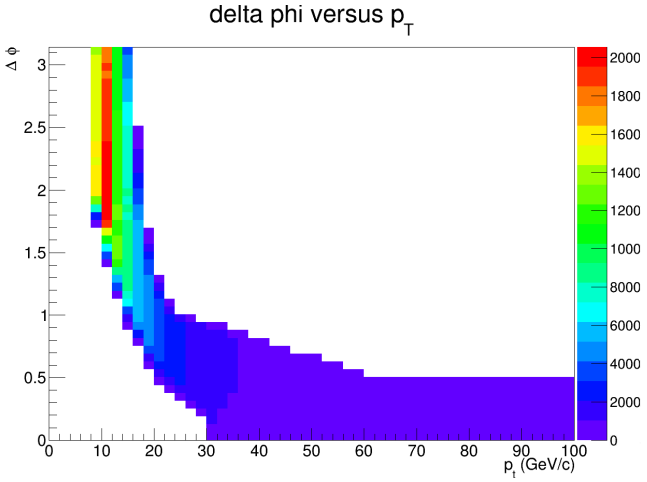

Figure 58: Invariant mass plots from ESD data.

Figure 59 shows a detailed part of figure 61 plot 9. The background is fitted through the red curve which has the function $f(x) = exp(p0 + p1 * x) - p2 * x^2 + p3$. For the fit parameters $p(i)$ the following values were determined: p0: 8.29419e+00; p1: -2.21108e-01; p2: -3.59919e+00 and p3: -7.50680e+02. The expected positions for the Υ-resonances are marked with arrows. It appears that there are hints for the 1S and the 3S state. With higher statistics it might be possible to distinguish the signal better from the background.

There are also two collections of plots shown in figures 60 and 61 . The first shows plots with information from ESD, the second one additional plots with the requirement of existing GTU-data. All plots in both figures are numbered and all of them show invariant mass spectra. In the first plot the un-like-sign signal from the ESD tracks is displayed. The second plot displays the corresponding like-sign distribution, the background. Plot 3([46]) then shows distribution 2 minus distribution 1. The background shows the appopriate pattern, but it needs to be scaled to fit perfectly. The already described cut for $\Delta\phi/p_T$ was used in plot 4 and 5. Just as before, plot 4 includes un-like-sign pairs and plot 5 the background with like-sign pairs. In these two plots an interesting pattern occurs, a bump around a

[46]For better readablility the numbers are given as number and not written-out.

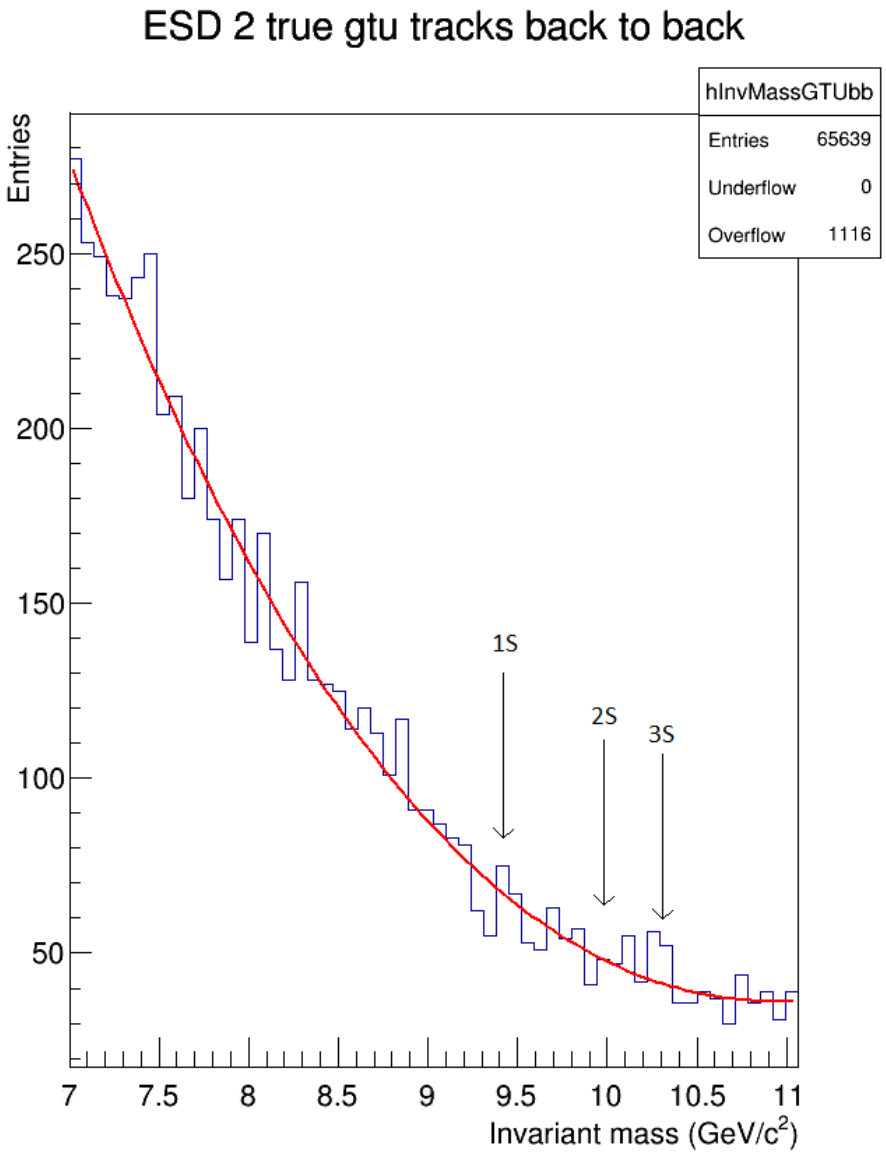

Figure 59: Invariant mass plots from ESD data with two GTU tracks, filtered for back to back correlation. See text for details on the fit function in red. Arrows with 1S, 2S and 3S mark the point where the corresponding Υ-resonances are expected.

mass of 5 GeV/c^2. Plot number 6 is then the difference of 4 und 5. The background is also not scaled to fit, because it is shown later, that fitting with a function is sufficient for this small data sample.
Now in figure 61 the structure of the plots is the same as in figure 60, but with the condition that both tracks have a GTU track. Information on the particle is still derived from the ESD track. The figure starts again with un-like-sign distribution (plot 6) and like-sign (plot 7) without any further cuts. Plot 8 is then the difference from 6 minus 7. Plot 9 (un-like-sign) and 10 (like-sign) include the $\Delta\phi/p_T$ -cut. Plot 11 gives last but not least the difference of 9 and 10.
Figure 62 and 63 show again all plots, but only around the interesting region of approx 9.5 GeV/c^2 . Cutting around 180 degrees difference of the daughter particles brought also no success for the low statistics, but might be useful for large results to select low p_T Υ-mesons.

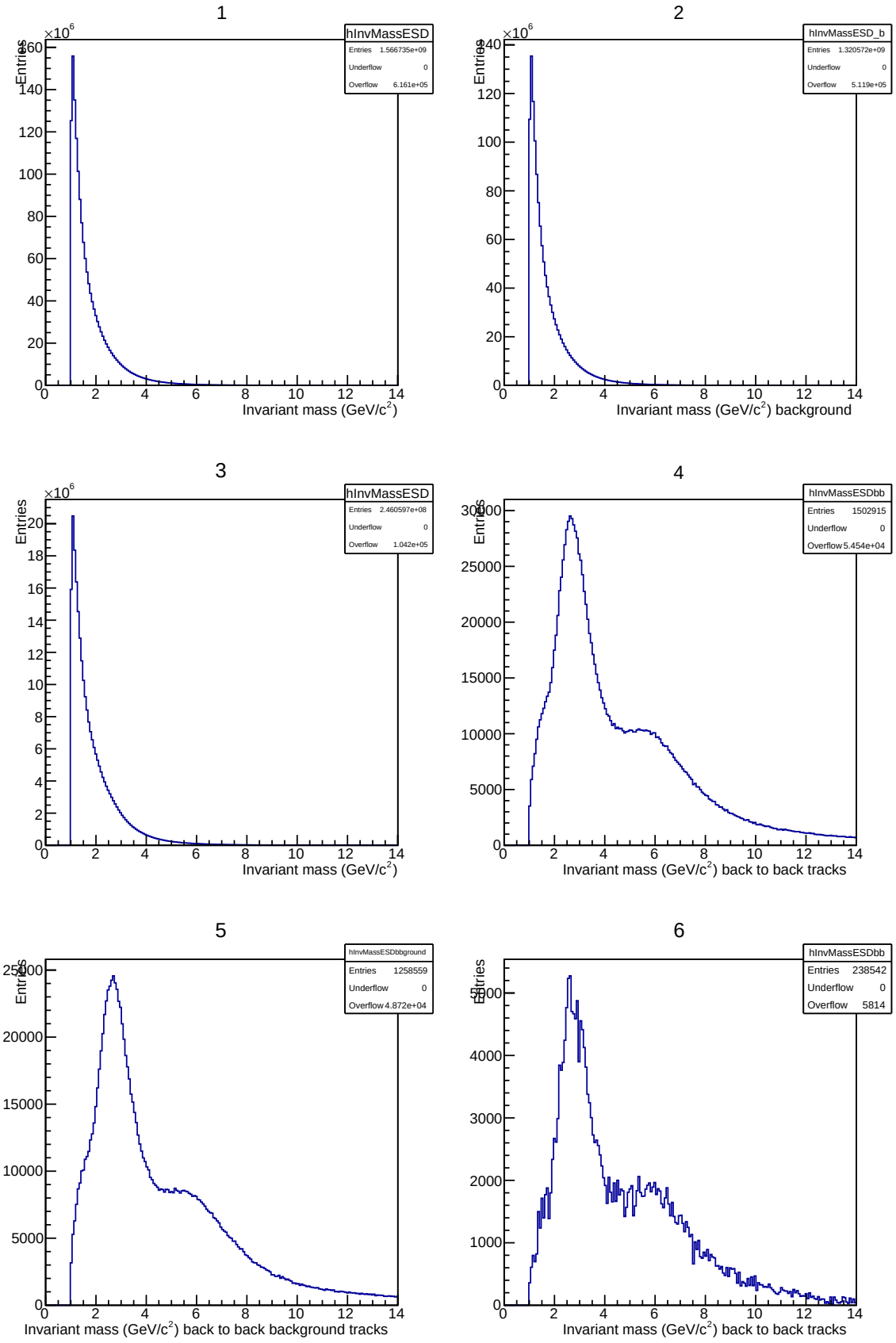

Figure 60: Invariant mass plots from the ESD data.

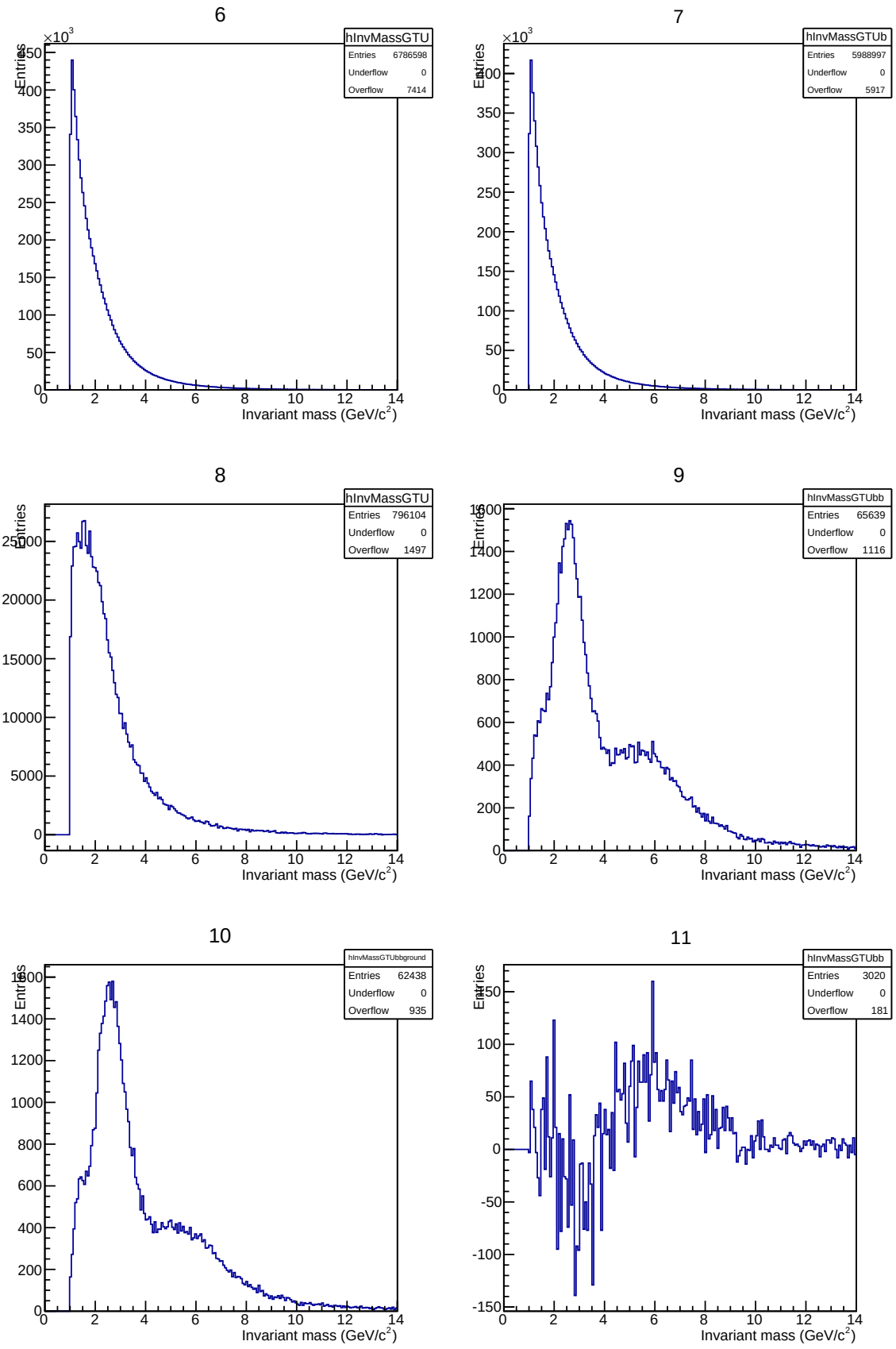

Figure 61: Invariant mass plots from the GTU data.

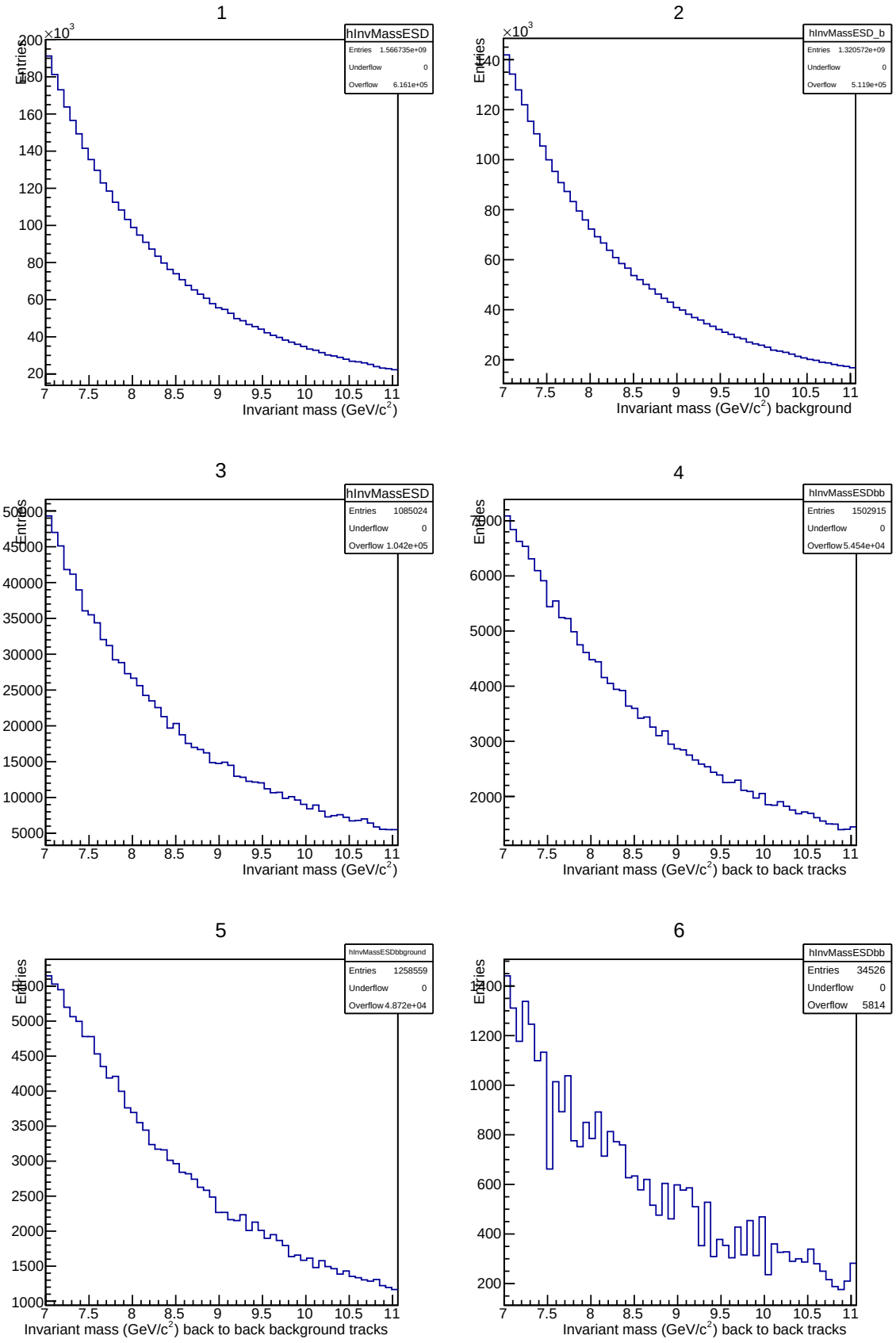

Figure 62: Invariant mass plots from the ESD data, showing the range $p_T = [7, 11]$ GeV.

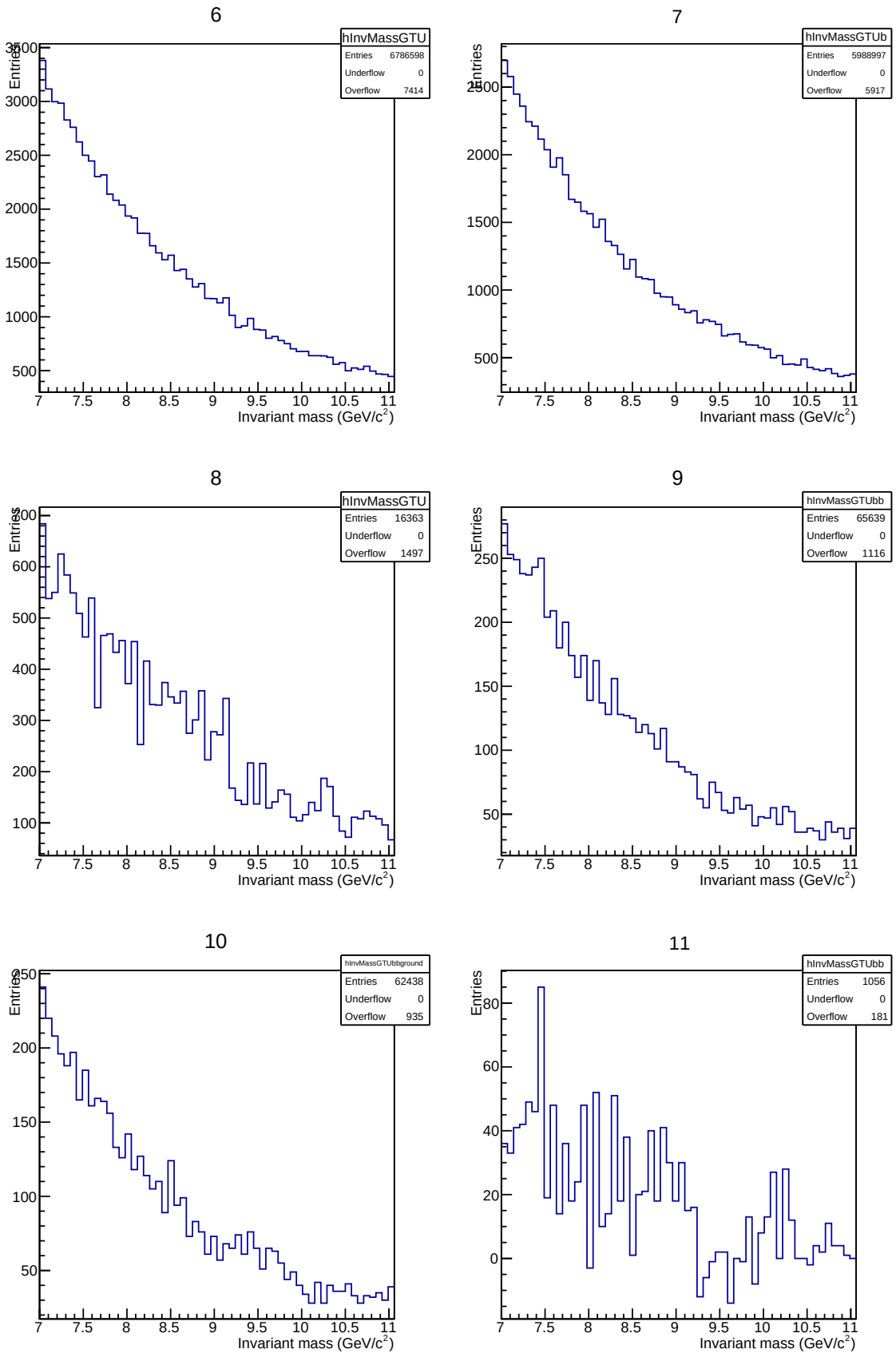

Figure 63: Invariant mass plots from the GTU data, showing the range $p_T = [7, 11]$ GeV.

4.9.4 Analysis on the LHC13f_AOD dataset (di-muon)

The analysis is also possible with muons detected from central barrel detectors, not from the muon arm, here avoided through a selection in rapidity. Note that this rapidity selection is included in the condition for the GTU signal, since the ESD information might include tracks from the muon arm. The only difference to the analysis presented in the chapter before is the setting of GetPID()=1 (for muons) instead of 0 (for electrons). This analysis also includes only run number197388 from LHC13f dataset. For the meaning of the plots see the chapter before, the numbering scheme is the same. The peak around 3.1 GeV/c^2, visible in figure 64 plot 4,5 and 6 and figure 64 plot 9 and 10 might be the J/Ψ-resonance.

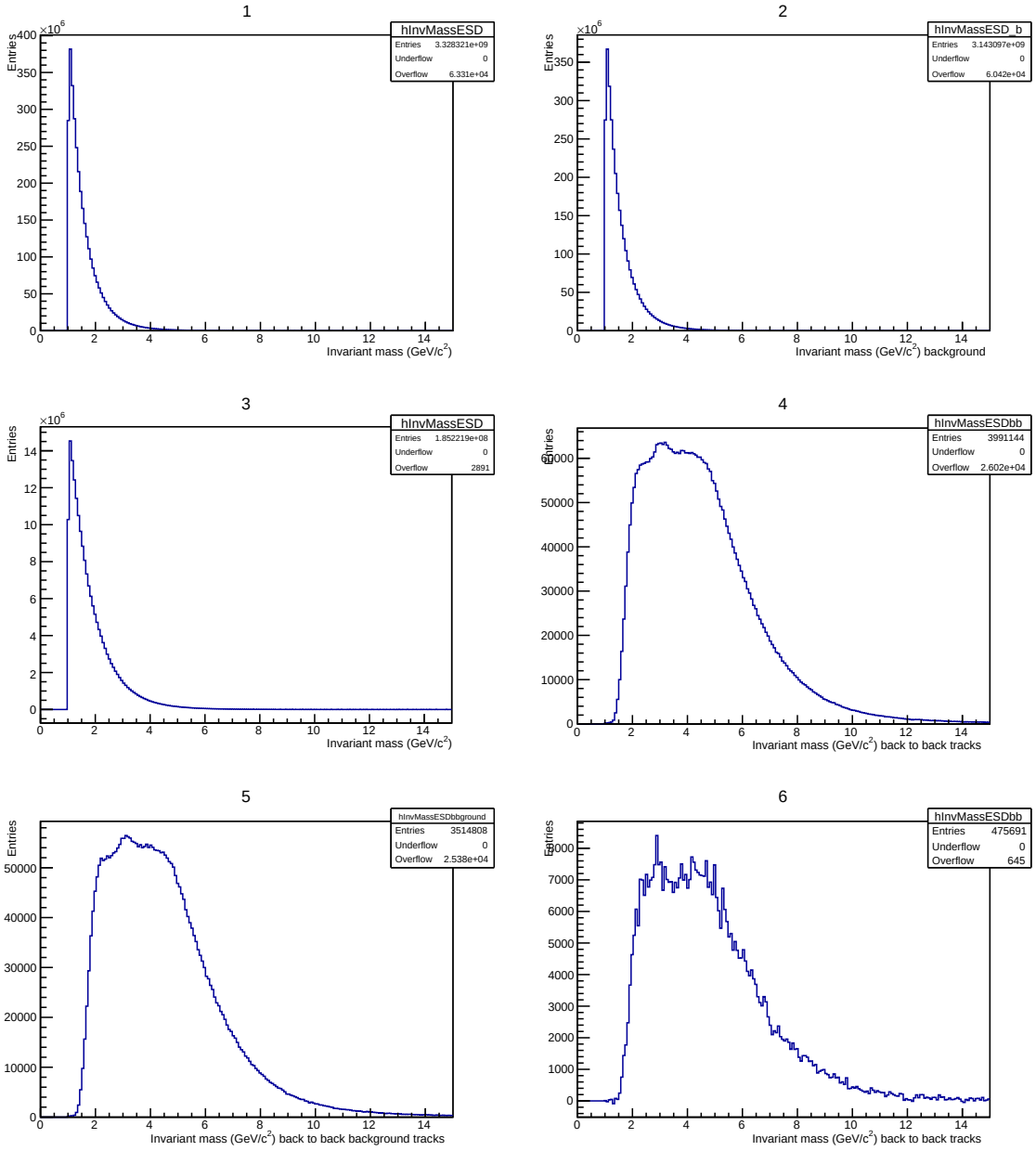

Figure 64: Invariant mass plots from the ESD data.

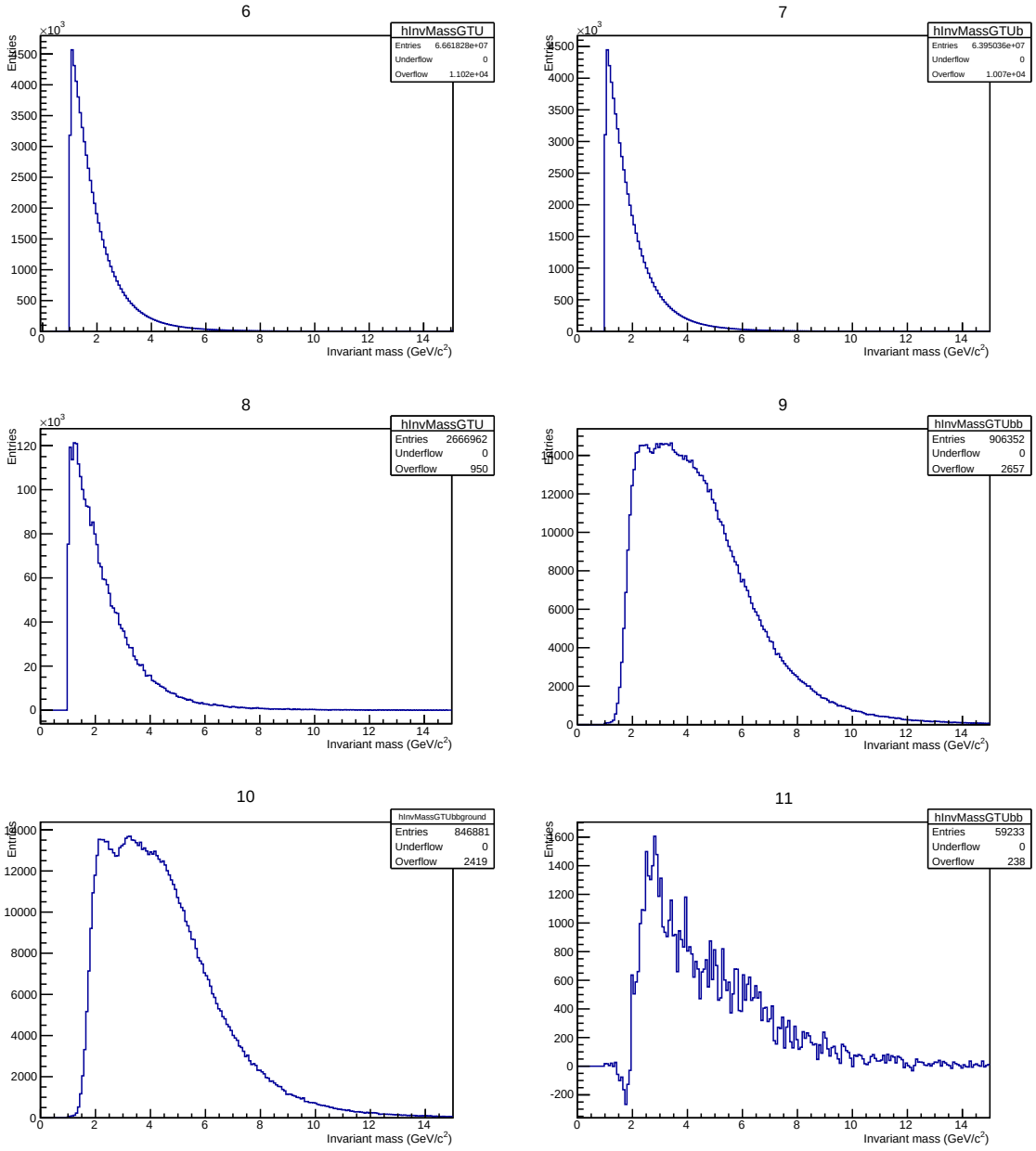

Figure 65: Invariant mass plots from the GTU data.

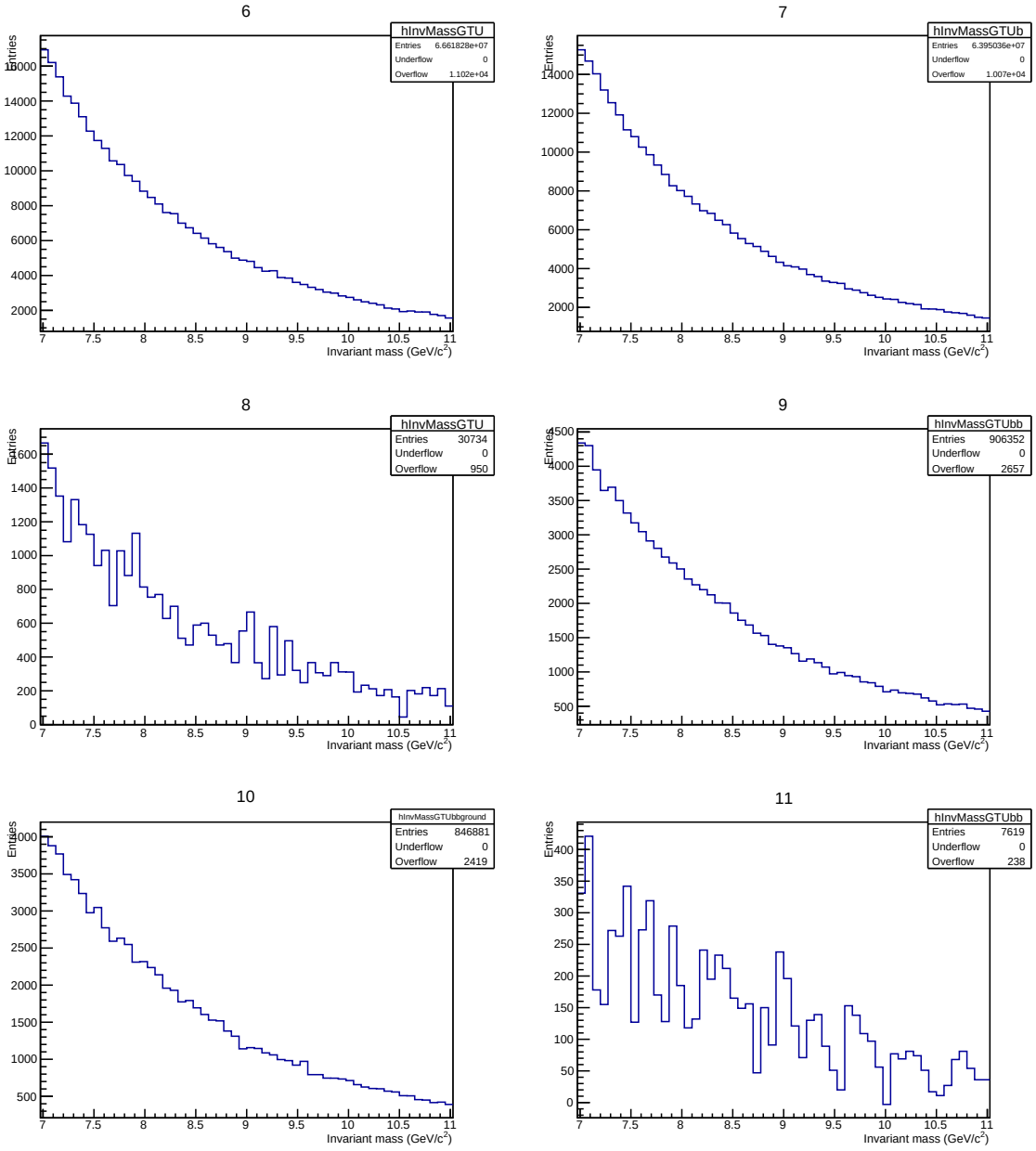

Figure 66: Invariant mass plots from the GTU data, showing the range $p_T = [7, 11]$ GeV.

5 Conclusion

This thesis included several detailed descriptions of methods and some comparisons to existing studies. The framework for the simulation of the three different Υ-states 1S, 2S and 3S was described and also the analysis on simulation data and measured data. Further research on this trigger can be based on the information given here. For this reason the sourcecode is given in the appendix, too.
The efficiency and acceptance found here follows the ranges of other experiments (CMS was mentioned before). The influence of some parameters (eta, phi cuts, geometrical acceptance of the TRD) was evaluated. Finally the implementation of the presented cuts in analysis code was done for the ESD and GTU data; the latter having no TRD information available so far, respectively needing further functions in the analysis code. Unfortunately the results lack sufficient statistics, why the analysis has to be rerun on larger datasets to reduce statistic fluctuations. Anyhow this thesis furnished a proof of concept on filtering the events.
Through this analysis of very large datasets, it might be possible to measure a satisfactory signal in pp, p-Pb and even Pb-Pb. It might be even possible to find additional meson resonances with di-lepton decay, especially di-electron or di-muon. As p_T cuts on single particles are not that efficient for the Υ-signal as the cuts on lepton pairs shown in this thesis, using data from the other existing TRD triggers is recommended to enhance the signal. In addition it might be also a possibility to make cuts smaller in $\Delta\phi$. The filter function concerning $\Delta\phi/p_T$ can be a useful purpose for the High Level Trigger instead of only compressing data. A requirement for this would be checking pairs of electrons for the fulfilment of this condition in a very fast time.

6 Appendix

6.1 Theory

6.1.1 Color superconductor

A color superconductor is equivalent to the superconductor for electrical currents. The quarks form cooper pairs, which attract each other under the exchange of gluons. Because of the different flavour and color charges of the quarks there are more types of color superconductors possible than of electrical superconductors. These additional parameters make the predictions from theoretical calculations more complicated.
In a color superconductor gluon properties can change. One possibility is that it becomes massive, when it interacts with cooper pairs made of quarks. The other possibility is the mixing of gluons with photons. [Alf08]

6.1.2 Invariant mass

The invariant mass is a good parameter to calculate particle collisions or decays. The mass M_x of a particle X which decays can be reconstructed through the invariant mass:

$$M_X^2 c^4 = \left(\sum_i E_i\right)^2 - \left(\sum_i p_i c\right)^2$$

E_i is the energy and p_i is the momentum of one daughter particle i after the decay. The spectrum of the invariant mass shows the decayed particles as peaks. [Pov06]

6.1.3 Rapidity and pseudorapidity

For the definition of rapidity and pseudorapidity the space-time momentum vector p^μ is needed:

$$p^\mu = (p^0, p^1, p^2, p^3) = (E, \mathrm{p}) = (E, \mathrm{p}_t, p_z) = (E, p_x, p_y, p_z)$$

Rapidity is defined as:

$$\mathrm{y} = \frac{1}{2}\ln\left(\frac{p_0 + p_z}{p_0 - p_z}\right)$$

It is a dimensionless quantity. More useful for experiments is the use of pseudorapidity:

$$\mathrm{y} = \frac{1}{2}\ln\left(\frac{|\mathrm{p}| + p_z}{|\mathrm{p}| - p_z}\right)$$

It is easier to use because momentum and energy have to be measured for the calculation of rapidity, whereas to calculate the pseudorapidity the angle θ between beamline and the direction of momentum p is required:

$$\mathrm{y} = -\ln[\tan(\frac{\theta}{2})]$$

The ALICE TRD covers the range in eta (pseudorapidity) from -0.9 up to 0.9, which is nearly 45°. In a relativistic approximation both values are nearly the same. [Won94]

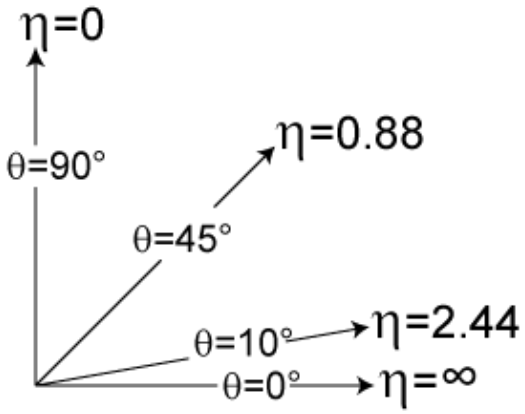

Figure 67: Some values in pseudorapidity and angle θ [wiki3]

6.1.4 Center of mass energy

The center of mass energy is defined as [PDG12]:

$$\sqrt{s} = \sqrt{\left(\sum_{i=1}^{n} P_i^{\mu}\right)^2}$$

P_i^{μ} is the four momentum vector of the colliding particle i. Two colliding protons (in the LHC) have a center of mass energy of:

$$\sqrt{s} = \sqrt{\left(\begin{pmatrix} E \\ p_x \\ p_y \\ p_z \end{pmatrix} + \begin{pmatrix} E \\ -p_x \\ -p_y \\ -p_z \end{pmatrix}\right)^2} = 2 \cdot E$$

For different masses the calculation is more complicated [ALI04] (for atoms):

$$\sqrt{s_{NN}} = E_{\text{per beam}} \cdot \sqrt{\frac{Z_1 Z_2}{A_1 A_2}}$$

Z_i is the number of protons in the nucleus, A_i the total number of nucleons. The index NN means that the center of mass energy is given per nucleon-nucleon pair. [ALI04]

6.1.5 Rapidity shift

In p-Pb collisions at the LHC there occurs an asymmetric effect. Due to their design, the magnets appropriated in the LHC have the same magnetic rigidity for the two beams:

$$p_{\text{Pb}} = Q \cdot p_{\text{proton}}$$

$Q = Z = 82$ is the atomic number of the used lead isotope $^{208}_{82}$Pb. The result is a shift in rapidity of:

$$\Delta y \approx \frac{1}{2}\log\frac{Z_1 A_2}{A_1 Z_2} = 0.46$$

Because of this shift in central rapidity in p-Pb collisions, the experiment will take p-Pb and Pb-p runs to exclude symmetric effects. The shift means that all tracks are deflected in direction of the lighter proton beam. [lhc11]

6.1.6 Coordinate system of ALICE

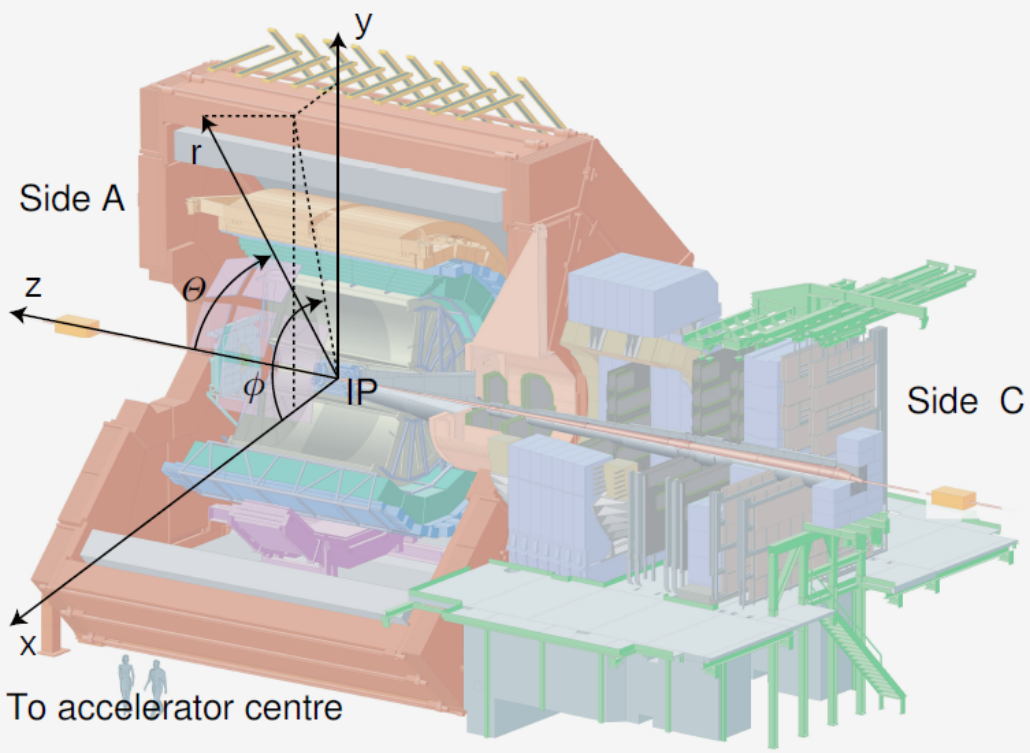

Figure 68: ALICE coordinate system [Heß11] (Definition of coordinates after[Be+03])

For the calculation of rapidity from Θ see 6.1.3.

6.2 Experimental Results

6.2.1 Upsilon parametrizations in Aliroot

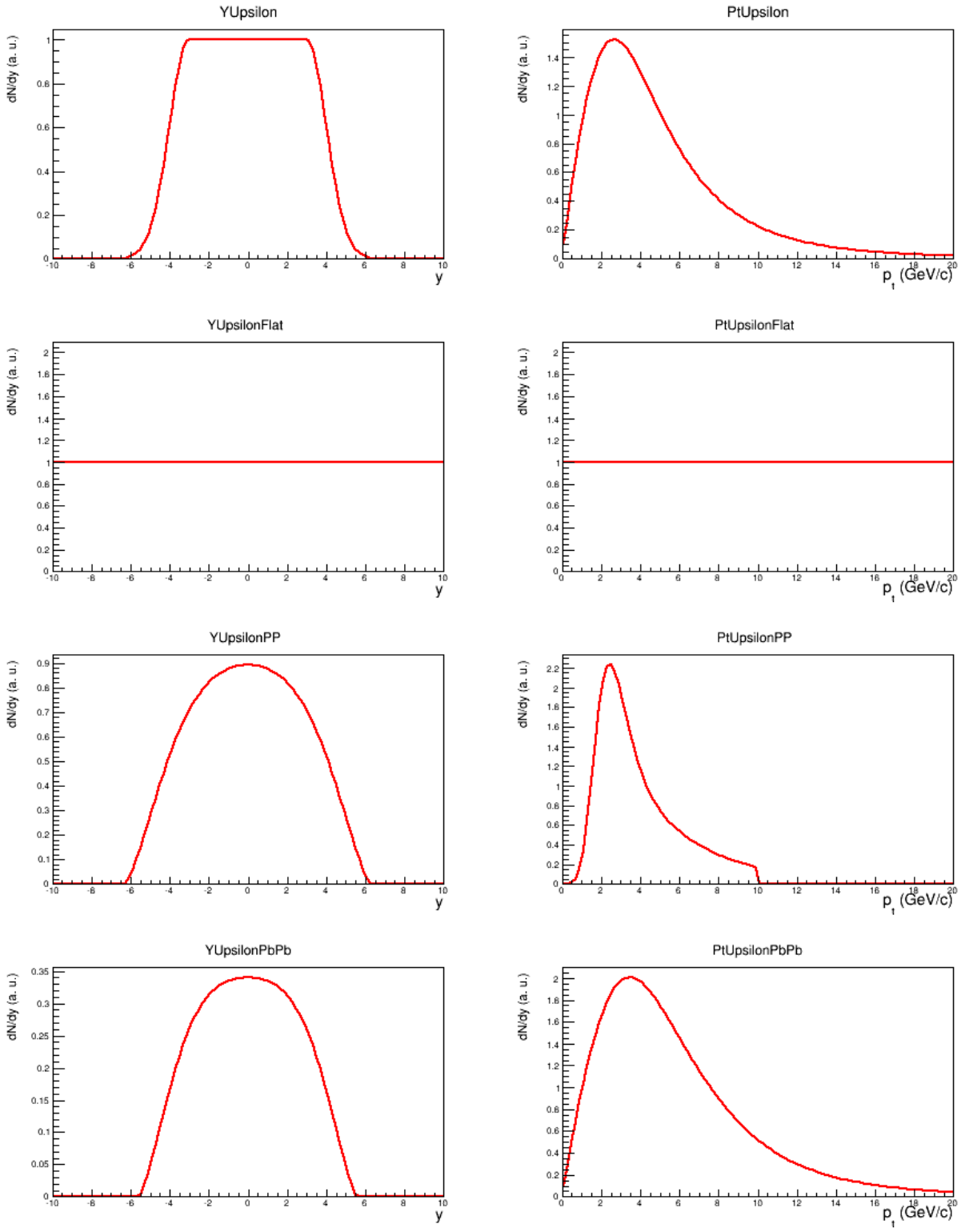

Figure 69: Parametrizations from the class AliGenMUONlib used by AliGenParam, part 1.

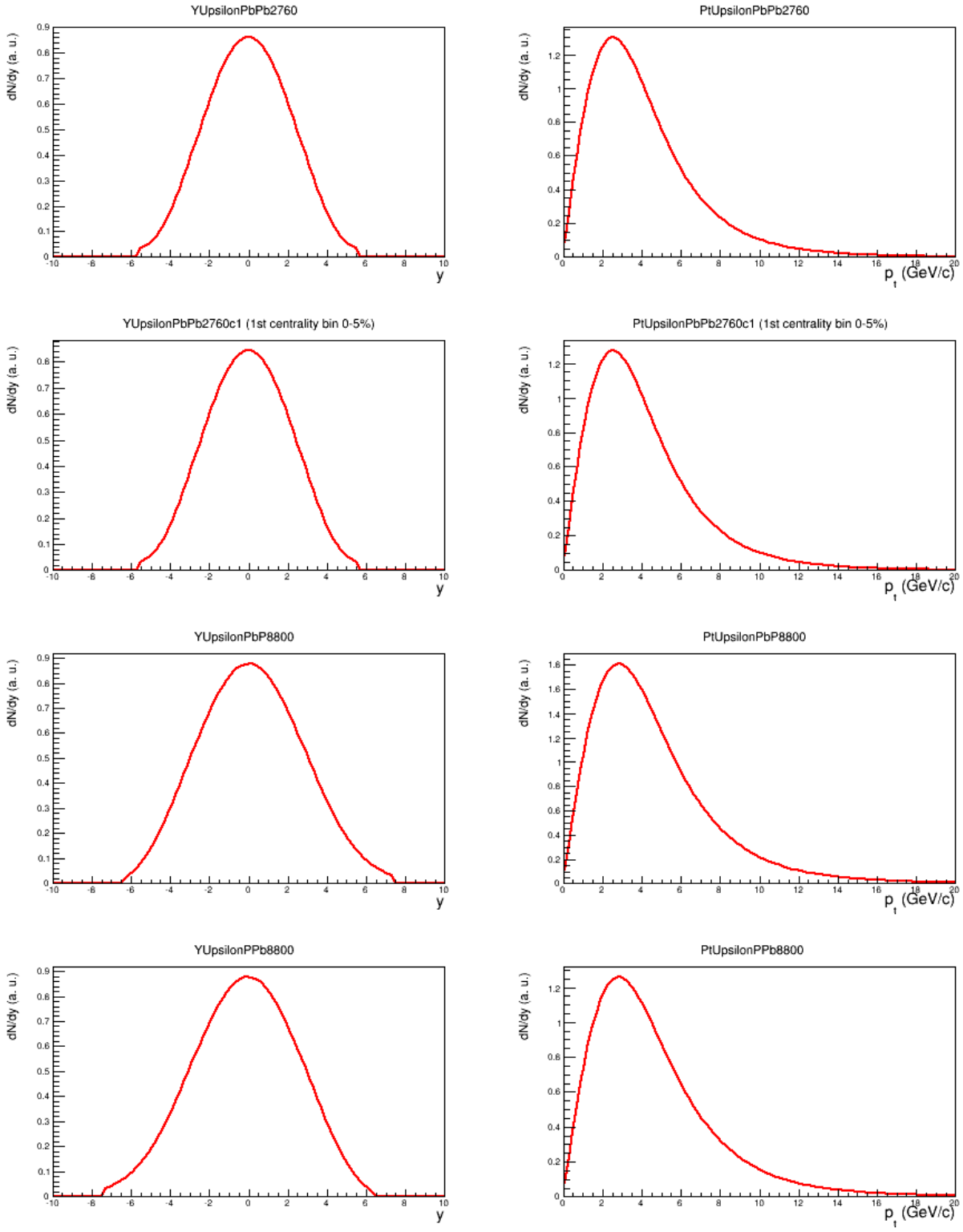

Figure 70: Parametrizations from the class AliGenMUONlib used by AliGenParam, part 2.

6.2.2 Functions SetChildYRange and SetChildThetaRange in Aliroot

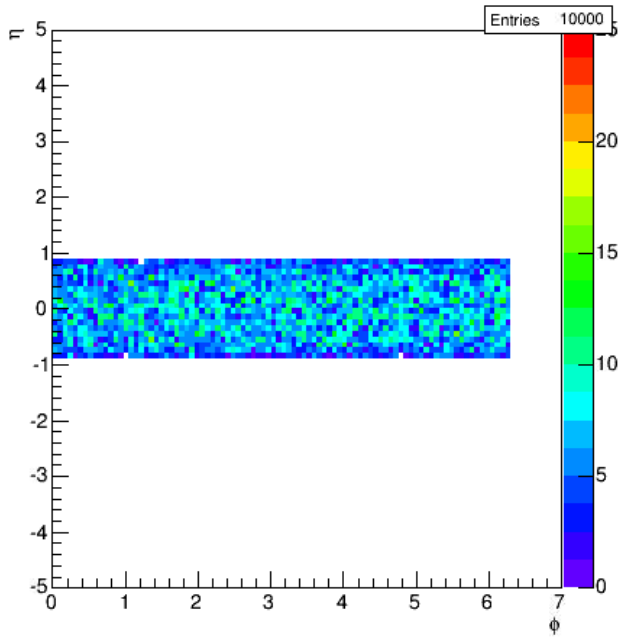

Figure 71: First electron daughter particle from Υ-particle with settings: gener->SetChildYRange(-5,5); gener->SetChildThetaRange(45.,135.);

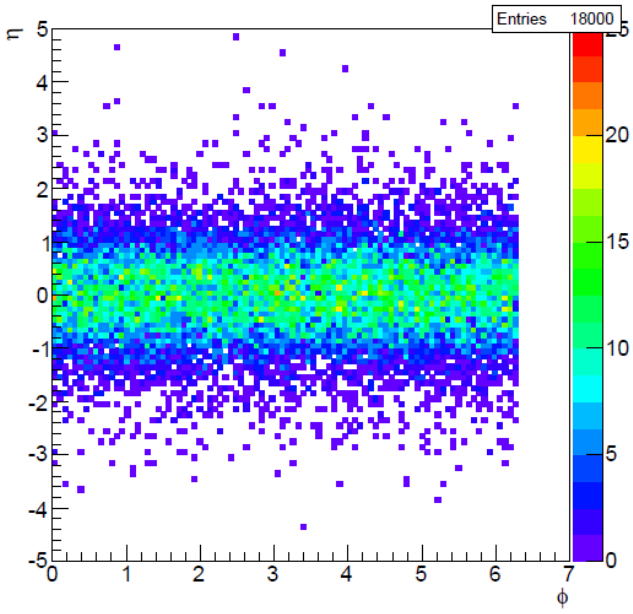

Figure 72: First electron daughter particle from Υ-particle with no cuts on child particle.

6.2.3 Acceptance of upsilon particle in units of pseudorapidity

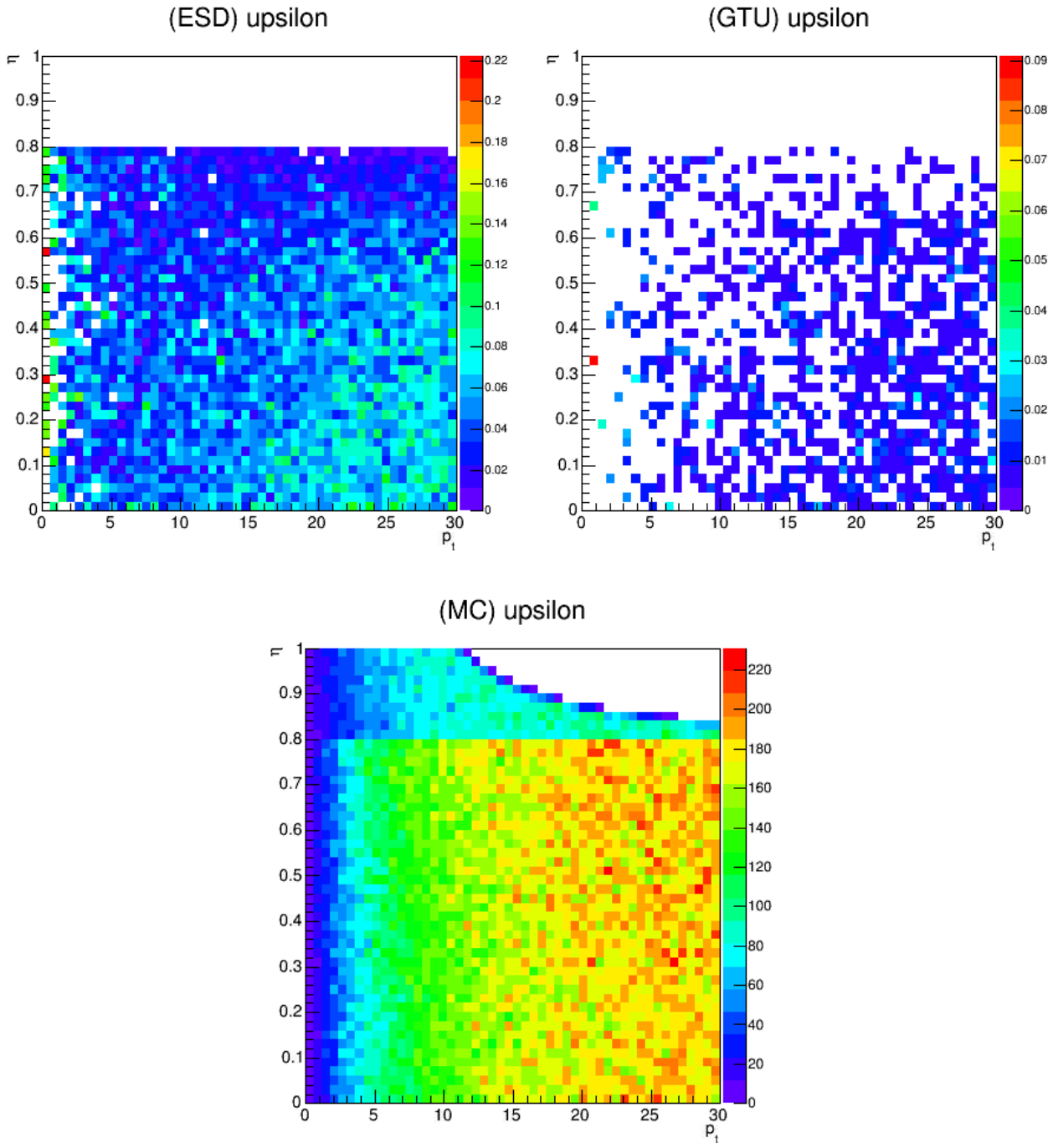

Figure 73: Acceptance for Υ-mesons - pseudorapitdity distribution - from a simulation up to 30 GeV p_T. The left plot shows the acceptance for Υ-mesons when the two decay tracks are existing ESD tracks. The right side shows the same for two GTU tracks from the decay. The bottom plot shows the simulated Monte Carlo Υ distribution. Cuts at all particles with $\eta = [-0.8, 0.8]$ (inclusive).

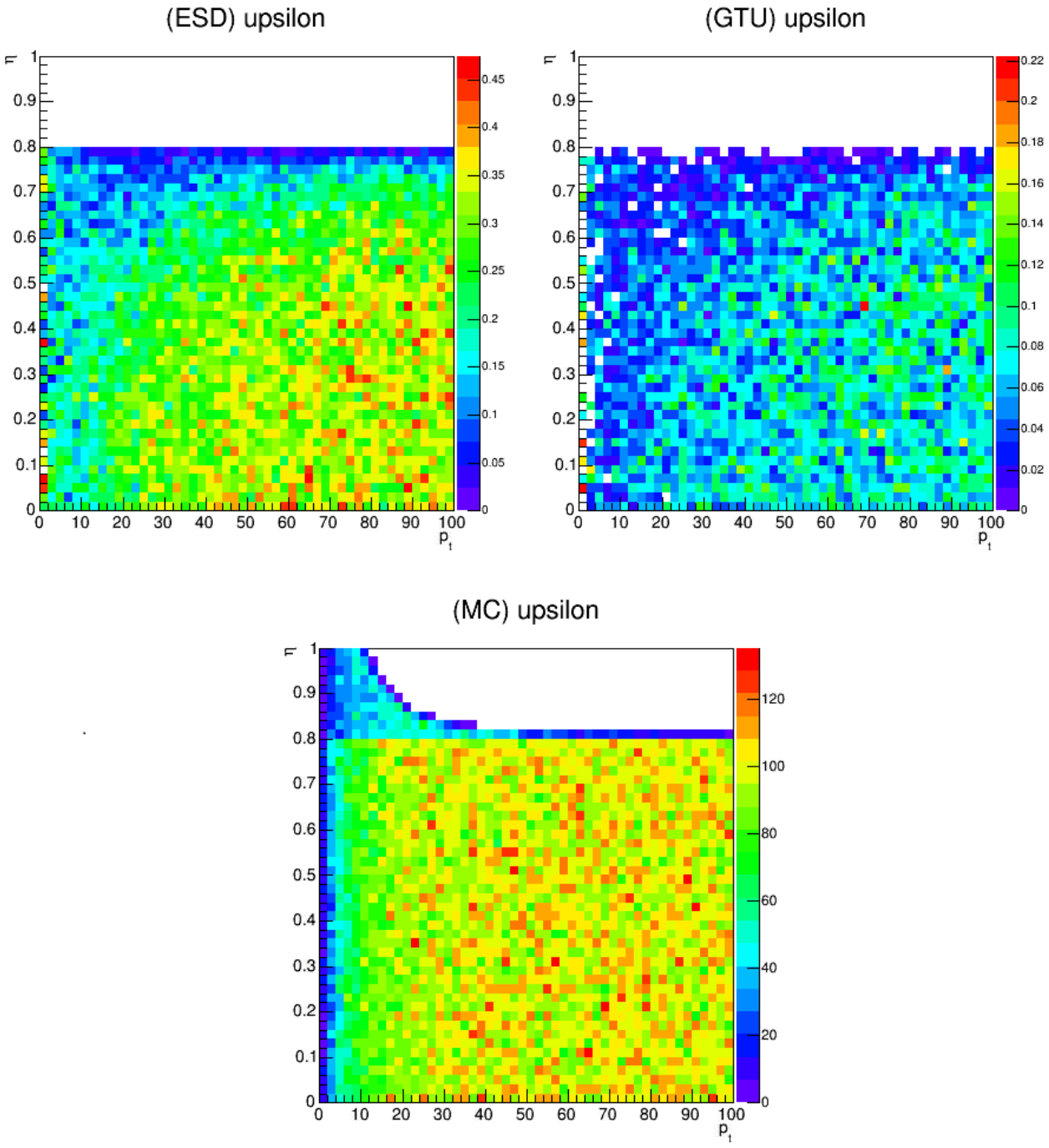

Figure 74: Acceptance for Υ-mesons - pseudorapitdity distribution - from a simulation up to 100 GeV p_T. The left plot shows the acceptance for Υ-mesons when the two decay tracks are existing ESD tracks. The right side shows the same for two GTU tracks from the decay. The bottom plot shows the simulated Monte Carlo Υ distribution. Cuts at all particles with $\eta = [-0.8, 0.8]$ (inclusive).

6.2.4 Numbering of the TRD sectors

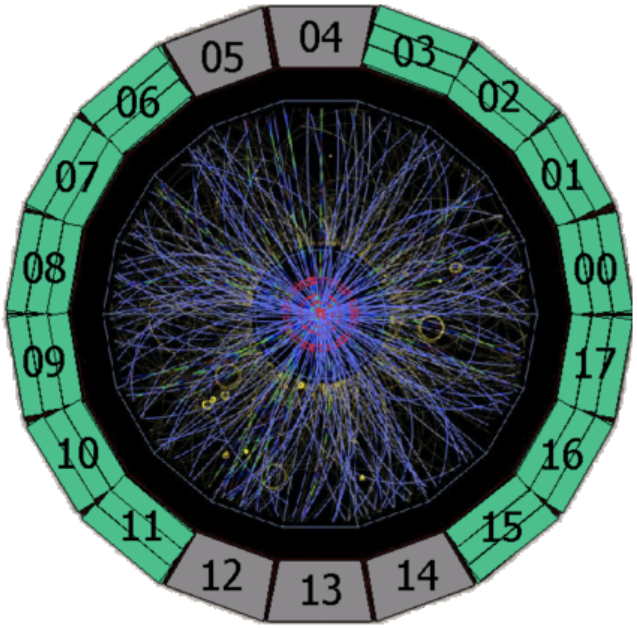

Figure 75: Numbering of the TRD supermodules. Green sectors represent installed moduls (status at begin of a long shutdown feb. 2014).

6.2.5 Data points for fit functions for transverse momentum cuts

low threshold p_T	$\Delta\phi$
5	3.1
10	1.5
15	1.0
20	0.7
25	0.5
30	0.4
high threshold p_T	$\Delta\phi$
15	3.1
20	1.3
25	1.0
30	0.9

Table 6

6.2.6 100GEV upsilon simulation

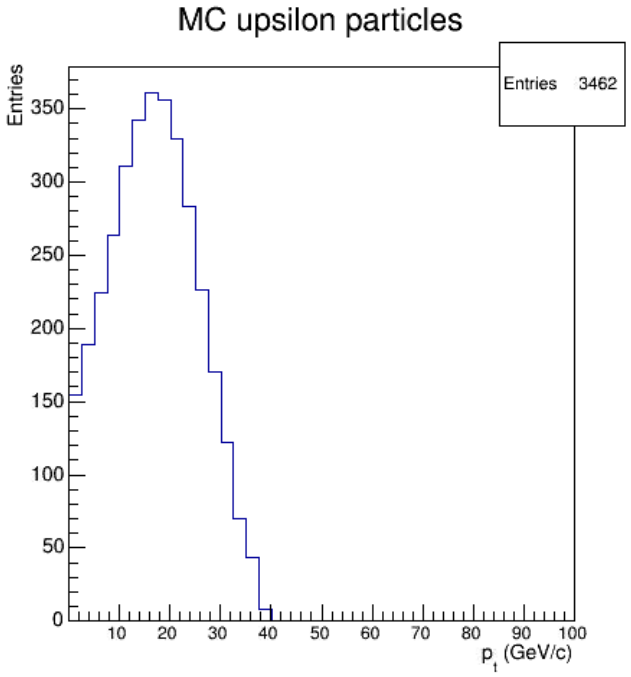

Figure 76: High p_T simulation up to 100GeV Υ-particles, with η=[-0.8,0.8] cut on decay leptons. No signal greater than 40GeV.

6.2.7 Full listing of AliTRDUpsilonTask.cxx source code

```
//-----------------------------------------------------
//
// This is the AliTRDUpsilonTask written by martin.kohn@cern.ch
// based on the macro:
//    This is the PROOF-enabled version of TRD/Macros/AliTRDComparisonV2.C macro
    .
//    Origin:  Andrei.Zalite@cern.ch
//
//-----------------------------------------------------
#include "TChain.h"
#include "TTree.h"
#include "TH1F.h"
#include "TH2F.h"
#include "TList.h"
#include "TClonesArray.h"
#include "TCanvas.h"
#include "TFile.h"
#include "TLorentzVector.h" // for invariantmass
#include "TNtuple.h" // for easier local analysis
#include "AliLog.h"
#include "AliVEvent.h"
#include "AliESDEvent.h"
#include "AliAODEvent.h"
#include "AliMCEvent.h"
#include "AliESDtrack.h"
#include "AliAODTrack.h"
#include "AliESDTrdTrack.h"
#include "AliTrackReference.h"
#include "AliStack.h"
#include "AliESDtrackCuts.h"

#include "AliPID.h"
#include "AliTRDUpsilonTask.h"
#include <iostream>
using namespace std;

ClassImp(AliTRDUpsilonTask)

AliTRDUpsilonTask::AliTRDUpsilonTask()
  : AliAnalysisTaskSE("AliTRDUpsilonTask"),
    fListOfHistos(0),
    hInvMassESD(0),
    hInvMassESD_b(0),
    hInvMassGTU(0),
    hInvMassGTUb(0),
    hInvMassGTUbb(0),
    hInvMassGTUbbground(0),
    hInvMassESDbb(0),
    hInvMassESDbbground(0),
    hInvMassESDbb_old(0),
    hInvMassESDbbground_old(0),
    check1(0),
    checkf(0),
    nTtracks(0)
{
  // Default constructor
  AliInfo("Default constructor AliTRDUpsilonTask");
  // Define input and output slots here
  // Input slot #0 works with a TChain
  DefineInput(0, TChain::Class());
  // Output slot #1 TList
  DefineOutput(1, TList::Class());
}

AliTRDUpsilonTask::AliTRDUpsilonTask(const char* name)
  : AliAnalysisTaskSE(name),
    fListOfHistos(0),
    hInvMassESD(0),
    hInvMassESD_b(0),
    hInvMassGTU(0),
    hInvMassGTUb(0),
    hInvMassGTUbb(0),
```

```
    hInvMassGTUbbground(0),
    hInvMassESDbb(0),
    hInvMassESDbbground(0),
    hInvMassESDbb_old(0),
    hInvMassESDbbground_old(0),
    check1(0),
    checkf(0),
    nTtracks(0)
{
  // Constructor
  AliInfo("Constructor AliTRDUpsilonTask");
  // Define input and output slots here
  // Input slot #0 works with a TChain
  DefineInput(0, TChain::Class());
  // Output slot #1 TList
  DefineOutput(1, TList::Class());
}

void AliTRDUpsilonTask::UserCreateOutputObjects()
{
  // Create histograms
  // Called once
  AliInfo("AliTRDUpsilonTask::UserCreateOutputObjects");
  // Create output container
  fListOfHistos = new TList();
  fListOfHistos->SetOwner(); // MANDATORY! To avoid leaks in merging

  hInvMassESD = new TH1F("hInvMassESD", "1; Invariant mass (GeV/c^{2}); Entries"
      , 200, 0., 14.);
  hInvMassESD_b = new TH1F("hInvMassESD_b", "2; Invariant mass (GeV/c^{2})
      background ; Entries", 200, 0., 14.);
  hInvMassGTU = new TH1F("hInvMassGTU", "ESD 2 true gtu tracks; Invariant mass (
      GeV/c^{2}); Entries", 200, 0., 14.); // one ot two tracks have a GTU track
  hInvMassGTUb = new TH1F("hInvMassGTUb", "ESD 2 true gtu tracks background;
      Invariant mass (GeV/c^{2}); Entries", 200, 0., 14.); // one ot two tracks
      have a GTU track
  hInvMassGTUbb = new TH1F("hInvMassGTUbb", "ESD 2 true gtu tracks back to back;
       Invariant mass (GeV/c^{2}); Entries", 200, 0., 14.); // one ot two tracks
       have a GTU track
  hInvMassGTUbbground = new TH1F("hInvMassGTUbbground", "ESD 2 true gtu tracks
      back to back background; Invariant mass (GeV/c^{2}); Entries", 200, 0.,
      14.); // one ot two tracks have a GTU track

  hInvMassESDbb = new TH1F("hInvMassESDbb", "4; Invariant mass (GeV/c^{2}) back
      to back tracks  ; Entries", 200, 0., 14.);
  hInvMassESDbbground = new TH1F("hInvMassESDbbground", "5; Invariant mass (GeV/
      c^{2}) back to back background tracks  ; Entries", 200, 0., 14.);

  hInvMassESDbb_old = new TH1F("hInvMassESDbb_old", "4; Invariant mass (GeV/c
      ^{2}) back to back tracks  ; Entries", 200, 0., 14.);
  hInvMassESDbbground_old = new TH1F("hInvMassESDbbground_old", "5; Invariant
      mass (GeV/c^{2}) back to back background tracks  ; Entries", 200, 0., 14.)
      ;

  check1 = new TH2F("check1", "delta phi versus p_{T}; p_{t} (GeV/c); #Delta #
      phi", 50, 0., 100., 50,0.,3.141);
  checkf = new TH2F("checkf", "delta phi versus p_{T}; p_{t} (GeV/c); #Delta #
      phi", 50, 0., 100., 50,0.,3.141);

  nTtracks = new TNtuple("tracks","tracks", "run:event:id:pt:px:py:pz:E:M:phi:
      eta:pid:charge");

  fListOfHistos->Add(hInvMassESD);
  fListOfHistos->Add(hInvMassESD_b);
  fListOfHistos->Add(hInvMassGTU);
  fListOfHistos->Add(hInvMassGTUb);
  fListOfHistos->Add(hInvMassGTUbb);
  fListOfHistos->Add(hInvMassGTUbbground);
  fListOfHistos->Add(hInvMassESDbb);
  fListOfHistos->Add(hInvMassESDbbground);

  fListOfHistos->Add(hInvMassESDbb_old);
```

```
  fListOfHistos->Add(hInvMassESDbbground_old);

  fListOfHistos->Add(check1);
  fListOfHistos->Add(checkf);

  fListOfHistos->Add(nTtracks);


  PostData(1, fListOfHistos);
}


void AliTRDUpsilonTask::UserExec(Option_t *)
{

  //runs for each event!

  ////////////////////////////////////
  //track cuts for reduction of fake tracks:
  AliESDtrackCuts* trackcut1 = new AliESDtrackCuts;
  trackcut1->SetMaxDCAToVertexXY(0.05);
  trackcut1->SetMaxDCAToVertexZ(0.5);
  //trackcut1->SetMaxDCAToVertexZ(0.50);
  //trackcut1->SetMaxDCAToVertexXY(0.50);
  //trackcut1->SetMaxDCAToVertexZPtDep("0.50pt");
  //trackcut1->SetMaxDCAToVertexXYPtDep("0.50pt");
  trackcut1->SetEtaRange( -0.8 , 0.8 );
  //trackcut1->SetPRange(4.,50.);
  trackcut1->SetAcceptKinkDaughters(kFALSE);
  //trackcut1->SetRequireITSRefit(kTRUE);
  trackcut1->SetRequireTPCRefit(kTRUE);
  trackcut1->SetPtRange(1.,1e30);
  trackcut1->SetMinNClustersTPC(70);
  trackcut1->SetMaxChi2PerClusterTPC(4);


  // Main loop
  // Called for each event

  //currently not used
  //TNtuple daughterinfo("daughterinfo", "the mc information of all daughters
      from upsilon decay", "x:y:z" ,32000);

  //invariant mass
  TLorentzVector mcfV1, mcfV2, mcfVtot;
  TLorentzVector esdfV1, esdfV2, esdfVtot;
  TLorentzVector gtufV1, gtufV2, gtufVtot;

  // for combined analysis with only one loop include esd event here
  // ESD information
  //AliESDEvent* esdEvent = InputEvent();
  AliVEvent* event = InputEvent();
  if (!event) {
    Printf("ERROR: Could not retrieve event");
    return;
  }

  // AliAODEvent* aodEvent = dynamic_cast<AliAODEvent*>(event);
  AliESDEvent* esdEvent = dynamic_cast<AliESDEvent*>(event);

Double_t E2, E3;
Double_t px2, px3;
Double_t py2, py3;
Double_t pz2, pz3;
TLorentzVector v2;

 Int_t naodtracks = esdEvent->GetNumberOfTracks(); // esd or aod

for (Int_t j = 0; j < naodtracks; j++) {
AliESDtrack* aodtrack = esdEvent->GetTrack(j);
//Find the pi(+). If this is the track of the pi(+), set the variables equal to
    the properties
```

```
//of the pi(+) and enter the next loop which finds the pi(-) and fills the
    histogram
if(aodtrack->Charge() == -1) {
//Double_t p=esdtrack->P();
E3 = aodtrack->E();

//cutting on electron, positrons flagd as electron with charge +
//if(!(aodtrack->GetMostProbablePID()==0)) continue; //aod
if(!(aodtrack->GetPID()==1)) continue; //esd


px3 = aodtrack->Px();
py3 = aodtrack->Py();
pz3 = aodtrack->Pz();

for(Int_t k = j+1; k < naodtracks; k++) {//importent j+1 (combinatorical) do not
     match track with itself

AliESDtrack* aodtrack2 = esdEvent->GetTrack(k);

//if(!(aodtrack2->GetMostProbablePID()==0)) continue;   //aod
if(!(aodtrack2->GetPID()==1)) continue;   //esd was getpid


if(aodtrack2->Charge() == 1) {     //positron
//check1->Fill(aodtrack->Pt()+aodtrack2->Pt(),DeltaPhi(aodtrack->Phi(),aodtrack2
    ->Phi()));

E2 =aodtrack2->E();
px2 = aodtrack2->Px();
py2 = aodtrack2->Py();
pz2 = aodtrack2->Pz();
v2.SetE(E2 + E3);
v2.SetPx(px2 + px3);
v2.SetPy(py2 + py3);
v2.SetPz(pz2 + pz3);
if (v2.Mag()<1.) continue; // Cut below 1GEV
hInvMassESD->Fill(v2.Mag());

////////////////////////////////////////////
///TRD TRACKS
////////////////////////////////////////////

Int_t nesdtrdtracks =0;
if (esdEvent->GetNumberOfTrdTracks())
{
        nesdtrdtracks = esdEvent->GetNumberOfTrdTracks();
}
else{}
if((esdEvent->GetTrdTrack(j))||(esdEvent->GetTrdTrack(k)))
{hInvMassGTU->Fill(v2.Mag());}

////////////////////////////////////////////////////
///     backtoback
////////////////////////////////////////////////////


if (FilterMomentum(aodtrack->Pt(),aodtrack2->Pt(),aodtrack->Phi(),aodtrack2->Phi
    (),aodtrack->Eta(),aodtrack2->Eta() ))
{
if((esdEvent->GetTrdTrack(j))||(esdEvent->GetTrdTrack(k)))
 {hInvMassGTUbb->Fill(v2.Mag());}
hInvMassESDbb->Fill(v2.Mag());
checkf->Fill(aodtrack->Pt()+aodtrack2->Pt(),DeltaPhi(aodtrack->Phi(),aodtrack2->
    Phi()));
}

//old cuts (170 up to 190 degrees)
if (FilterMomentumOld(aodtrack->Pt(),aodtrack2->Pt(),aodtrack->Phi(),aodtrack2->
    Phi()))
{
 hInvMassESDbb_old->Fill(v2.Mag());
```

```
}

}//end positron

//////////////////////////////////////
//////////////////////////////////////
///// BACKGROUND

if(aodtrack2->Charge() == -1) {

E2 =aodtrack2->E();
px2 = aodtrack2->Px();
py2 = aodtrack2->Py();
pz2 = aodtrack2->Pz();
v2.SetE(E2 + E3);
v2.SetPx(px2 + px3);
v2.SetPy(py2 + py3);
v2.SetPz(pz2 + pz3);
if (v2.Mag()<1.) continue; // Cut below 1GEV
hInvMassESD_b->Fill(v2.Mag());    //unfiltered

if((esdEvent->GetTrdTrack(j))||(esdEvent->GetTrdTrack(k)))
 {hInvMassGTUb->Fill(v2.Mag());}


if (FilterMomentum(aodtrack->Pt(),aodtrack2->Pt(),aodtrack->Phi(),aodtrack2->Phi
    (),aodtrack->Eta(),aodtrack2->Eta()))
 {
if((esdEvent->GetTrdTrack(j))||(esdEvent->GetTrdTrack(k)))
 {hInvMassGTUbbground->Fill(v2.Mag());}

hInvMassESDbbground->Fill(v2.Mag());
checkf->Fill(aodtrack->Pt()+aodtrack2->Pt(),DeltaPhi(aodtrack->Phi(),aodtrack2->
    Phi()));
 }
//old cuts
if (FilterMomentumOld(aodtrack->Pt(),aodtrack2->Pt(),aodtrack->Phi(),aodtrack2->
    Phi()))
{
        hInvMassESDbbground_old->Fill(v2.Mag());
}
}
} // fi second esdtrack          } // charge ==1
} //fi esdtracks

  // Post output data.
 PostData(1, fListOfHistos);
}

}// end of user exec

//________________________________________________________________________
void AliTRDUpsilonTask::Terminate(Option_t *) {
  // Draw result to the screen
  // Called once at the end of the query
  fListOfHistos = dynamic_cast<TList*>(GetOutputData(1));
  if (!fListOfHistos) {
    Printf("ERROR: fListOfHistos not available");
    return;
  }

  hInvMassESD = dynamic_cast<TH1F*>(fListOfHistos->At(0));
  hInvMassESD_b = dynamic_cast<TH1F*>(fListOfHistos->At(1));
  hInvMassGTU = dynamic_cast<TH1F*>(fListOfHistos->At(2));
  hInvMassGTUb = dynamic_cast<TH1F*>(fListOfHistos->At(3));
  hInvMassGTUbb = dynamic_cast<TH1F*>(fListOfHistos->At(4));
  hInvMassGTUbbground = dynamic_cast<TH1F*>(fListOfHistos->At(5));
  hInvMassESDbb = dynamic_cast<TH1F*>(fListOfHistos->At(6));
  hInvMassESDbbground = dynamic_cast<TH1F*>(fListOfHistos->At(7));
  hInvMassESDbb_old = dynamic_cast<TH1F*>(fListOfHistos->At(8));
  hInvMassESDbbground_old = dynamic_cast<TH1F*>(fListOfHistos->At(9));
```

```
  check1 = dynamic_cast<TH2F*>(fListOfHistos->At(10));
  checkf = dynamic_cast<TH2F*>(fListOfHistos->At(11));

  nTtracks = dynamic_cast<TNtuple*>(fListOfHistos->At(12));

  TFile fc("Pt.ESD.1.root","RECREATE");

  hInvMassESD->Write();
  hInvMassESD_b->Write();
  hInvMassGTU->Write();
  hInvMassGTUb->Write();
  hInvMassGTUbb->Write();
  hInvMassGTUbbground->Write();
  hInvMassESDbb->Write();
  hInvMassESDbbground->Write();
  hInvMassESDbb_old->Write();
  hInvMassESDbbground_old->Write();
  checkf->Write();

  fc.Write();

  fc.Close();
  Printf("Written result to Pt.ESD.1.root");
}


bool AliTRDUpsilonTask::FilterMomentum(Double_t pT1,Double_t pT2,Double_t phi1,
    Double_t phi2, Double_t eta1,Double_t eta2) {
Double_t diff = phi1 - phi2;
if (diff>3.141)
      {
 Double_t x=diff;
 diff = 3.141-(x-3.141);
  }
  else
  {
         //change nothing in this case
   }
        Double_t pTsum = pT1+pT2;

        if(pTsum<9.) return 0;
        if((TMath::Abs(eta1-eta2))>1) return 0;

        //Double_t diff2 = diff;
        if(pTsum < 30)
  {if ( (diff>( exp(1.612-0.105*pTsum) )) && (diff < (exp( 5.938-0.343*pTsum )
      +0.905 )) )
   { return 1;}else{return 0;}}

        if((pTsum>30)&&(pTsum<60))
  {if (diff<(1.336-(0.0140*pTsum)))
   { return 1;}else{return 0;}
  }

        if(pTsum>60)
  {if (diff<0.5)
  { return 1;}else{ return 0;}
  }

}

bool AliTRDUpsilonTask::FilterMomentumOld(Double_t pT1,Double_t pT2,Double_t
    phi1,Double_t phi2) {
Double_t diff = phi1 - phi2;
 if (diff>3.141)
   {
        Double_t x=diff;
        diff = 3.141-(x-3.141);
   }
        else
   {
```

```
          //change nothing in this case
    }

Double_t pTsum = pT1+pT2;

 if (diff<(exp(1.00082-0.069216*pTsum)) || diff >(exp(1.17245-0.0458376*pTsum)))
 { return 0;
 }
        else
        { return 1;
  }
}

Double_t AliTRDUpsilonTask::DeltaPhi(Double_t phi1,Double_t phi2) {
Double_t diff = phi1 - phi2;
        if (diff>3.141)
  {
          Double_t x=diff;
          diff = 3.141-(x-3.141);
  }
  else
  {
          //change nothing in this case
  }
        return diff;
}
```

6.2.8 AliEVE

AliRoot has a build-in visualization tool (AliEVE)[47] for displaying events with all tracks and detector signals (clusters).
It can access local data and also data from the Grid. Whereas the use with files from the Grid is documented on the web page, the syntax for local data is given here.
To display each event one by one, run the following line in the directory with the data files (AliESDs.root):

```
alieve visscan_local.C
```

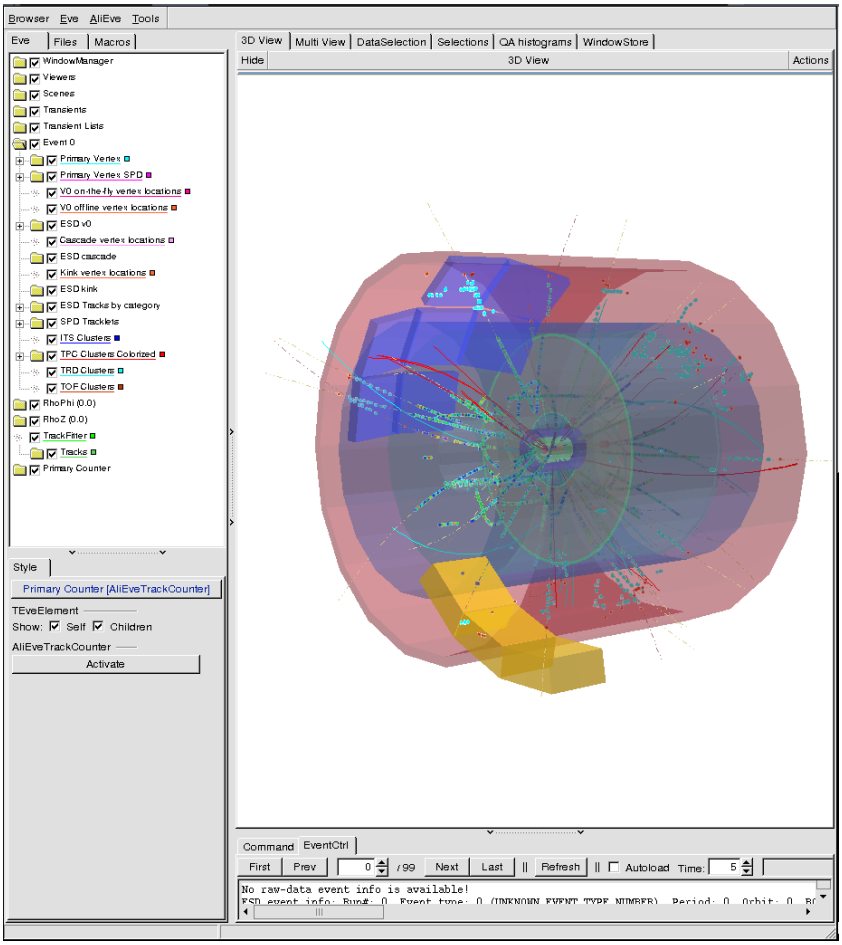

Figure 77: 3D view in AliEVE on a simulation of Υ-particle with pp background data.

If AliEVE is executed for the first time, it takes some minutes for AliRoot to compile the required libraries. After the compilation it displays event number 0 with the given detector structures in visscan_local.C. In the bottom menu one can navigate through the different events.
In the 3D view, as shown in figure 77, the navigation follows standard principles on mouse input[48].

[47] http://aliweb.cern.ch/Offline/Activities/Visualisation/index.html

[48] Usage: mouse wheel or right mouse button down: Zoom; left button down: change angle; both mouse buttons down: move total object

7 Bibliography

[ain12] https://aliceinfo.cern.ch/Figure/node/3402 - 13.09.12

[ADr09] Axel Drees, Stony Brook University, Stony Brook, NY 11777, USA, Dileptons And Photons At RHIC Energies, Nuclear Physics A 830 (2009) 435c-442c http://dx.doi.org/10.1016/j.nuclphysa.2009.10.036

[Alf08] Mark G. Alford, Krishna Rajagopal, Thomas Schaefer, Andreas Schmitt - Color superconductivity in dense quark matter - v.2 2008 - arXiv:0709.4635 [hep-ph]

[ALI01] ALICE Collaboration, ALICE Transition Radiation Detector : Technical Design Report ALICE-TDR-9 ; CERN-LHCC-2001-021 - Geneva : CERN, 3 October 2001

[ALI04] ALICE Collaboration, ALICE: Physics Performance Report, Volume I J. Phys. G: Nucl. Part. Phys. 30 (2004) 1517-1763 doi:10.1088/0954-3899/30/11/001

[ALi07] ALICE Collaboration, The ALICE Offline Bible, http://aliweb.cern.ch/Offline/AliRoot/Manual.html - 2007

[ALI08] K. Aamodt, et al. [ALICE Collaboration], The ALICE experiment at the CERN LHC doi:10.1088/1748-0221/3/08/S08002

[An+11] A. Andronic, J.P. Wessels, Transition Radiation Detectors - arXiv:1111.4188v1 - 2011

[And13] Anton Andronic - private communication - 21.01.2013

[ATL08] ATLAS Collaboration, The ATLAS Experiment at the CERN Large Hadron Collider doi:10.1088/1748-0221/3/08/S08003

[ATL12] ATLAS Collaboration et al, Observation of a new particle in the search for the Standard Model Higgs boson with the ATLAS detector at the LHC http://dx.doi.org/10.1016/j.physletb.2012.08.020

[Bas05] Steffen A. Bass, Invited plenary talk at the 5th Int. Conf. on Physics and Astrophysics of the QGP, Kolkata, India, 2005 http://www.phy.duke.edu/~bass/kolkata05.ppt

[Be+03] L. Betev,P. Chochula, Definition of the ALICE Coordinate System and Basic Rules for Sub-detector Components Numbering ALICE-INT-2003-038 https://edms.cern.ch/file/406391/2/

[BMS07] Peter Braun-Munziger and Johanna Stachel - The quest for the quark-gluon plasma Nature Vol 448 19 July 2007 doi:10.1038/nature06080

[BrW06] Peter Braun-Munzinger, Jochen Wambach, Extreme Materie, Physik Journal 5 (2006) Nr. 10 - 2006 Wiley-VCH Verlag GmbH & Co. KGaA, Weinheim

[CAR12] Renè Brun, Federico Carminati,Giuliana Galli Carminati : From the Web to the Grid ans Beyond Springer 2012

[CAL04] ALICE Collaboration, ALICE trigger data-acquisition high-level trigger and control system : Technical Design Report ALICE-TDR-10 ; CERN-LHCC-2003-062. - Geneva : CERN, 2004

[CEM08] ALICE Collaboration, ALICE Electromagnetic Calorimeter Technical Design Report CERN-LHCC-2008-014 ; ALICE-TDR-014. - 2008

[CER84] ECFA-CERN Workshop on Large Hadron Collider in the LEP tunnel - 21 - 27 Mar 1984 - Lausanne, Switzerland -
http://cdsweb.cern.ch/record/155724/files/cern-84-10-V-2.pdf

[CIT99] ALICE Collaboration, ALICE Inner Tracking System (ITS) : Technical Design Report ALICE-TDR-4 ; CERN-LHCC-99-012. - Geneva : CERN, 1999

[CHM98] ALICE Collaboration, ALICE high-momentum particle identification : Technical Design Report ALICE-TDR-1 ; CERN-LHCC-98-019. - Geneva : CERN, 1998

[CMS08] The CMS Collaboration et al 2008, The CMS experiment at the CERN LHC 2008 JINST 3 S08004 doi:10.1088/1748-0221/3/08/S08004

[CMS11] CMS Collaboration, Indications of Suppression of Excited Υ States in Pb-Pb Collisions at $\sqrt{s_{NN}} = 2.76$ TeV doi:10.1103/PhysRevLett.107.052302

[CMS12] CMS Collaboration, Observation of a new boson at a mass of 125 GeV with the CMS experiment at the LHC http://dx.doi.org/10.1016/j.physletb.2012.08.021

[CMU99] ALICE Collaboration, ALICE dimuon forward spectrometer : Technical Design Report ALICE-TDR-5 ; CERN-LHCC-99-022. - Geneva : CERN, 1999

[Cou08] Prof. H.-J. Pirner, Prof. H.-C. Schultz-Coulon - Lecture: The Standard Model of Particle Physics
http://www.kip.uni-heidelberg.de/~coulon/Lectures/SM/ - 08.01.2013

[CPH99] ALICE Collaboration, Technical Design Report of the Photon Spectrometer (PHOS) : Technical Design Report ALICE-TDR-2 ; CERN-LHCC-99-04. - Geneva : CERN, 1999

[CrB97] P. Crochet and P. Braun-Munzinger, Investigation of background subtraction techniques for high mass dilepton physics,
http://hal.archives-ouvertes.fr/docs/00/01/71/97/PDF/democrite-00013585.pdf

[CTP00] ALICE Collaboration, ALICE time projection chamber : Technical Design Report CERN-OPEN-2000-183 ALICE-TDR-7 ; CERN-LHCC-2000-001. - Geneva : CERN, 2000

[CTO00] ALICE Collaboration, ALICE Time-Of-Flight system (TOF) : Technical Design Report ALICE-TDR-8 ; CERN-LHCC-2000-012. - Geneva : CERN, 2000

[DAQ06] ALICE Collaboration, Architecture and Implementation of the ALICE Data-Acquisition System - 15th International Conference on Computing In High Energy and Nuclear Physics, Mumbai, India, 13 - 17 Feb 2006, pp.142-148
https://cdsweb.cern.ch/record/1079672?ln=de

[Dya70] Sidney D. Drell and Tung-Mow Yan , Massive Lepton-Pair Production in Hadron-Hadron Collisions at High Energies, Stanford Linear Accelerator Center, Stanford University, Stanford, California 94305 doi: 10.1103/PhysRevLett.25.316

[ED+04] E.Dumonteil and P.Crochet, Measuring the pt dependence of the Y´ / Y ratio with the ALICE Muon Spectrometer ALICE Internal Note - ALICE-INT-2005-002 version 1.0 http://cdsweb.cern.ch/record/814358/files/INT-2005-002.pdf

[EIa12] Edmond Iancu, QCD in heavy ion collisions arXiv:1205.0579v1 2 May 2012

[Ev+05] Evans, D. et al., The ALICE central trigger system 07/2005;
DOI:10.1109/RTC.2005.1547458 ISBN: 0-7803-9183-7 In proceeding of: Real Time Conference, 2005. 14th IEEE-NPSS

[Fac13] Pietro Daccioli, The return of quarkonia, CERN Courier July/August 2013 http://cerncourier.com/cws/article/cern/54038 02.10.2013

[FSa76] F. Sauli - Principles of operation of multiwire proportional and drift chambers. Lectures given in the Academic Training Programm of CERN 1975-1976 https://cdsweb.cern.ch/record/117989/files/CERN-77-09.pdf 18.10.1012

[Gin91] V. L. Ginzburg und V. N. Tsytovich - Transition Radiation and Transition Scattering (Series on Plasma Physics) Institute of Physics Publishing (Februar 1991)

[Gin96] Vitalii L Ginzburg - Radiation by uniformly moving sources (Vavilov-Cherenkov effect, transition radiation, and other phenomena)
1996 Phys.-Usp. 39 973 doi:10.1070/PU1996v039n10ABEH000171

[gun03] Taku Gunji, Study of Electron Identification Capability of the ALICE Transition Radiation Detector,
http://www-alice.gsi.de/trd/papers/dipl/gunji.pdf

[Had01] Simon Hands - The Phase Diagram of QCD -
doi: 10.1080/00107510110063843 http://arxiv.org/abs/physics/0105022v1

[Heß11] Benjamin Andreas Heß, Online Electron Identification for Triggering with the ALICE Transition Radiation Detector
http://www.physi.uni-heidelberg.de//Publications/diplomathesis_hess.pdf

[HMü96] John W. Harris, Berndt Müller, THE SEARCH FOR THE QUARKGLUON PLASMA
arXiv:hep-ph/9602235v2 8.Feb.1996

[IaV03] Edmond Iancu, Raju Venugopalan, The Color Glass Condensate and High Energy Scattering in QCD
arXiv:hep-ph/0303204v3

[jkl11] Jochen Klein, et al. [ALICE Collaboration], Triggering with the ALICE TRD arXiv:1112.5110V1 21 Dec 2011

[Kal11] Alexander Kalweit for the ALICE Collaboration, Particle identification in the ALICE experiment 2011 J. Phys. G: Nucl. Part. Phys. 38 124073
http://stacks.iop.org/JPhysG/38/124073

[KKo11] K. Koch for the ALICE Collaboration, π^0 and η measurement with photon conversions in ALICE in proton-proton collisions at $p_s = 7TeV$ - Nuclear Physics A 00 (2011) 1-4 arXiv:1103.2217v1 11 Mar 2011

[lhc08] http://lhcb-public.web.cern.ch/lhcb-public/en/Detector/Detector-en.html - 20.07.2012

[lhc11] C. A. Salgado (editor) Proton-Nucleus Collisions at the LHC: Scientific Opportunities and Requirements arXiv:1105.3919v1

[LoI12] https://cdsweb.cern.ch/record/1475243/files/LHCC-I-022.pdf - 10.09.2012

[LWe07] Fu-Ming Liu, Klaus Werner, A Systematic Study on Direct Photon Production from Central Heavy Ion Collisions, arXiv:0712.3619v2 [hep-ph] 29 Dec 2007

[Mat10] The CMS Collaboration, Upsilon production cross section in pp collisions at $\sqrt{s}$ = 7 TeV, arXiv:1012.5545v1 [hep-ex] 26 Dec 2010

[Mat11] M. De Mattia (Purdue University) for the CMS Collaboration, Upsilon production with CMS, 9/04/2011
https://indico.cern.ch/event/114069/session/3/material/slides/0?contribId=25

[MBo08] Marek Bombara, ALICE trigger system for newcomers -
http://www.ep.ph.bham.ac.uk/twiki/bin/view/ALICE/AliceTriggerIntroduction - 15.12.2012

[McL01] Larry McLerran, The Color Glass Condensate and Small x Physics: 4 Lectures - arXiv:hep-ph/0104285v2

[McL12] Larry McLerran, Summary: 8th International Workshop on High pT Physics at LHC 2012 20-24 October 2012 Wuhan, China
https://indico.cern.ch/conferenceDisplay.py?ovw=True&confId=181834 - 18.01.2013

[MUl49] Nicholas Metropolis, Stanislaw M. Ulam, The Monte Carlo Method, Journal of the American Statistical Association, Vol. 44, No. 247. (Sep., 1949), pp. 335-341. http://www.jstor.org/stable/2280232

[MZi10] Markus Zimmermann: Bachelor thesis, Study of the Response of Different Jet-Algorithms for the ALICE-Experiment, 2010
http://qgp.uni-muenster.de/thesisdb/batch-zimm-10.pdf

[Nay06] J.L. Nagle, The letter "s" (and the sQGP) Eur. Phys. J. C 49, 275-279 (2007) doi:10.1140/epjc/s10052-006-0061-1

[New13] Dr. D. Newbold, First-Level Triggering, Lecture
http://www.stfc.ac.uk/PPD/resources/pdf/yr11_lecture07_newbold.pdf

[PDG06] S.Eidelman et al. [Particle Data Group], Phys. Lett. B 592, 1 (2004) and 2005 partial update for edition 2006 (URL: http://pdg.lbl.gov)

[PDG12] J.Beringer et al. [Particle Data Group], Particle Physics Booklet July 2012 (URL: http://pdg.lbl.gov)

[PDG12a] J.Beringer et al. [Particle Data Group], The Review of Particle Physics, chapter 27. Passage of particles through matter Phys. Rev. D86, 010001 (2012)

[Pei09] Thomas Peitzmann, Direct Photon Production in Heavy Ion Reactions, Utrecht University
http://agenda.nikhef.nl/getFile.py/access?resId=5&materialId=0&confId=536

[Pov06] Povh, Rith, Schloz, Zetsche, Teilchen und Kerne Berlin: Springer Verlag, 7.th edition 2006

[PSt12] Peter Steinberg, First results from the LHC heavy ion program
doi:10.1088/1367-2630/14/3/035006

[PTS11] http://alice.physi.uni-heidelberg.de/oyama/PreTrigger/pkwk/
- 20.07.2012

[PZS11] P. Z. Skands, Tuning Monte Carlo Generators: The Perugia Tunes, arXiv:1005.3457v4 [hep-ph] 5 May 2011

[RaL99] Johann Rafelski, Jean Letessier (Department of Physics, University of Arizona, Tucson, AZ and LPTHE-Universite Paris 7, France) Hadron Freeze-out and QGP Hadronization - arXiv:hep-ph/9902365v1

[RFi01] Rick Field, Run 2 Monte-Carlo Workshop April 20, 2001
http://cepa.fnal.gov/patriot/mc4run2/MCTuning/run2mc/R_Field.pdf
- 29.01.2013

[RIc11] Raphaëlle Ichou, for the ALICE collaboration, ALICE potential for direct photon measurements in pp and Pb-Pb collisions, arXiv:1101.1244v2 [hep-ex]
28 Jan 2011

[SaS10] S. Sarkar, H. Satz, B. Sinha(Editors) The physics of the quark-gluon plasma: introductory lectures. Berlin: Springer Verlag, 2010.

[SUr82] R.U. Sexl, H.K.Urbantke: Relativität, Gruppen, Teilchen: Spezielle Relativitätstheorie als Grundlage der Feld- und Teilchenphysik, Springer (1. Februar 1982)

[TPC12] Weilin Yu, For the ALICE TPC Collaboration Particle identification of the ALICE TPC via dE/dx doi:10.1016/j.nima.2012.05.022,

[UHe13] Universität Heidelberg Bildgalerie des Physikalischen Institutes -
http://www.physi.uni-heidelberg.de/Galerie/allpics.php - 17.01.2013

[Ven08] Raju Venugopalan, From Glasma to Quark Gluon Plasma in heavy ion collisions - arXiv:0806.1356v2 [hep-ph] 11 Jun 2008

[Ver12] Marta Verweij - Measurement of jet spectra with charged particles in Pb-Pb collisions at $\sqrt{s_{NN}}$=2.76 TeV with the ALICE detector at the LHC -
https://indico.cern.ch/contributionDisplay.py?contribId=444&confId=181055
18 Nov 2013 (see also inherent paper: arXiv:1210.8264v1)

[VLi04] Volker Lindenstruth, Ivan Kisel: Overview of trigger
systems doi:10.1016/j.nima.2004.07.267

[VUL04] Vulpescu, Bogdan: ALICE TRD trigger algorithms and performance for Upsilon detection
http://www-alice.gsi.de/trd/transp/HERA_LHC.pdf - 05.04.2014

[wiki2] http://en.wikipedia.org/wiki/Standard_Model - 22.10.2012

[wiki3] http://en.wikipedia.org/wiki/Pseudorapidity - 24.10.2012

[wiki4] http://en.wikipedia.org/wiki/File:Drell-Yan.svg - 29.01.2013

[Wil12] Martin Wilde for the ALICE Collaboration, Measurement of Direct Photons in pp and Pb-Pb Collisions with ALICE, arXiv:1210.5958v2 [hep-ex] 23 Oct 2012

[Won94] Wong, Cheuk-Yin , Introduction to high energy heavy ion collisions, World Scientific Publishing Co Pte Ltd (Dezember 1994)

Eidesstattliche Erklärung des Studierenden

Hiermit versichere ich, dass die vorliegende Arbeit selbstständig verfasst worden ist, dass keine anderen Quellen und Hilfsmittel als die angegebenen benutzt worden sind und dass die Stellen der Arbeit, die anderen Werken - auch elektronischen Medien - dem Wortlaut oder Sinn nach entnommen wurden, auf jeden Fall unter Angabe der Quelle als Entlehnung kenntlich gemacht worden sind.

_____

(Münster, 25. April 2014 Paul Martin Kohn)

Ich erkläre mich mit einem Abgleich der Arbeit mit anderen Texten zwecks Auffindung von Übereinstimmungen sowie mit einer zu diesem Zweck vorzunehmenden Speicherung der Arbeit in eine Datenbank einverstanden.

_____

(Münster, 25. April 2014 Paul Martin Kohn)

Danksagung:

Danke an alle.
Es war eine schöne Zeit und ich habe viel gelernt!